GEND-INF-060-V2

GEND-INF-060,Vol.II
May 1985

Cy 1

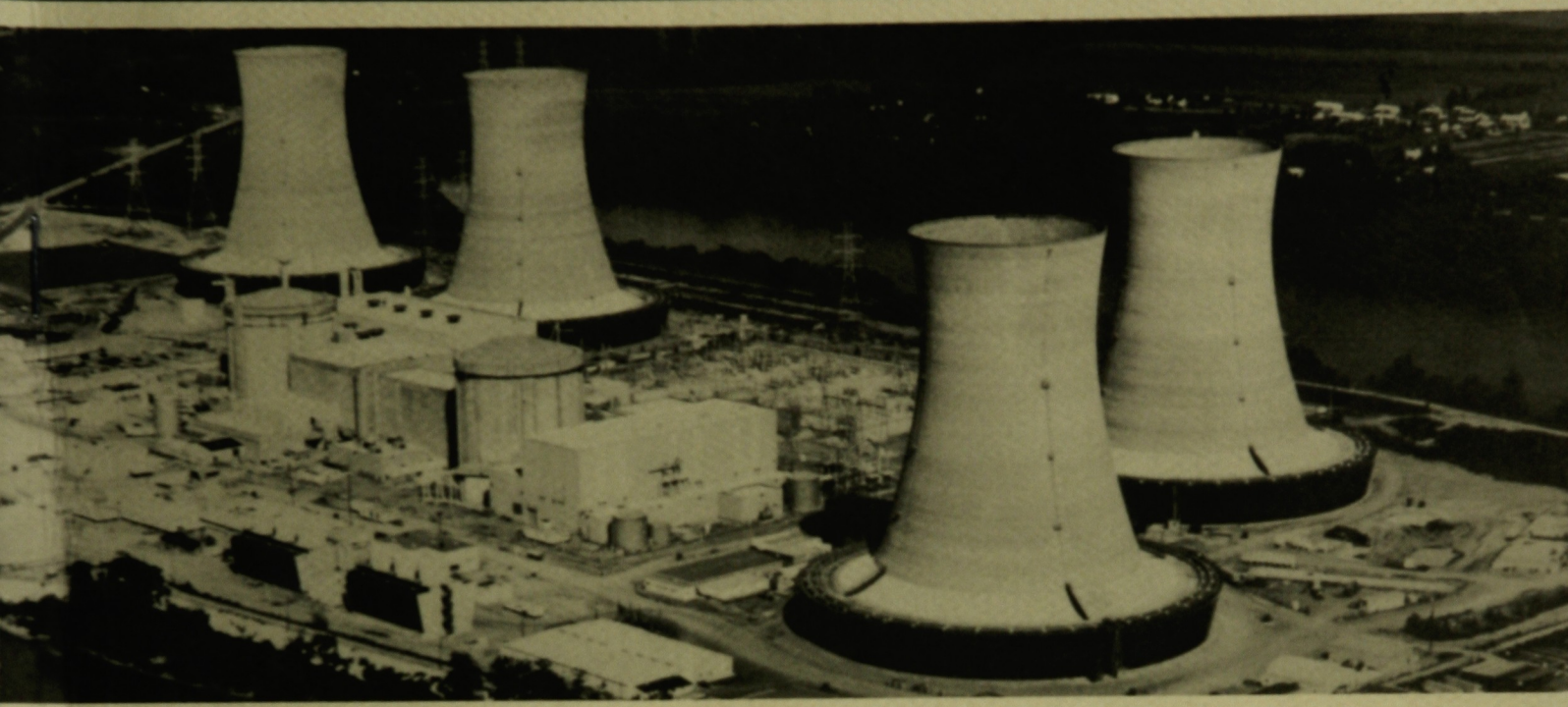

GEND

General Public Utilities • Electric Power Research Institute • U.S. Nuclear Regulatory Commission • U.S. Department of Energy

TMI-2 H8A CORE DEBRIS SAMPLE EXAMINATION

FINAL REPORT

George O. Hayner

Prepared for the
U.S. Department of Energy
Three Mile Island Operations Office
Under Contract No. DE-AC07-76ID01570

TMI-2 H8A CORE DEBRIS SAMPLE EXAMINATION FINAL REPORT

George O. Hayner

Published May 1985

Babcock and Wilcox Company
Research and Development Division
Lynchburg Research Center
Lynchburg, Virginia

Prepared for EG&G Idaho, Inc.
and the U.S. Department of Energy
Three Mile Island Operations Office
Under DOE Contract No. DE-AC07-76ID01570

CONTENTS

LIST OF TABLES

LIST OF FIGURES

ACKNOWLEDGMENTS

The author would like to acknowledge those persons who contributed to the completion of this report.

Gary Bain	- Initial inspection
Bobby Dudley John Henderson	- Hot cell activities
Todd Hardt Lloyd Collins	- Radiochemistry
John Bullard	- Chemistry
Bernard Parham	- Metallography
Woody White	- Scanning electron microscopy
Colin Caldwell	- Consultation
Susan Haghi	- Report preparation

SUMMARY

An examination of a TMI-2 core debris sample removed from position H8 was performed by the Babcock & Wilcox Company Lynchburg Research Center (LRC). The sample was obtained at a depth of three inches below the top of the rubble bed using a specially designed pointed sampling device. The sample was composed of ceramic, resolidified metallic and "rock-like" materials. Many particles contain external open porosity and appear to be a high temperature reaction product from portions of two or more core components. Small pieces can be identified as fuel pellet fragments, oxidized cladding, or combinations with reaction product material. The debris sample is resistant to chemical dissolution in strong boiling mineral acids. The sample contains a wide range of particle sizes with at least 4 w/o of the sample less than 70-100 microns.

The bulk of the sample was composed of U, Zr, and Fe present as undefined alloys or compounds. Ni, Cr, Ag, Sn, Al, and In were also present in smaller amounts. All of these elements were present in the as-built core materials, therefore, it is not surprising that these elements are present in the core debris. About 7 w/o of the sample was determined to be ferromagnetic. The magnetic fractions contained higher Fe, Ni, and Cr, as expected, but also contained higher Ag levels. The magnetic fractions also contain less U in all size ranges. About 70% of the Curie content of the sample material results from Ce/Pr-144 activity. Cs-137 accounts for most of the remaining Curie content and gamma activity. The Cs-137 activity is depleted (10-30% of the code predicted value) for all size fractions and not preferentially depleted for the fine size fractions. This lack of correlation with specific surface area suggests that water leaching of the rubble material is probably not the controlling factor in the Cs-137 depletion observed.

1. INTRODUCTION

Acquisition and examination of debris grab samples from the TMI-2 rubble bed are part of the core internals examination program. The objectives and interests of the examination performed and data presented in this report support data requirements of GPU Nuclear for reactor recovery. The core debris sample examination is a part of other examinations being performed to acquire data on the extent, nature of damage and post-accident condition of the TMI-2 core. The results obtained are intended to assist GPU Nuclear in assessing the tooling and procedures required for defueling. The principal core debris sample examination objectives were to:

1. Determine the physical form of the particulate core debris including information concerning particle size, shape, morphology, components of origin, etc.
2. Determine the chemical form of the debris.
3. Quantify the fission products in the debris.

The examination performed based on these objectives provides information that supports defueling operations in several ways. The physical form of the debris is significant since small sized particles may be suspended in the water during defueling and cause cloudiness. Particle size distribution information is needed to determine the type, number, and effectiveness of filters used for cleaning the water. Information regarding the type of material in the rubble bed will influence the design of tools and the method of defueling. The levels of radionuclides present in the core debris are needed to define the core source term and the levels of leachable radionuclides (such as Cs-137) that could potentially dissolve in the water during defueling operations. The report provides the examination results obtained for one of six samples removed from the TMI-2 rubble bed during September-October, 1983 by lowering sampling devices through leadscrew openings at two locations: H8 (mid-core) and E9 (mid-radius). Samples were

obtained from three depths: surface of the rubble bed, 3 and 22 inches deep in the bed. Following removal, all six samples were shipped to EG&G, Idaho. Sample number 2 removed from the 3-inch depth at location H8 (designated H8A) was shipped to the LRC for examination and analysis. The other five samples were examined at EG&G, Idaho. These grab samples are the first material to be extracted from the rubble bed since the accident in March, 1979.

Two different sampling devices were designed by EG&G, Idaho and used to extract the samples from the rubble bed. A clamshell type tool was used to remove surface samples. A pointed tool with a rotational door opening on each side was used to remove the subsurface samples. A photograph of the subsurface sampling tool is given in Figure 1. All of the tools were attached to long poles which were manipulated from a working platform above the reactor.

2. RESULTS

Following receipt of the H8A sample from EG&G, Idaho in a shielded container, the sampler was unloaded, beta/gamma surveyed, and transferred into hot cell 1 for initial inspection. The inside of the shielded container contained smearable contamination. The inside of the container contained several particles at the bottom on the pad. This shows that the sampler leakage was minimal during shipment. No attempt was made to retrieve these particles. Following initial inspection, particle size and magnetic separation was also performed in hot cell 1. Several selected coarse particles were removed and transferred to the radiochemistry laboratory for immersion density and quantitative gamma scan examinations. One of these particles was also given a preliminary metallographic and scanning electron microscope (SEM) examination. Most of the material from each size fraction was dissolved in order to obtain representative and uniformly dispersed samples for quantitative gamma isotopic assay and elemental examinations. Archive samples from each size fraction were set aside for possible future use. A powder camera X-ray diffraction examination was performed on a sample from the residue remaining following chemical dissolution. A flow diagram of the examinations performed and the weight of material distributed to each step is given in Figure 2.

2.1 Initial Inspection

Following transfer into hot cell 1, the following tasks were performed:

1. Gamma-ray profile of the sampler
2. Sample weight
3. Unloading sampler
4. Visual examination
5. Bulk density

2.1.1 Gamma-Ray Profile

A gamma-ray spectral profile of the sampler was performed prior to unloading. Twenty-eight gamma spectra were acquired using an intrinsic high purity Ge detector with a relative efficiency of 5%. The detector was located outside the hot cell. The sample was viewed through a 43-inch long lead collimator that extended through the cell wall. The sampler was located 13.4 inches in front of the collimator end and centered by a guide sleeve. The opening in the collimator was set at 0.1 inch and spectra were taken every 0.2 inch for 2.6 inches. The sampler was scanned at 0° and 180° orientations corresponding with the sampler window locations.

A typical gamma-ray spectra at 0° orientation is given in Figure 3. The following radionuclides were detectable in the debris specimen: Co-60, Ru-106, Cs-134, Cs-137, Ce/Pr-144, Sb-125, Eu-154, and U X-ray. These radionuclides are typically found in irradiated PWR fuel assemblies. Plots of gamma-ray activity versus length for all radionuclides detected are given in Appendix A. No significant segregation was seen for most radionuclides. The sample length in the sampler was 1.7-1.8 inch. This indicates that the cavity of the sampler was full as-received.

2.1.2 Sample Weight

The sampler was weighed prior to unloading. All in-cell weight measurements were performed using a top loading Mettler electronic balance, Model PE1600 with a precision of $\pm$5 mg. Balance calibration was performed using standard calibration weights. Balance readout was reported to the nearest 10 mg.

The weight of the sampler and debris sample was 489.62 grams. The weight of empty sampler number SN-2 used at location H8A was provided by EG&G Idaho as 363.5 grams. Following sample unloading and cleaning, the sampler was reweighed as 363.4 grams. Therefore, the weight of the as-received H8A Sample was 126.1-126.2 grams. The sample was not weighed after unloading.

2.1.3 Sample Unloading

Prior to sample unloading, the sampler door was opened and the debris sample was visually examined and photographed (Figure 4). No sample segregation was seen in the sampler. The sample appeared to be fairly dry and filled the cavity of the sampler. The approximate elapsed time between removal of the sampler from the shielded container and unloading of core debris material from the sampler was one month.

The sample was unloaded into a large polyethylene tray.

2.1.4 Visual Examination

Visual examination of the debris sample was performed using an ITI hot cell periscope. The sample was distributed uniformly over the surface of the tray, visually examined and photographed. Most photographs were taken using 35 mm color negative daylight film color corrected for tungsten light using an 80A filter. Typical photographs are given in Figure 5. Observations seen during the visual examination are given below:

- Particle size range - 1 cm down to pan fines.
- Sample consists of ceramic, resolidified metallic and "rock-like" materials.
- Many particles have orange surface deposits.
- Most particles have a brown coloration (light-to-dark) and have rough edges.
- Some particles have smooth edges and surface porosity.
- Some larger fragments have a curved surface.
- Approximately 1/3 of coarse material contains substantial surface porosity.

During the visual examination, high intensity lights were required in order to provide adequate illumination for photography through the wall periscope.

These lights produced considerable heat (more than anticipated) and melted the top layer of the polyethylene tray. This effectively bonded a large portion of the debris sample to the tray. Several attempts using different techniques were made to remove this material. However, these attempts were largely unsuccessful and 57.4 grams of material were lost on the tray. Subsequent handling of the material in- cell was performed using porcelain coated steel containers. A discussion of the significance of this material loss is given in Section 3.3.

2.1.5 Bulk Density

A bulk density determination was performed on 68.7 grams of material (the remainder of the debris sample). The volume of the material was determined using a 50 ml graduated cylinder with slight tapping to settle the material. A bulk density of 4.2 g/cc was obtained.

2.2 Particle Size and Magnetic Separation

Particle size separation was performed on 68.7 grams of material. ASTM procedure C-92 was used as a guide for performing these measurements. A set of 8 half height, 3 inch diameter US standard screens made by Tyler with a Tyler RX-24 motor driven portable sieve shaker was used for particle size separation. The screens were shaken for one hour. All screens were US standard wire mesh. The following screens were used: 5, 10, 16, 24, 48, 100, 200 and 325. The particle size distribution results are given in Table 1.

Separation of magnetic material was performed on 62.7 grams of the sample. Magnetic separation was not performed on the individual particles examined in Section 2.7. Separation was performed using a permanent magnet separated from the sample by a 1/16 inch layer of polyethylene. The magnetic separation results are given in Table 2. Representative photographs of each size fraction are given in Appendix B.

The most significant problem that occurred during the examination was the loss of 57.4 grams of sample during initial inspection. This resulted in 68.7 grams of sample being subjected to particle sizing. This working sample accounts for approximately 55% of the sample weight. Based on visual observation, about 45% of the sample that bonded to the tray was representative of the total sample rather than a specific size fraction.

2.3 Sample Dissolution

Following magnetic separation, adjacent size fractions were combined in order to maintain approximately the same number of samples. Archive samples from most size fractions were removed and stored in hot cell 1. Selected coarse particles were removed for detailed examination. A sample weight of 53.3 grams was subjected to the dissolution process in order to provide a representative sample from each combined size fraction. Each combined size fraction was further separated into a magnetic and non-magnetic portion for a total of 10 samples ranging from a weight of 0.17 to 21.49 grams.

Each of the samples was initially immersed in 8M nitric acid and kept at boiling for 2-4 hours. This step was intended to dissolve any UO_2, U_3O_8, and silver present in the sample. For the most part, large chunks of debris still existed as undissolved particles after this step. The nitric acid solution was decanted and the undissolved residue was washed into a teflon beaker. Concentrated HF and HCl were added sequentially to the residue to further dissolve any Zr and Fe compounds in the residue. After heating to dryness twice, the chlorides were driven off with nitric acid and the solution was filtered through a 0.45 micron Millipore paper. All the large chunks remaining after the first HNO_3 step were either dissolved or reduced to a fine powder in subsequent dissolution steps. Both solutions were combined, made up to a known weight, and sampled for gamma spectroscopy. The filter paper with the remaining residue was dried and weighed to determine the amount of undissolved solids. An average of 95% of each fraction was soluble in this treatment. A residue of 2.9 grams remained

following the dissolution process. Distribution of archive and dissolution samples are given in Table 3.

Each Millipore filter containing the undissolved portion of the debris fractions was put into a one-liter container with 500 ml of deionized (DI) water. This mixture was then subjected to five minutes of ultrasonic agitation in order to knock the residues loose from the filter papers and create a suspension of particulates. An additional 500 ml of DI water was added to make up a volume of 1000 ml. It appeared that a very uniform suspension was created by this method although not all of the debris was removed from each filter paper. A 1-ml aliquot of the suspension was taken, placed on a Millipore paper, dried and weighed. This sample contained 1.8 mg of material and was analyzed by gamma-ray spectroscopy for gamma emitting isotopes.

2.4 Radionuclide Distribution

Quantitative isotopic gamma scanning was performed on an aliquot of each dissolved sample given in Table 3. All of the radionuclides which were gamma counted should have been retained by the dissolution process. The uncertainty on the absolute detector efficiency is 10% for gamma rays above 300 keV in energy and 15-20% for lower energy gamma rays. The gamma scan results (in microCuries/gram sample) by size fraction are given in Table 4. The activity values are decay corrected to November 11, 1983 at 1200. The results are also corrected for mass attenuation. The percent error values are based on one sigma uncertainties for counting statistics. All gamma-ray peaks measured were identified. Gamma-ray spectrum for the -24 +100 mesh magnetic and non-magnetic dissolved size fractions are given in Figure 6. The weighted averages of the gamma scan results by radionuclide are given in Table 5. The weighted averages were calculated by the following equation:

$$\text{Wt. Avg.} = \frac{\Sigma A_i \cdot WT_i}{\Sigma WT_i}$$

where:

A = activity of radionuclide in fraction (microCuries/gram)
WT = net dissolved weight of fraction
i = fraction

2.5 Elemental Examination

Graphite electrodes were packed with 10 ± 0.5 mg of high purity graphite. The standards were prepared by pipetting 10 microliter aliquots of certified standard solutions into the electrodes and drying under a heat lamp. The volume of standard solutions was corrected on a mass basis with a maximum mass of 0.2 mg for any one element. The sample volumes were also based on obtaining a sample mass of approximately 0.2 mg. A dilution was made for samples with concentration exceeding 0.2 mg/10 microliters. It was necessary to measure the density of the solutions to determine the mass of material in a given volume since the sample solutions were prepared on a mass/mass basis. A Ge internal standard was added to all samples to help correct for variations in the burn conditions. The electrodes were burned to completion in a DC arc operated at 9-10 amp. Emission from the elements of interest was recorded on photographic plates. Emission line intensities were measured on a digital densitometer. All sample intensities were ratioed to the intensities of the internal standard lines. Ratioed intensity data from the standards were used to construct calibration curves to quantify the elements present in the samples. The estimated precision of this technique is ±20% relative. The results for the elemental analysis by size fraction is given in Table 6 for the dissolved samples. The weighted average results by element for the total dissolved sample, magnetic and non-magnetic materials is given in Table 7. Analysis for Cu, Cd, Co, Mo, Mn and B was also performed, but results were less than detectability limit.

A qualitative analysis was performed on the undissolved solids. All of the solids from the size fraction were well mixed in a plastic bottle containing one liter of water. Aliquots from the slurry were pipetted into graphite

electrodes and burned in a DC arc. The elements in the sample were identified by comparison to standards. The results obtained are given in Table 8.

2.6 X-Ray Diffraction of Residue

An aliquot of the well-mixed solids slurry was evaporated almost to dryness with a heat lamp. Part of the residue was rolled into a thin rod with Duco cement. The rod was mounted in an X-ray powder diffraction camera. X-rays were generated with a Cu X-ray tube operated at 35 kv and 20 ma. The identified phases were UO_2 and ZrO_2. One or more unidentified phases are also present. The diffraction data obtained are listed in Appendix E. The data obtained are qualitative and the detectability limit is typically about 5%.

2.7 Examination of Selected Coarse Particles

Six particles were selected from the +5 mesh size fraction for more detailed examination. The examinations performed are given below:

- Immersion density determination of each particle
- Quantitative isotopic gamma scanning of each particle
- Detailed macroscopic inspection
- Metallography and SEM examination of one particle

2.7.1 Immersion Density Determination

Immersion density measurements were made on particles 1-6. LRC Technical Procedure LRC-TP-98, "Density Determination of Porous Ceramics by an Immersion Technique," was used as a guide for performing these measurements. This is the method normally used for irradiated fuel pellet fragments. This procedure is similar to ASTM procedure C-830.

Each of the samples was placed in a separate beaker and dried on a hot plate at 100°C for 12 hours. After the samples cooled to room temperature, they were weighed. All weight measurements were performed using an analytical balance in the Radiochemistry Laboratory. Sample 4 split into two pieces spontaneously during the drying. Both pieces were measured together throughout the experiment. The dry weights are given in Table 9.

Following the dry weight measurements, the samples were placed under a vacuum for one hour. Then the samples were covered with water by filling the tubes holding the samples. The water was added without interrupting the vacuum. Each sample remained underwater in a vacuum for an additional hour. During loading of sample 3 into the vacuum chamber, it split into two large pieces and one small piece. The two large pieces were measured together throughout the experiment. The small piece was weighed and the sample dry weight was corrected. The small piece was not used.

The suspended weight measurements were made by using a basket suspended in water in place of the normal weight pan used for the analytical balance. The samples were weighed in the suspended basket to obtain the suspended weight. These weights are also given in Table 9. Finally, the samples were dried on a wet paper towel and weighed to obtain the saturated weight, also given in Table 9. The temperature of the water was 24°C and a density of 0.99732 grams/cm^3 was used for the calculations.

The results of the calculations are given in Table 10. The following results were calculated for each sample: open porosity (cm^3); pellet volume (cm^3); matrix volume, percent open porosity (%); and, matrix density of sample (grams/cm^3). The formulas used in the calculations of these results are listed below. The pellet volume considers open porosity but the matrix volume and density considers only closed porosity.

$$\text{Open porosity} = \frac{\text{Saturated weight - dry weight}}{\text{Fluid density}}$$

$$\text{Matrix volume} = \frac{\text{Dry weight - suspended weight}}{\text{Fluid density}}$$

$$\text{Pellet volume} = \frac{\text{Saturated weight - suspended weight}}{\text{Fluid density}}$$

$$\text{Percent open porosity} = \frac{\text{Open porosity}}{\text{Matrix volume}} \times 100\%$$

$$\text{Matrix density of sample} = \frac{\text{Dry weight}}{\text{Matrix volume}}$$

2.7.2 Gamma Scanning

The six particles measured for immersion density in Section 2.7.1 were gamma scanned. All samples except number 5 were measured at a calibrated distance of 195 cm from the detector. Sample 5 was measured at a calibrated distance of 38 cm. The uncertainty on the absolute efficiency is 10% for gamma rays above 300 keV in energy and 15-20% for lower energy gamma rays.

Tables 11 and 12 give the results of the analyses. The results are not corrected for mass attenuation but the data is available to perform this correction. However, based on the size and composition of the particles, significant mass attenuation would be expected only for the 133.5 keV Ce-144 gamma-ray peak. Therefore, the Ce-144 results are not reliable for the individual particles. The data given are the identified radionuclides, their activity in microCuries per gram of sample and the percent error. The activity values are decay corrected to November 11, 1983, at 1200. The percent error values are based on one sigma uncertainties for counting statistics and are unrealistically low in terms of overall uncertainty. This results because the system used is not calibrated for particle geometry but is normally used for small liquid samples of the type measured in Section 2.4.

In Table 11 some activation products were not detected in all samples. In those cases, the values are given as less than the minimum detectable activity (MDA) values.

Table 12 includes the results for fission products or daughter products from fission products. The case of Ce-144 and Pr-144 presents a confusing situation. The Ce-144 and Pr-144 are in equilibrium and thus should have the same activity. These discrepancies may be partially explained in terms of differential gamma-ray attenuation. The Ce-144 activity is computed on the basis of a 134 keV gamma ray while the Pr-144 is computed on the basis of a 696 keV gamma ray. These two gammas are attenuated to different extents, with the 134 keV gamma being significantly attenuated by a high density, high Z material. This is supported by the results from the smallest size and lowest density sample, number 5, which has the closest agreement in the two nuclides. Therefore, the Pr-144 results were used in all discussions concerning Ce-144 distribution of the individual particles.

Table 13 shows the parameters used in the identification of the nuclides and the decay corrections made. The half-life used for Pr-144 is that for its parent, Ce-144. The parameters also pertain to the results given in Tables 4 and 5 except that the Pr-144 data was not calculated. The gamma-ray spectra of the six samples are given in Appendix C. Major peaks in the spectra are labeled.

2.7.3 Macroscopic Inspection

Detailed macroscopic inspection at 5 to 25X magnification was performed on each particle using a Nikon stereo macroscope. Stereo 35 mm photographs of each particle were taken using daylight color negative film and an 80A filter for color correction. Generally, most of the observations noted during initial visual examination pertain to these particles. The exception was particle 5. During handling, this particle appeared to be a piece of rubber. This particle is, therefore, assumed to be contamination from the

hot cell (probably from the slave fingers). Particle 1 had a curved surface on one side that appeared to be a piece of oxidized cladding. The other side was "rock-like" in appearance with some surface porosity present. Particle 2 was "rock-like" in appearance with extensive surface porosity. Particle 2 had about the same medium brown coloration as Particle 1. Particles 3 and 6 were similar. These particles were almost black, contained orange and silver colored surface deposits, and contained extensive surface porosity. Most of the surfaces were rough, however, a curved surface in Particle 3 was noted. Particle 4 appeared to be a fractured piece of UO_2 fuel. Photographs of these particles taken during visual examination are given in Appendix D. The background grid seen on some photographs is 1/4-inch square.

2.7.4 Metallographic/SEM Examination

The small portion of particle 3 (see Appendix D for photograph) was metallographically mounted and prepared in a conventional manner. Deionized water was used with the polishing media during preparation. The specimen was examined using the hot cell metallograph in the as-polished condition. A photomosaic of a portion of the specimen is given in Figure 7. A large amount of both fine and coarse internal porosity was seen. Also, one corner of the specimen (right side of Figure 7) contained considerable cracking of the type normally seen in ceramic UO_2 fuel following irradiation. Other areas of the specimen did not contain this type of extensive cracking. The specimen was then etched with a 5% Nital solution with the hope of revealing other phases present rich in Fe, Ni or Cr. This etchant revealed a dark gray phase as indicated in Figure 8. Figure 8 was taken at the same magnification as Figure 7 in the lower left quadrant.

Further examination was performed on this specimen in the etched condition using the scanning electron microscope (SEM) system. The specimen was sputter coated with Au to facilitate examination. A composite photograph of most of the specimen cross section is shown in Figure 9. The specimen was

examined in greater detail at locations A, B, C, D, E, 1 and 2 noted on Figure 9. Energy dispersive X-ray (EDX) spectra were obtained at locations A, B, E, 1 and 2. The cracked area noted previously appears lighter in the SEM secondary electron composite photograph. The small areas of porosity seen in Figure 7 are more difficult to see in Figure 9 because they are only slightly lighter than the grey matrix seen in most of the specimen. Detailed photographs of areas A, B, C, D and E are given in Figures 10, 11, 12, 13, and 14, respectively. The EDX spectra from areas 1 and 2 are given in Figures 15 and 16, respectively. All EDX spectra have the same integrated counts and the same vertical scale and, therefore, can be directly compared. Inspection of Figures 10-16 reveals that rounded globular features are present on the inside of the small pores. The EDX analyses generally indicate that U and Zr are the only detectable elements present in the bulk material. These are qualitative results for elements with an atomic number $\geq$ 11. The darker area noted in Figures 13 and 14 contains U, Zr, Fe, Cr, and Al. This area appears to represent a second phase. As indicated previously, O is not detected by the system used for the examination, however, O is probably present due to the origin of the material and the probable elevated temperature history of particle 3. The lighter area seen containing the bulk of the cracking is more easily distinguished in Figure 9 than in Figure 7. The grey level change is probably due to either electrical conductivity changes or the contribution of detected backscattered electrons. Electrical conductivity changes in the specimen can sometimes be seen even with a thin sputter coated Au layer. Both of these effects imply a compositional change for an undetected element. For the reasons indicated previously, this element is probably O.

Table 1. Particle Size Distribution Obtained Following Screening

Sieve Range	Sieve Size, Inch (micrometer)	Size Fraction, %	Cumulative, % Less Than	Weight of Sample,* grams
+5	0.1560 (+4,000)	9.2	-	6.32
-5, +10	0.0650 (+1,700)	39.3	90.8	26.97
-10, +16	0.0390 (+1,000)	21.6	51.5	14.87
-16, +24	0.0276 (+710)	10.8	29.9	7.43
-24, +48	0.0116 (+300)	11.8	19.1	8.14
-48, +100	0.0058 (+150)	3.0	7.3	2.05
-100, +200	0.0029 (+75)	0.8	4.3	0.53
-200, +325	0.0017 (+45)	2.0	3.5	1.37
-325		1.5	1.5	1.01
			Total	68.69

*A total of 68.7 grams of material was screened. 2.4 grams of sample was not recovered following screening. The weight of the sample for each sieve range is the weight of the screen and sample minus the initial weight of the screen.

Table 2. Magnetic Separation Results

Sieve Range (micrometers)		Magnetic Fraction, %*
+5	(+4,000)	0
-5, +10	(+1,700)	9.2
-10, +16	(+1,000)	5.6
-16, +24	(+710)	6.4
-24, +48	(+300)	7.2
-48, +100	(+150)	10.5
-100, +200	(+75)	5.3
-200, +325	(+45)	10.9
-325		67.1

*Based on a sample weight of 62.7 grams.

Table 3. Distribution of Archive and Dissolution Samples

Fraction (micrometers)	Non-Magnetic			Magnetic		
	Initial Dissolution Sample (g)	Dissolved Sample (g)	Archive (g)	Initial Dissolution Sample (g)	Dissolved Sample (g)	Archive (g)
+10 (+1,700)	21.49	20.35 (95%)	4.3	1.78	1.40 (79%)	0.6
-10, +24 (+710)	18.10	17.57 (97%)	1.8	0.88	0.82 (93%)	0.4
-24, +100 (+150)	8.32	7.82 (94%)	0.8	0.66	0.63 (95%)	0.1
-100, +325 (+45)	1.18	1.08 (92%)	0.2	0.17	0.14 (82%)	-
-325	0.22	0.18 (82%)	0.1	0.53	0.45 (85%)	0.1
Total	49.31	47.00	7.2	4.02	3.44	1.2

Table 4a. Gamma Scan Results in microCuries/gram Sample by Size Fraction Dissolved

Magnetic Properties	Size Fraction	Mn-54 (±%)	Co-60 (±%)	Ru-106 (±%)	Cs-134 (±%)	Cs-137 (±%)
Magnetic	+10	0.9 (30)	121 (0.6)	495 (1)	101 (0.6)	1,680 (0.1)
Magnetic	-10, +24	2.9 (10)	169 (0.6)	318 (2)	76.9 (0.9)	1,330 (0.2)
Magnetic	-24, +100	3.3 (20)	334 (0.5)	1,680 (0.6)	83.4 (1)	1,380 (0.2)
Magnetic	-100, +325	2.2 (40)	369 (0.8)	775 (2)	87.6 (2)	1,430 (0.3)
Magnetic	-325	1.9 (20)	89.5 (0.9)	225 (3)	74.1 (1)	1,350 (0.2)
Non-magnetic	+10	0.6 (70)	24.8 (2)	109 (7)	72.5 (1)	1,360 (0.2)
Non-magnetic	-10, +24	1.2 (30)	17.3 (2)	287 (2)	41.8 (1)	826 (0.2)
Non-magnetic	-24, +100	1.1 (10)	37.5 (0.7)	150 (2)	48.3 (0.6)	916 (0.1)
Non-magnetic	-100, +325	1.3 (20)	62.8 (0.9)	173 (2)	50.8 (0.9)	918 (0.2)
Non-magnetic	-325	1.4 (40)	78.5 (2)	240 (4)	74.2 (2)	1,370 (0.3)

Table 4b. Gamma Scan Results in microCuries/gram Sample by Size Fraction Dissolved

Magnetic Properties	Size Fraction	Ce-144 (±%)	Sb-125 (±%)	Eu-154 (±%)	Eu-155 (±%)	Sample Analyzed (mg)	Counting Distance (cm)
Magnetic	+10	2,710 (0.2)	157 (1)	30 (2)	66 (2)	11	15
Magnetic	-10, +24	3,120 (0.3)	165 (1)	35 (3)	75 (3)	6	15
Magnetic	-24, +100	1,870 (0.4)	985 (.4)	22 (5)	46 (6)	5	15
Magnetic	-100, +325	1,400 (0.5)	1,070 (.7)	18 (9)	40 (10)	1	15
Magnetic	-325	3,420 (0.3)	302 (.9)	40 (3)	84 (4)	4	15
Non-magnetic	+10	3,800 (0.4)	91.4 (3)	-	7.1 (3)	69	29
Non-magnetic	-10, +24	3,820 (0.2)	66.2 (2)	-	6.7 (2)	66	29
Non-magnetic	-24, +100	3,800 (0.1)	179 (.6)	45 (1)	6.5 (1)	65	29
Non-magnetic	-100, +325	3,070 (0.2)	479 (.5)	37 (2)	72 (2)	9	15
Non-magnetic	-325	3,600 (0.5)	312 (1)	41 (5)	85 (3)	1	15

Table 5. Gamma Scan Results by Isotope

Weighted Averages (μCi/gm)

Isotope	Energy (kev)	Whole Sample (±%)	Magnetic Fraction (±%)	Non-Magnetic Fraction (±%)	Residue (±%)
Mn-54	834.8	1.1 (30)	2.0 (20)	0.9 (30)	2.4 (30)
Co-60	1,332.5	39.7 (1)	178 (0.7)	25.2 (2)	109 (1)
Ru-106	621.8	422 (3)	646 (2)	184 (3)	4,090 (0.5)
Cs-134	795.8	56.2 (1)	87.9 (1)	56.5 (1)	13.3 (5)
Cs-137	661.6	1,060 (0.2)	1,490 (0.2)	1,080 (0.2)	232 (0.6)
Ce-144	133.5	3,650 (0.4)	2,700 (.4)	3,790 (.3)	2,500 (0.5)
Sb-125	427.9	122 (1)	367 (1)	106 (1)	88 (3)
Eu-154	1,274.8	41 (4)	30 (4)	44 (3)	-
Eu-155	105.3	12 (4)	66 (5)	8.6 (2)	65 (5)
Total weight - gm		53.27	3.44	47.00	2.83
Total activity - μCi/gm		5,400	5,570	5,300	7,100

Table 6. Elemental Analysis Results by Size Fraction of Dissolved Sample

Magnetic Properties	Size Fraction	Elemental Analysis (Weight Percent)								
		U	Zr	Fe	Ni	Cr	Sn	Al	In	Ag
Magnetic	+10	63.3	11.8	26.7	7.2	2.6	<.50	<.50	<.50	1.0
Magnetic	-10, +24	70.5	15.8	11.6	4.7	1.7	<.50	<.50	<.50	2.0
Magnetic	-24, +100	47.0	21.8	10.3	3.9	1.2	1.3	0.81	2.2	5.0
Magnetic	-100, +325	29.7	27.8	13.9	5.6	1.8	1.6	1.8	2.4	6.3
Magnetic	-325	59.6	16.5	5.0	1.8	0.69	<.50	0.57	.50	1.8
Non-magnetic	+10	91.3	13.9	1.5	0.57	<.50	<.50	<.50	<.50	0.84
Non-magnetic	-10, +24	88.9	14.7	1.5	0.50	<.50	<.50	<.50	<.50	<.50
Non-magnetic	-24, +100	87.0	15.3	2.8	0.88	0.51	<.50	<.50	<.50	0.78
Non-magnetic	-100, +325	51.7	15.6	2.1	1.6	0.52	0.50	0.63	0.55	1.7
Non-magnetic	-325	64.9	17.2	3.1	1.5	.50	<.50	<.50	0.50	2.2

Table 7. Weighted Average of Elemental Results of Dissolved Sample

Element	Whole[1] Sample	Magnetic[1] Fraction	Non-magnetic Fraction
U	86.7 (82.6)	60.2 (59.0)	88.8 (84.1)
Zr	14.6 (13.9)	15.9 (15.6)	14.5 (13.7)
Fe	2.8 (2.7)	16.7 (16.4)	1.7 (1.6)
Ni	0.9 (.9)	5.2 (5.1)	0.6 (0.6)
Cr	-	1.8 (1.8)	-
Sn	-	-	-
Al	-	-	-
In	-	-	-
Ag	-	2.3 (2.3)	-

(1) Numbers in parentheses are normalized to 100%.

Table 8. Qualitative Elemental Analysis of Undissolved Residue

Element	Amount Detected*
U	M
Zr	M
Fe	M
Ni	m
Cr	M
Sn	m
Al	m
In	T
Ag	m
Si	m
Mn	T
Cu	T
B	T

*M = major (>10 w/o)

m = minor (1-10 w/o)

t = trace (<1 w/o)

Table 9. Summary of Sample Weights

	Dry Weight, grams	Saturated Weight, grams	Suspended Weight, grams
1	0.12285	0.12559	0.09620
2	1.08108	1.10912	0.93772
3	0.45887*	0.47000	0.40508
4	1.0572	1.07250	0.95154
5	0.06875	0.07959	0.01576
6	0.74307	0.76291	0.66100

*Sample weight corrected for a 0.01052-gram piece not used in density measurements.

Table 10. Immersion Density Results

Sample	Open Porosity (cc)	Pellet Volume (cc)	Matrix* Volume (cc)	% Open Porosity	Matrix Density (g/cc)
1	2.747E-3	2.947E-2	2.673E-2	9.32	4.59
2	2.812E-2	1.719E-1	1.437E-1	16.4	7.52
3	1.116E-2	6.509E-2	5.395E-2	17.1	8.50
4	1.534E-2	1.213E-1	1.059E-1	12.6	9.97
5	1.087E-2	6.400E-2	5.314E-2	17.0	1.29
6	1.989E-2	8.232E-2	8.232E-2	19.5	9.03

*Density of H_2O used, 0.99732 g/cc.

Table 11. Activation Products - microCuries/gram

Reference Date:
November 11, 1983 12:00

Sample	Co-60	% Error	Mn-54	% Error	Co-58	% Error
1	157	1.5	<0.93	-	<1.04	-
2	11.6	2.5	0.894	25	<0.47	-
3	10.8	3.6	<0.3	-	<0.61	-
4	<0.3	-	<0.53	-	<1.0	-
5	3.90	2.6	0.454	19	15.1	1.4
6	76.1	0.90	<0.42	-	<0.80	-

*Values with < were not detected, and are < or = to the minimum detectable activity (MDA). The value given is the MDA value.

Table 12. Fission Product - microCuries/gram

Reference Date:
November 11, 1983 12:00

Sample	Ru-106	% Error	Cs-134	% Error	Cs-137	% Error	Sb-125	% Error
1	151	6.9	48.4	2.8	771	0.5	111	3.7
2	73.3	4.8	52.1	0.8	876	0.17	66.9	2.2
3	74.1	7.9	92.7	0.87	1,500	0.19	17.1	12
4	1,590	0.60	127	0.80	2,530	0.13	148	2.1
5	5.90	9.0	2.28	3.1	23.3	0.74	6.41	3.3
6	1,650	0.47	8.54	5.3	166	0.53	104	1.8

Sample	Eu-154	% Error	Eu-155	% Error	Pr-144	% Error	Ce-144	% Error
1	10.6	14	19.9	20	911	7.4	572	1.8
2	54.6	1.6	51.2	3.9	3,280	0.99	1,090	0.42
3	57.7	2.3	48.8	5.8	3,620	1.2	1,120	0.62
4	48.2	2.7	34.2	8.8	4,070	1.4	704	1.0
5	0.483	15	0.782	18	25.7	12	27.4	1.7
6	52.0	2.2	36.5	6.1	4,160	1.01	785	0.66

Table 13. Radionuclide Peaks Used

Nuclide	Half-Life		Energy (keV)
Co-60	5.264	Y	1,332.5
Mn-54	312.5	D	834.8
Co-58	71.30	D	810.8
Ru-106	367	D	621.8
Cs-134	2.06	Y	795.8
Cs-137	30.17	Y	661.6
Ce-144	284.2	D	133.5
Sb-125	2.73	Y	427.9
Eu-154	8.50	Y	1,274.8
Pr-144	284.2	D	696.5
Eu-155	4.96	Y	105.3

Figure 1. Photograph of Subsurface Sampling Tool

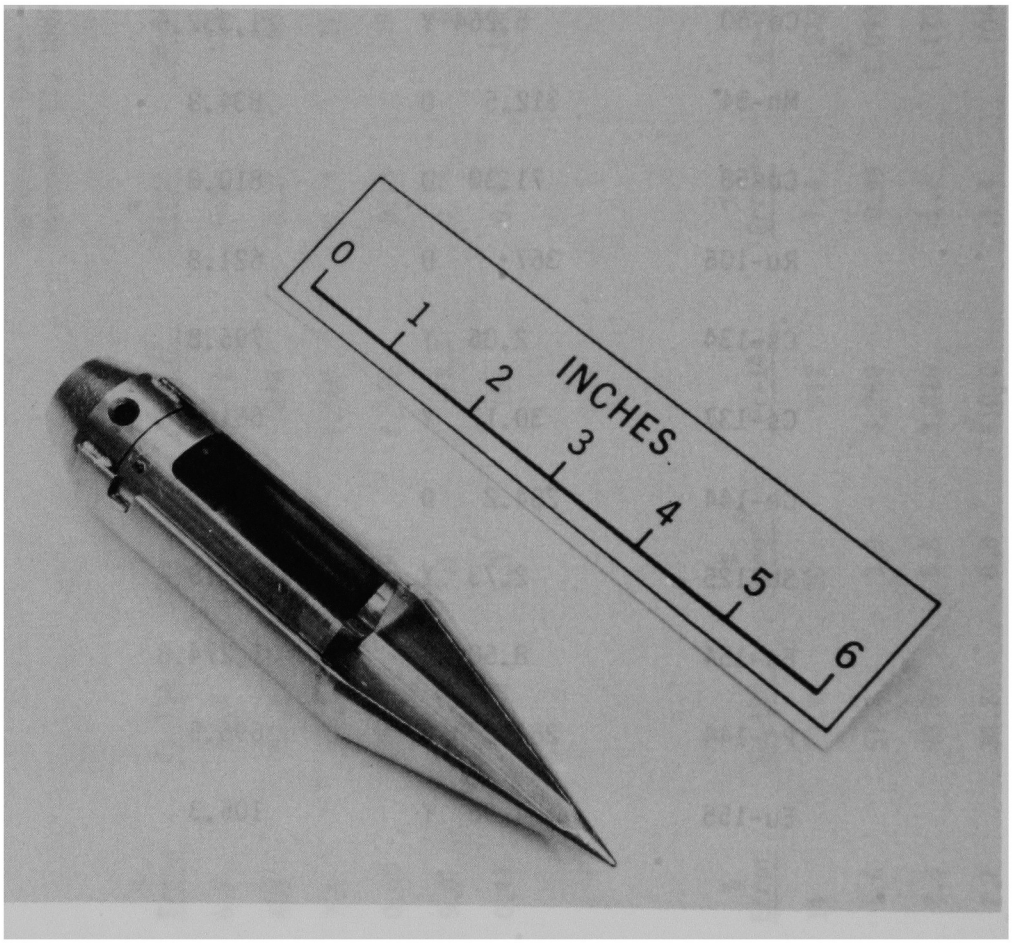

Figure 2. Flow Diagram of Examinations Performed and Distribution of Material by Weight

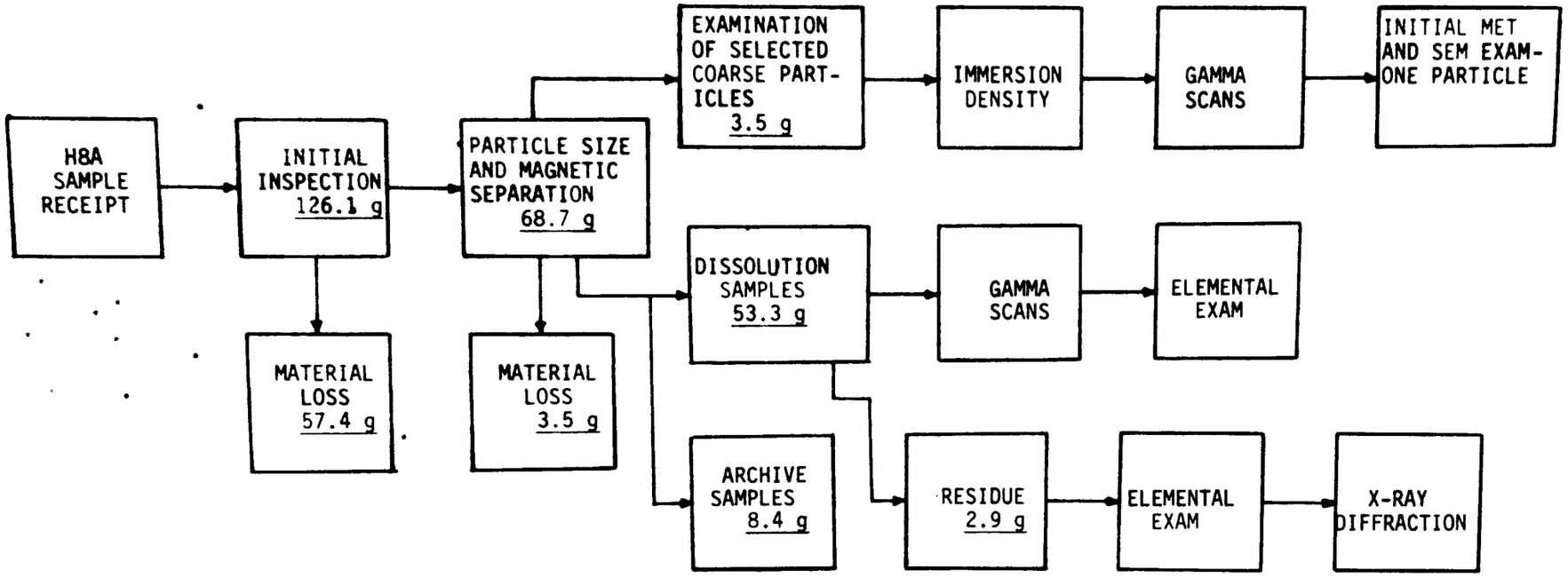

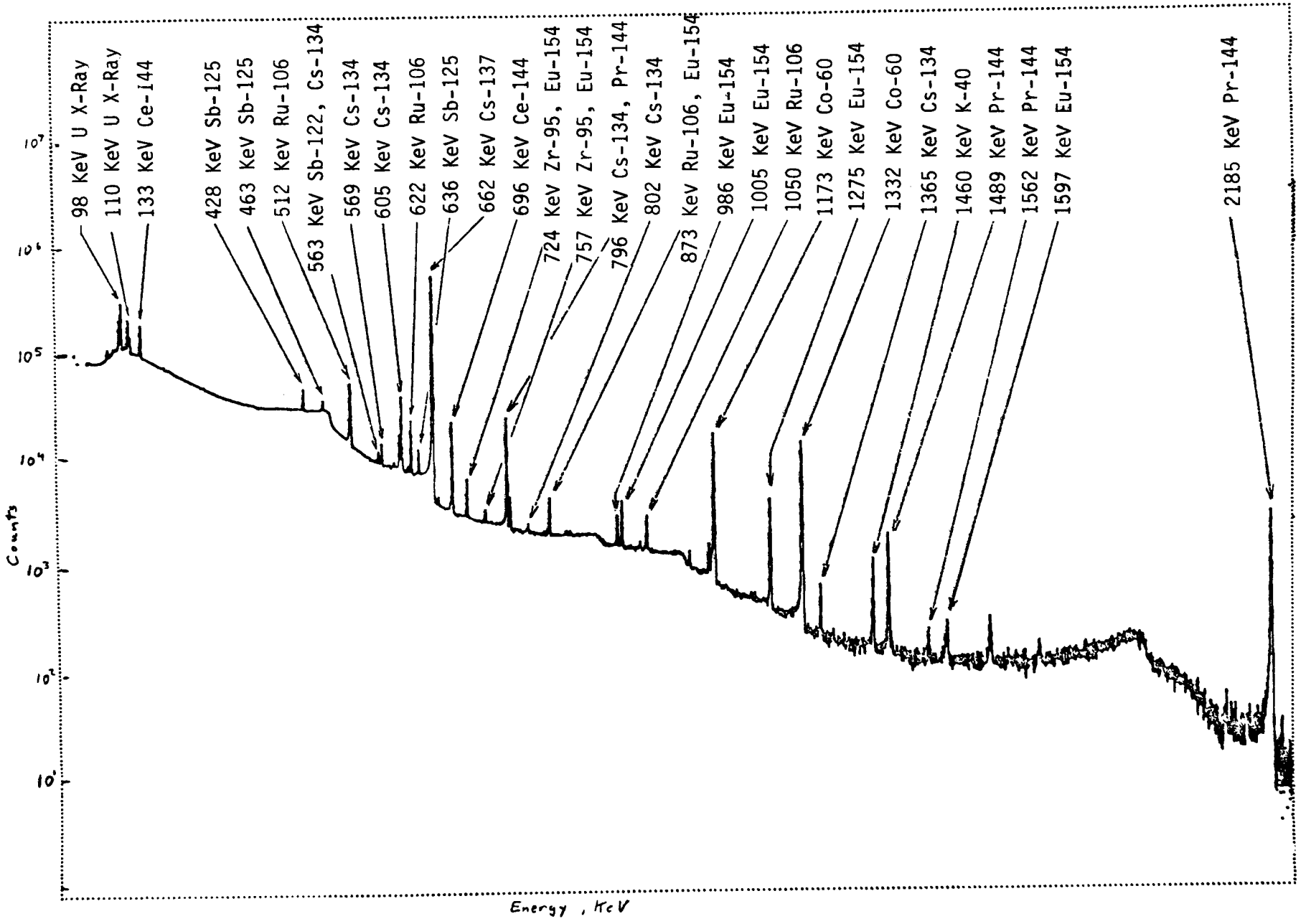

Figure 3. Typical Gamma-Ray Spectra of the TMI-2 Debris Sample in the Subsurface Sampling Tool. Spectra was taken at 49.80 inches (relative) and 0° orientation.

Figure 4. Photograph of Debris Sample in Sampler Prior to Unloading

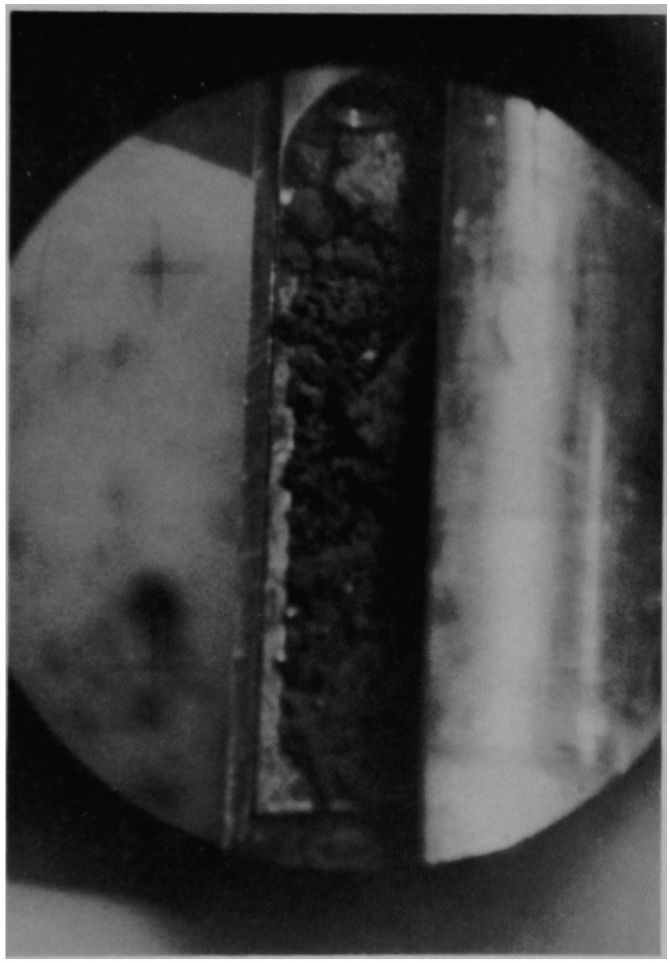

Figure 5. Typical Photographs of H8A Debris Sample Taken During Visual Examination

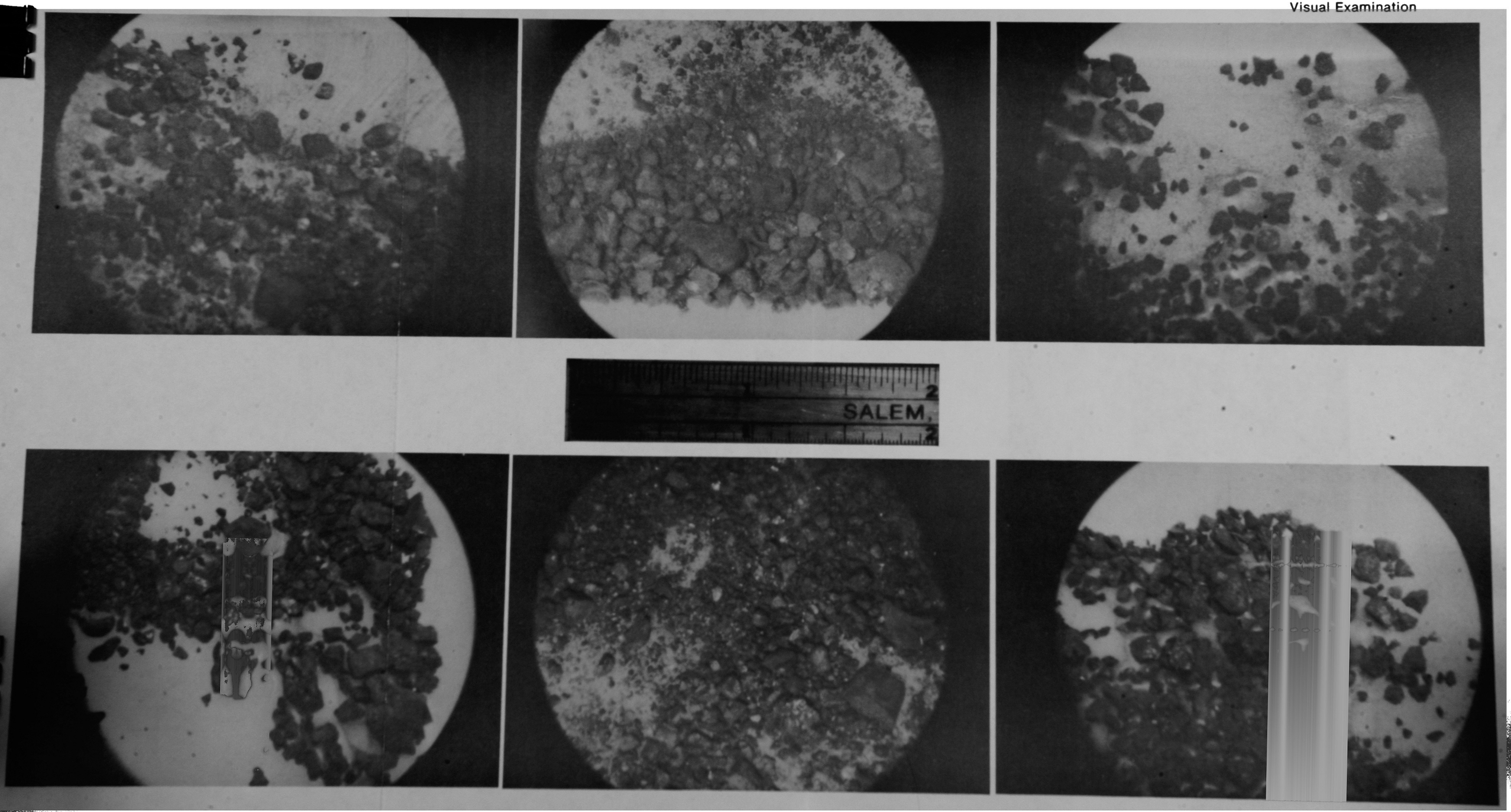

Figure 6a. Gamma-Ray Spectrum Obtained for Non-Magnetic -24 +100 Dissolved Sample

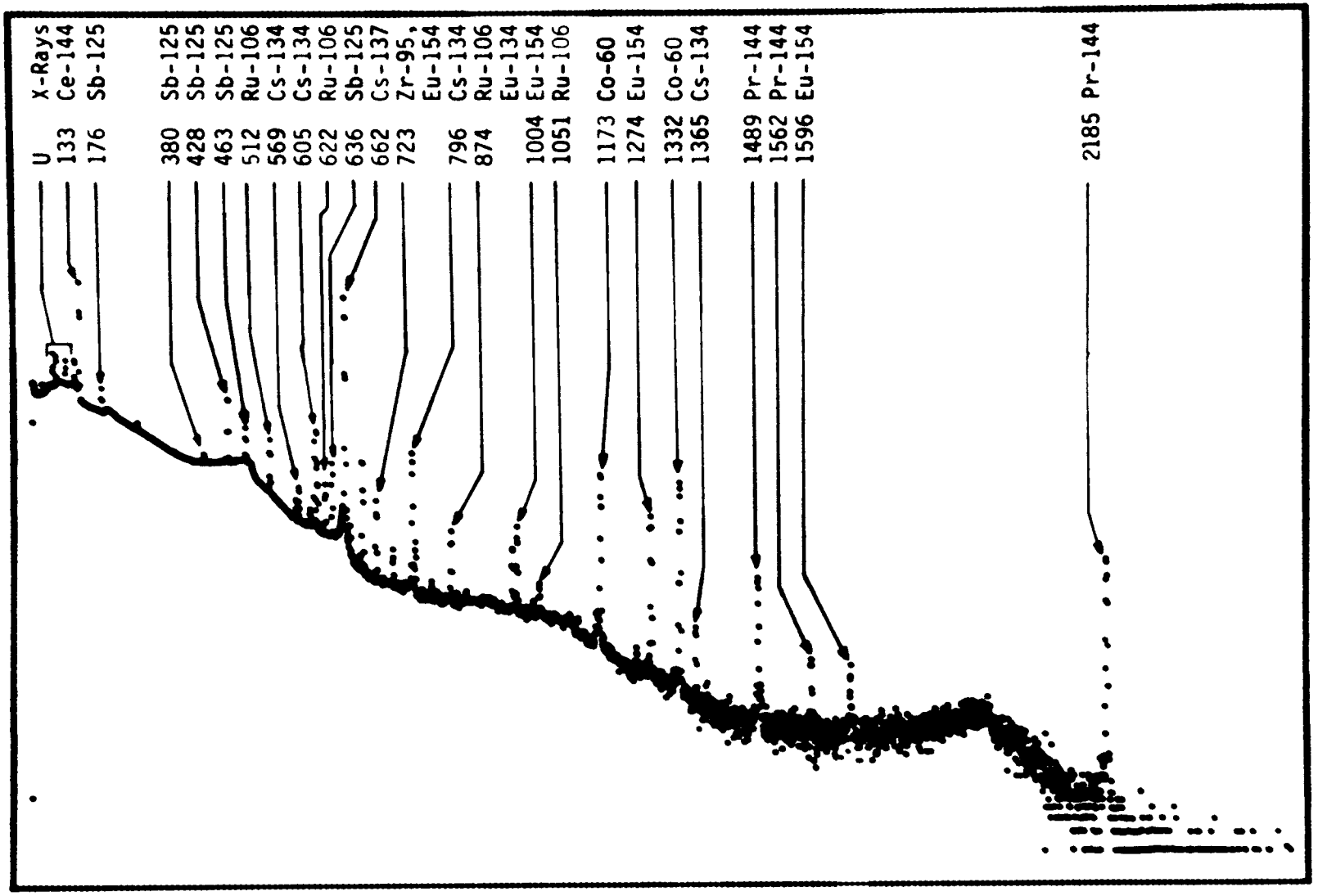

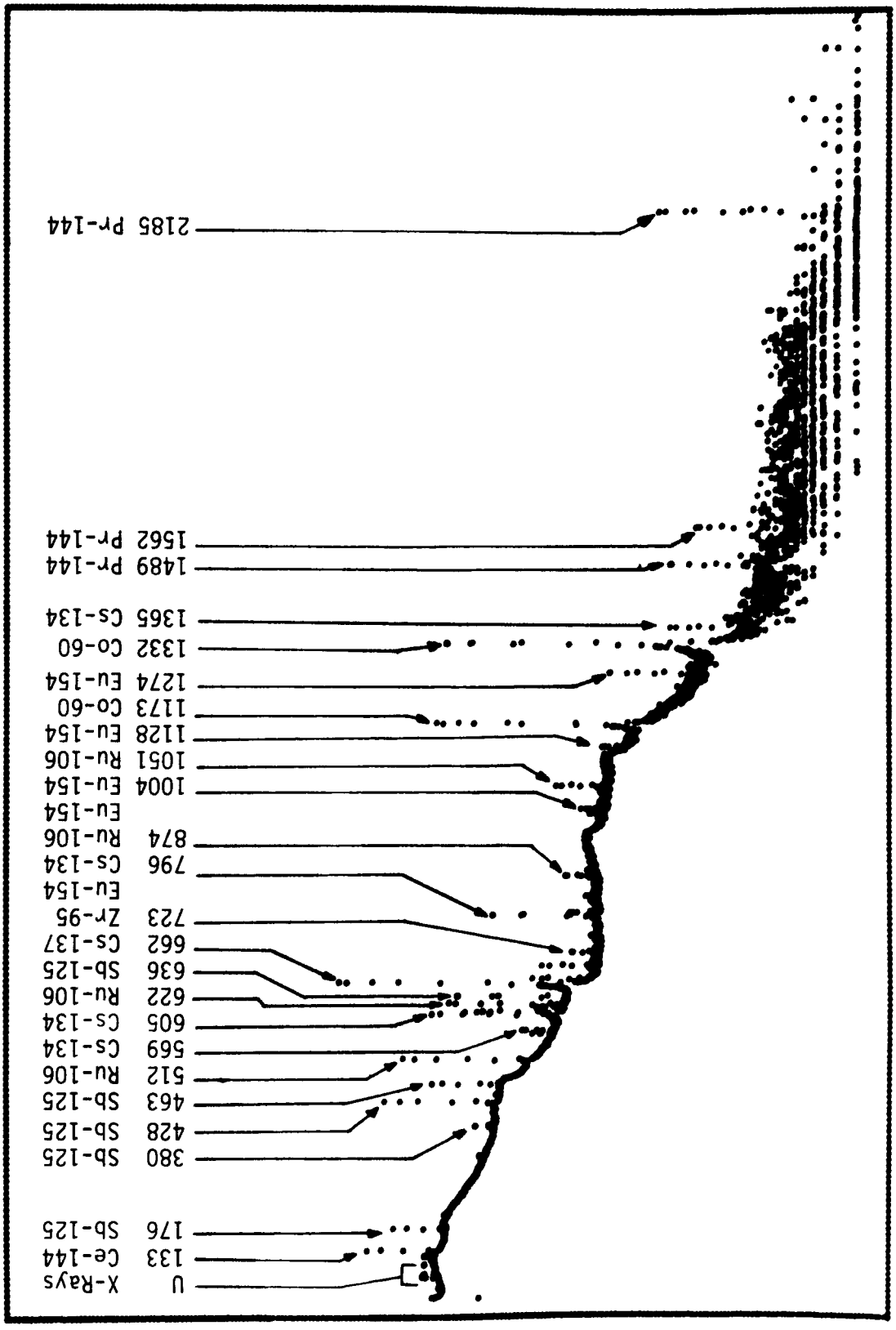

Figure 6b. Gamma-Ray Spectrum Obtained for Magnetic -24 +100 Dissolved Sample

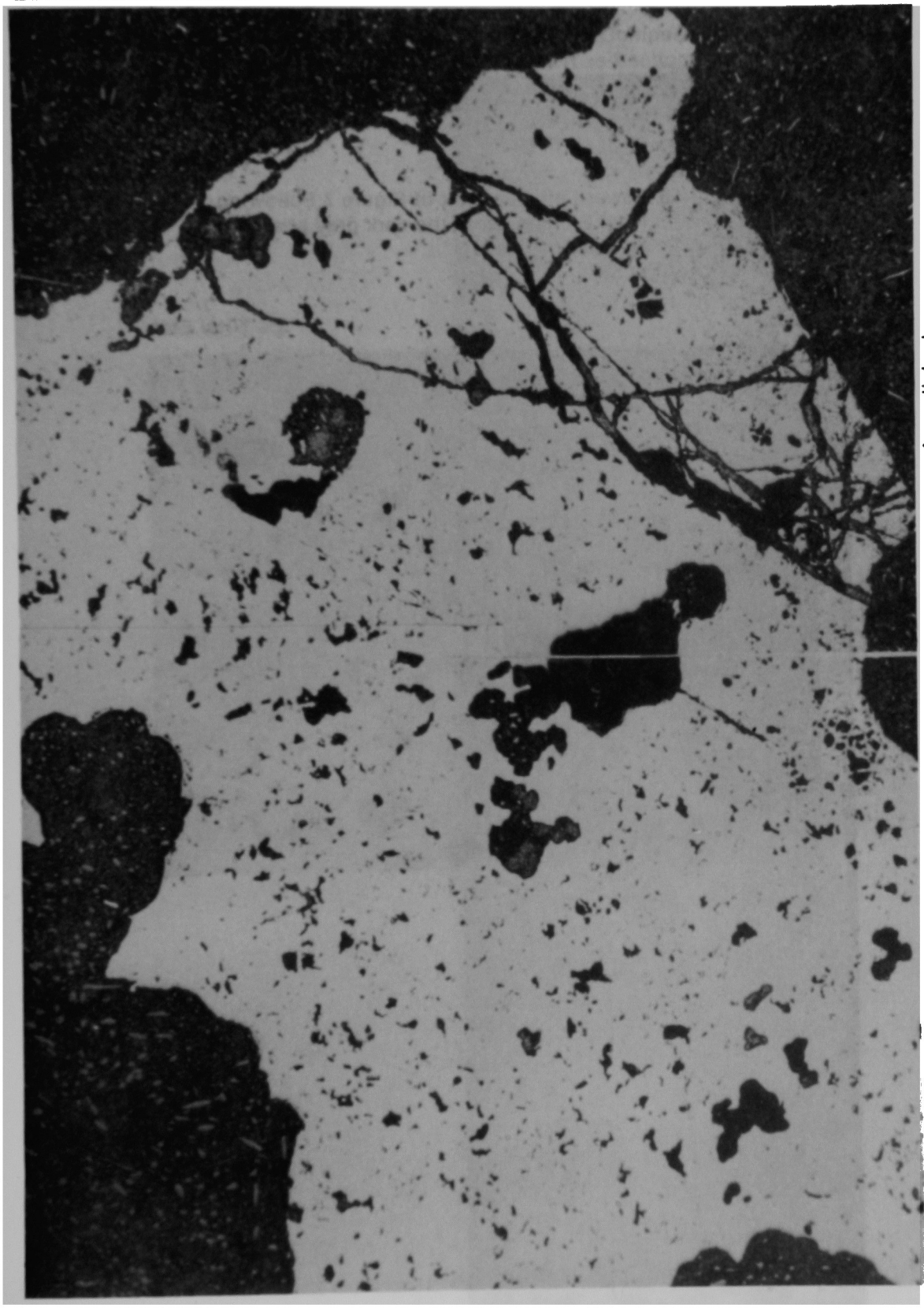

As-polished

100X

Figure 7. Photomosaic of Portion of Particle 3 Cross Section

Figure 8. Lower Left Quadrant of Figure 7 Following Nital Etching. Note the dark grey phase revealed.

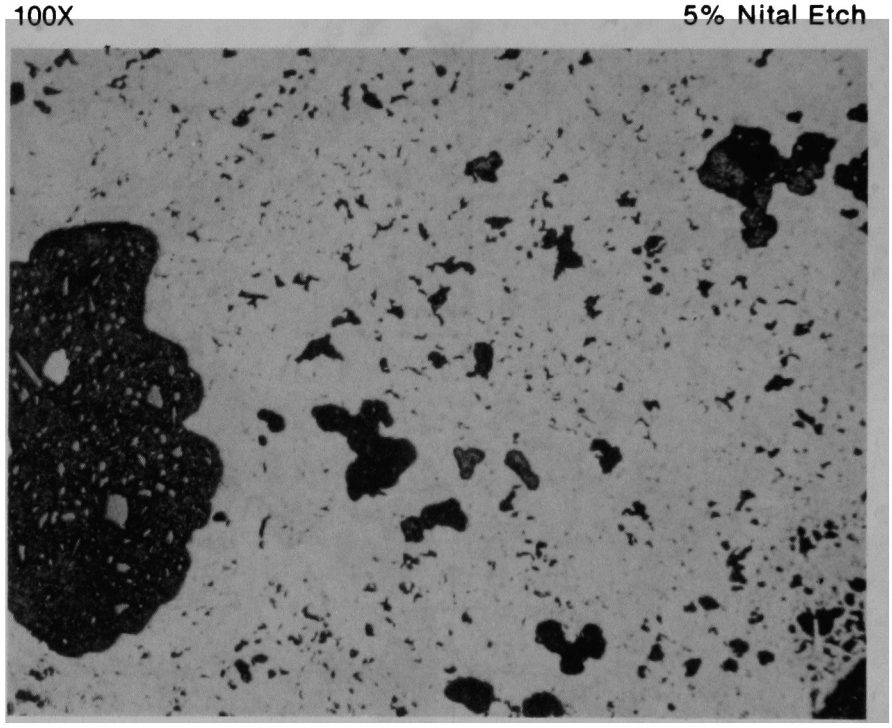

Figure 9. SEM Com[illegible] of Particle 3
Cross Sec[illegible]

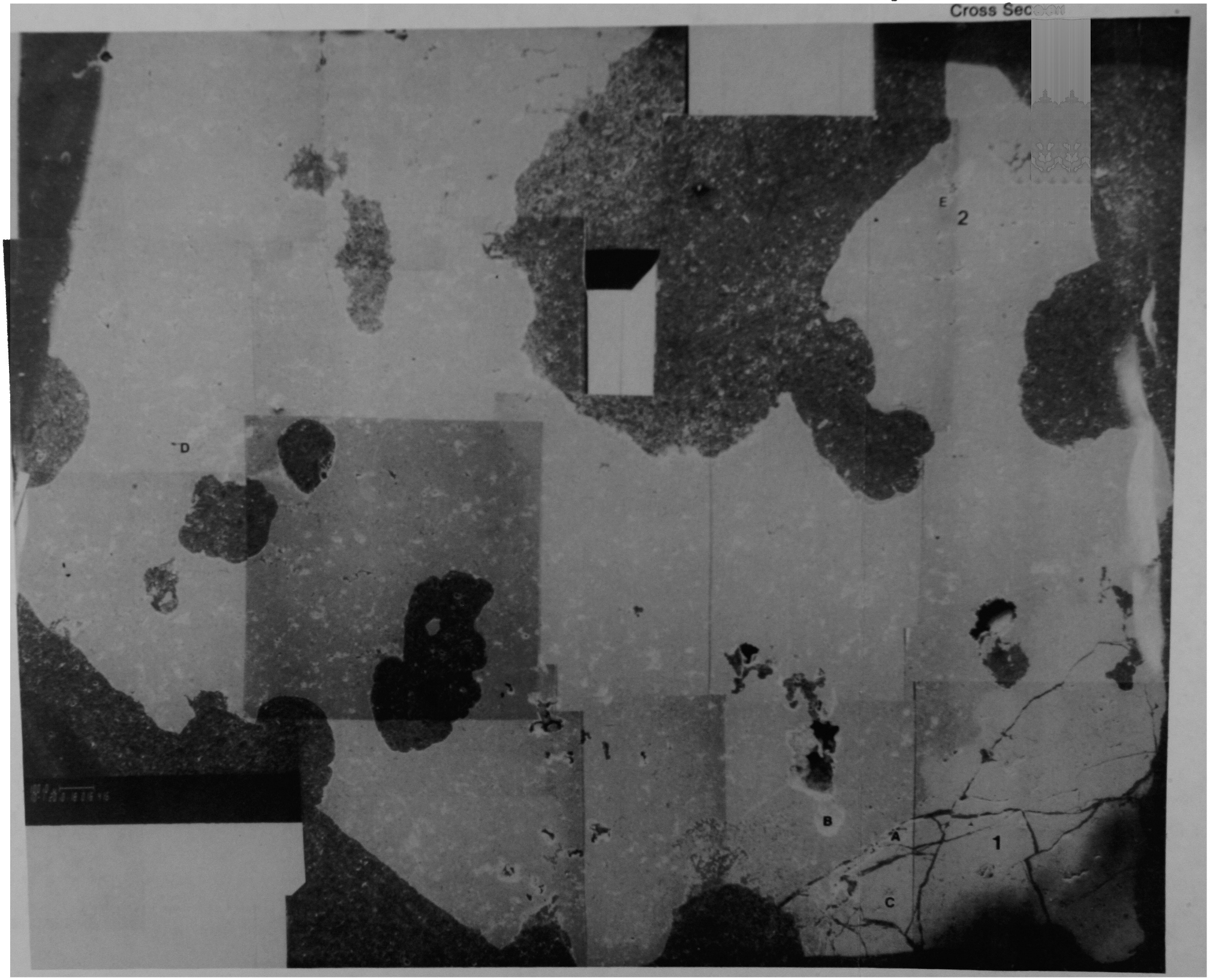

Figure 10. Detail of Area A (Figure 9). EDX spectra of Area A indicates that U and Zr are present. Specimen was Au coated.

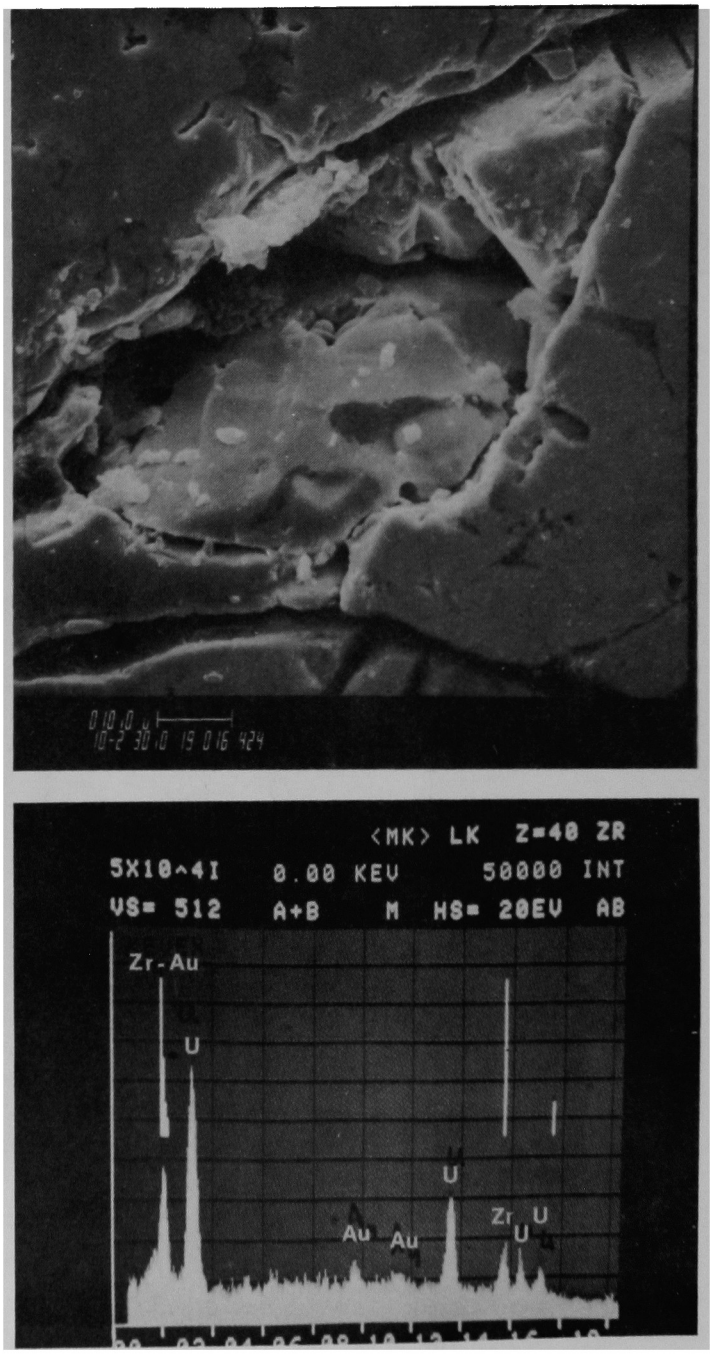

Figure 11. Detail of Area B (Figure 9). EDX spectra of Area B indicates that U and Zr are present. Specimen was Au coated.

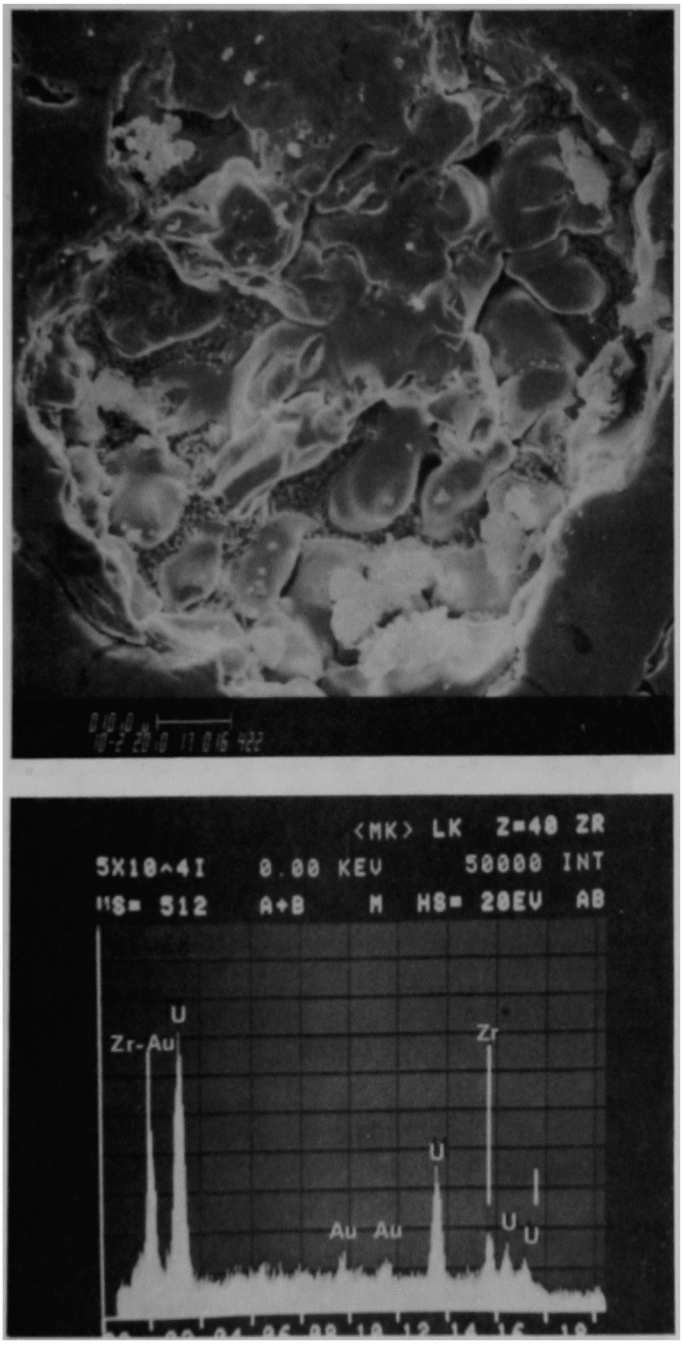

Figure 12. Detail of Area C (Figure 9).

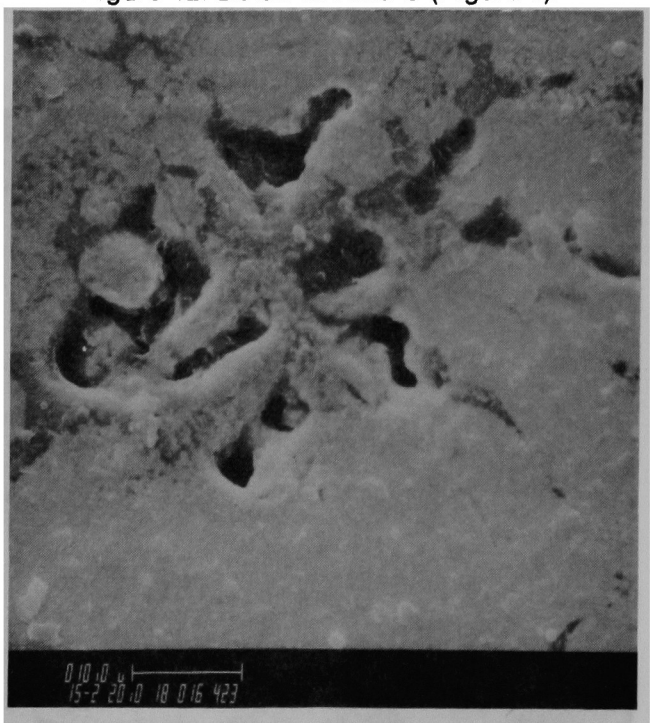

Figure 13. Detail of Area D (Figure 9).

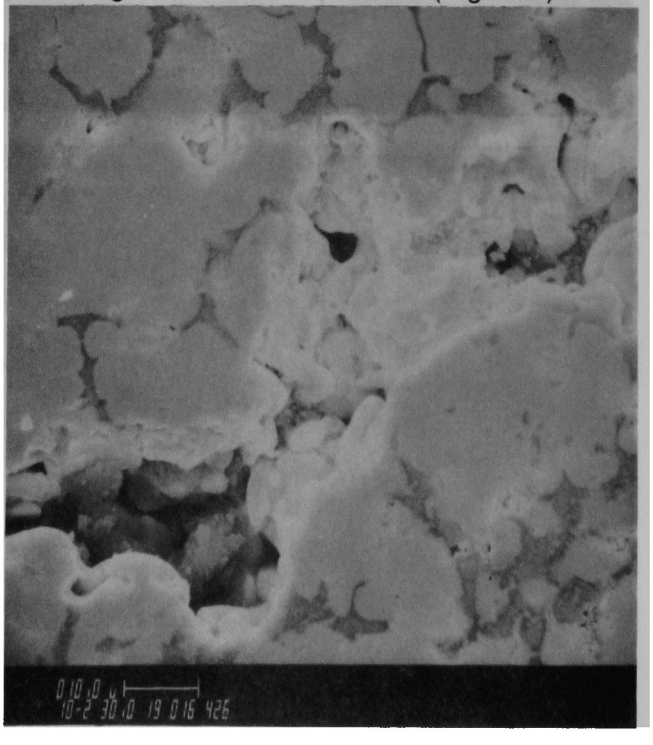

Figure 14. Detail of Area E (Figure 9). The EDX spectra is from a spot at the location indicated covering the dark phase only. U, Cr, Fe, Al, Au, and Zr are seen in the spectra. Specimen is Au coated.

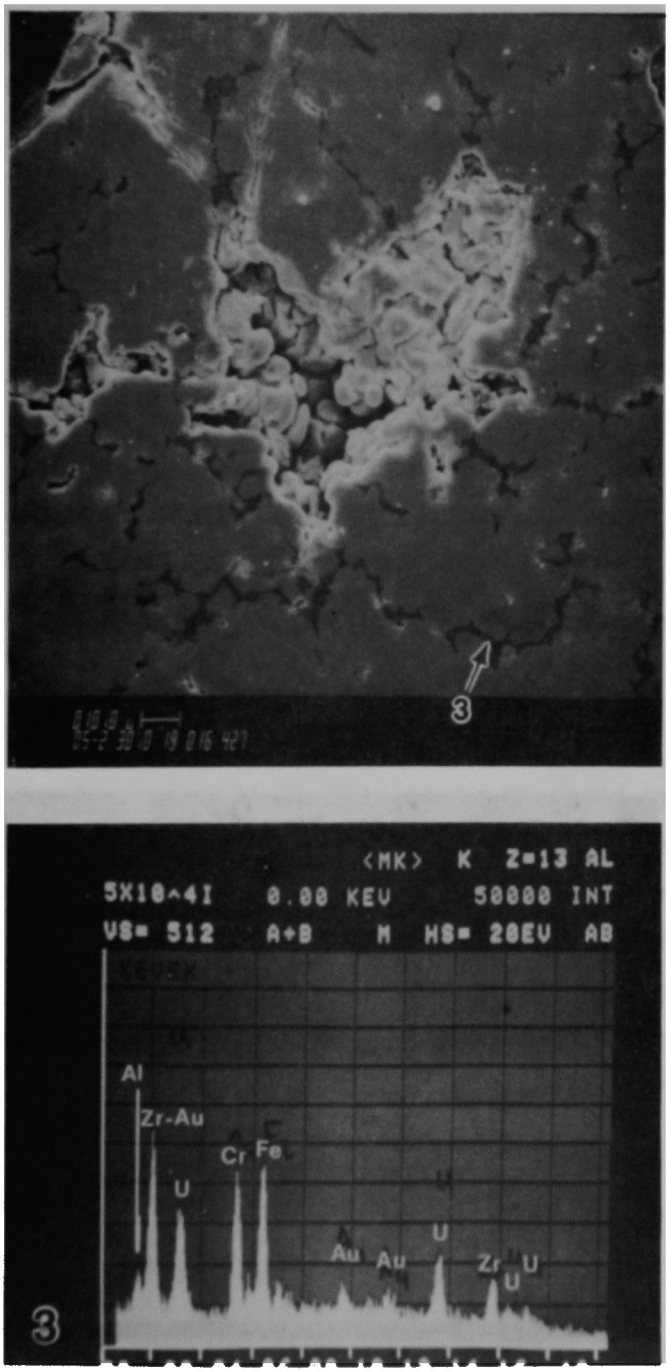

Figure 15. EDX Spectra of Area 1. U, Zr, and Au are present. Sample was Au coated.

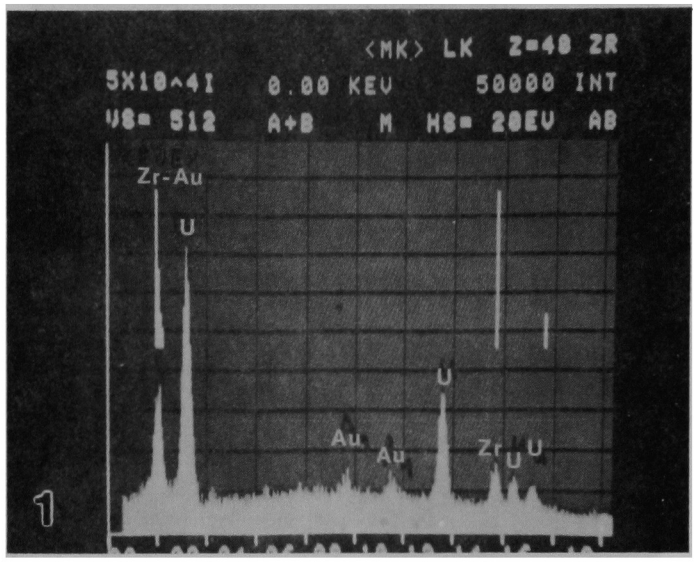

Figure 16. EDX Spectra of Area 2. U, Zr, and Au are present. Sample was Au coated.

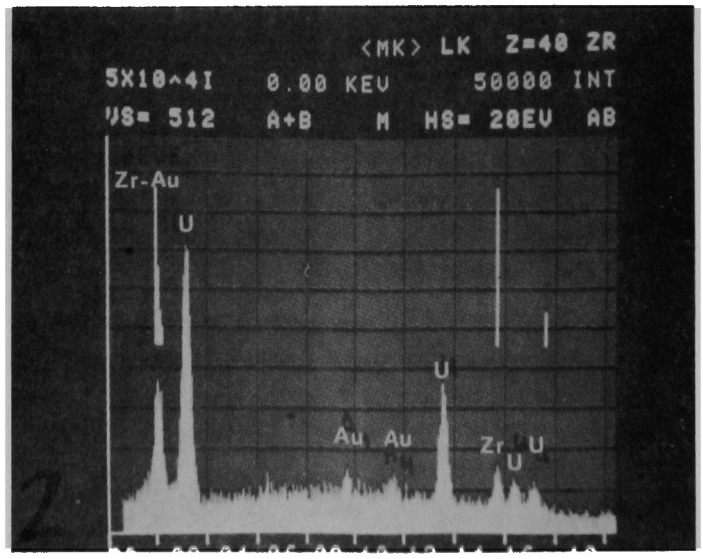

3. DISCUSSION

The discussion section will attempt to indicate the significance of key results presented in Section 2. The topics selected for discussion include the nature and amount of reaction product present and the significance of the radionuclide particle size, magnetic and elemental distributions.

3.1 Sample Composition

The sample was observed to be composed of at least four distinct types of particles. These were characterized based on visual examination as:

A. Rounded, rock-like particles with surface porosity visible. These particles often have a brown coloration.

B. Rounded, rock-like particles with little surface porosity and a much darker, almost black, glazed appearance.

C. Small particles which were from identifiable components such as fuel pellets or cladding.

D. Particles which show a composite structure of both a and c or b and c.

Type A particles represented a substantial percentage (up to 1/3) of the coarse particles examined visually. This is represented by particles 2 and 3 (see Section 2.7). Type B, C, and D particles are represented by particles 6, 4, and 1, respectively. These observations are based primarily on the visual examination but are supported by immersion density results of the six coarse particles, and the metallographic/SEM/EDS examination performed on particle 3. The rock-like particles appear to be some type of solid solution and/or reaction product formed at high temperature by combination of two or more core components such as UO_2 fuel cladding and structural alloy (stainless steel or Inconel components).

As a simple internal check on density, particles 2, 3, and 6 were treated as a simple mixture of UO_2, ZrO_2, and stainless steel in the ratios obtained during elemental examination of the dissolved bulk samples (Table 6). For purposes of the calculation, the elemental results from the coarse (+10) size fractions from the magnetic and non-magnetic samples were used to establish a range and to compare with the coarse particle immersion density measurements. This resulted in mixtures with weight fractions of:

1. Non-magnetic

   UO_2 - 0.84

   ZrO_2 - 0.14

   SS - 0.02

2. Magnetic

   UO_2 - 0.58

   ZrO_2 - 0.12

   SS - 0.30

Specific gravity values of 10.14, 5.6 and 7.9 were used for UO_2, ZrO_2, and stainless steel, respectively. The 10.14 value for UO_2 was calculated based on 92.5% theoretical density. This value was obtained from the as-built design and material characteristics of the TMI-2 core. This yielded composite densities of 9.0 g/cc for the coarse non-magnetic and 8.6 g/cc for the coarse magnetic fractions. The matrix densities calculated for particles 2, 3 and 6 (probable reaction product) are 7.5, 8.5, and 9.0 g/cc (Table 10), respectively. Note that these values are quite close to the calculated density range of the hypothetical mixture. This is also supported by the results of the metallographic/SEM/EDS examination given in Section 2.7.4. These results indicate that particle 3 contains at least three phases, contains considerable internal porosity, and is composed of U and Zr (major)

and Fe, Cr, and Al (minor). The amount of O present was not measured by either the elemental analysis techniques or the EDS examination. These results suggest that particle 3 formed by rapid solidification from a high temperature melt. Porosity probably resulted from trapped gaseous or vapor phases during solidification or shrinkage porosity following solidification. Probable high temperature exposure is also indicated by the Cs-137 data given in Table 12. Cs and Cs compounds are known to be volatile at high temperature and migration away from a localized high temperature area would be expected. The Pr-144 activity indicates that a large inventory of UO_2 is present in particles 2, 3, and 6. However, the Cs-137 activity is depressed, particularly for particle 6, when compared to particle 4. These results indicate high temperature exposure for particles 2, 3, and 6. The change in Cs-137 inventory for these particles may be related to time at temperature. Therefore, based on these results, particle 6 would have received the highest time/temperature exposure.

Particle 4 is apparently unreacted fuel as indicated by the visual and gamma scan results. This particle has a matrix density of 10.0 g/cc compared to a value of 10.14 g/cc for an as-fabricated fuel pellet. The gamma scan results given in Table 12 indicate that particle 4 has the highest Cs-137 inventory (2,530 microCuries/gram) and nearly the highest Pr-144 inventory (4,070 microCuries/gram). Both of these results would be expected for material composed of irradiated UO_2 which apparently saw a lower local peak time/temperature than particles 2, 3, or 6.

The percent open porosity value calculated for particle 4 (12.6%) appears high based on immersion density results performed in the LRC hot cells on numerous post-irradiation fuel pellet fragments. A more realistic value based on the above work is about 0.5%. The value calculated for percent open porosity is primarily dependent on saturated weight. The saturated weight is the sample weight obtained following removal from the water. Excess surface water on the sample is removed by absorption on a paper

towel. This step is technique dependent and it is not difficult to leave some surface water present on the sample which results in a high value of percent open porosity.

Particle 1 is composed of about 25% material similar to particles 2, 3, and 6 with Zr/ZrO_2 estimated to be the probable remaining material. This assessment is based on the ratio of Pr-144 of particle 1 to the average Pr-144 activity for particles 2, 3, and 6. The calculated matrix density of particle 1 is 4.6 g/cc. This is significantly less than the density of ZrO_2 (5.6 g/cc) or Zircaloy (6.5 g/cc). If the closed porosity of this particle is actually approximately 25-35%, this would put the corrected immersion density value in the range expected (5.6 - 6.4 g/cc). However, this level of closed porosity seems high for partially oxidized cladding. Therefore, the low immersion density value of particle 1 cannot be easily explained based on the data available.

A materials summary of the as-built TMI-2 active core region is given in Table 14. The as-built active core region contains about 94.5 w/o UO_2 + Zr-4 and approximately 2.3 w/o stainless steel + Inconel. The U/Zr ratio for the active core regions is 3.6. This indicates that the normalized whole sample data given in Table 7 is close to the average as-built active core elemental distribution, but with a higher ratio of U to Zr (approximately 5.9). The total of Ni, Cr, and Fe is about 1.3 w/o higher than the as-built active core.

The weighted averages of the elemental results presented in Table 7 indicate that close to 97% of the dissolved sample is U and Zr. This does not include elements not measured, such as O, which would also be expected to be present. This material is probably present as UO_2, Zr-4, ZrO_2, (U, Zr, O alloy) and alpha-Zr(O). The probable origin of this fraction of the sample is fuel rods. Most of the remaining material is Fe and Ni. This material is probably present as Fe, Ni(Cr) alloys or complex oxides. The probable

origin of this material is stainless steel and Inconel from the fuel and control assemblies. Other elements including Ag, Sn, Al, and In are present in the sample in very small amounts. These elements are apparently from control rods, APSRS, burnable poison assemblies, and Zr-4 cladding.

A comparison was made between a weighted average of the individual particle matrix densities given in Table 10 and the bulk density of the entire sample (4.2 g/cc) given in Section 2.1.5. If it is assumed that the total sample is approximated by the weight fractions of the individual particles (excluding particle 5), the weighted average matrix density obtained is 8.4 g/cc. It is expected that the packing fraction for this type of bulk density measurement is in the range of 0.5 to 0.6. Therefore, the bed density expected should be in the range of 4.2 to 5.0 g/cc. The value obtained (4.2 g/cc) is on the lower end of this range.

Approximately 8.5% of the sample is magnetic. As expected, this material contains a higher percentage (about 23 w/o) of Fe, Cr, and Ni and consequently less U and Zr. Also, this fraction contains approximately 2 w/o Ag which indicates that the Ag may be associated in some way with stainless steel. This is reasonable because control rod cladding material is stainless steel and Ag easily alloys with stainless steel.

The only as-built magnetic materials in the core region are from components fabricated from cast stainless steel such as the upper and lower fuel assembly end fittings. However, these components are not in the active core region. Other types of 300 grade stainless steels can become magnetic through certain heat treatments which do not retain austenite at room temperature. This results from any high temperature exposure near the melting point of stainless steel and subsequent slow cooling.

Recent work at Sandia (Reference 1) have shown that the outer reaction layer formed during high temperature steam oxidation of stainless steel is

primarily magnetite. The inner layer is a spinel structure (Fe and Cr oxides). Earlier work performed at GE-NMPO by White and Fuji (References 2 and 3) also identified the formation of magnetite and spinel. In addition, the crud which is present in a normal core is magnetic. The magnetic separation removes the ferrite and magnetite rich materials. Therefore, the possible sources of magnetic material are adequate to account for the magnetic material seen in the debris sample. The coarser magnetic material probably resulted from sources such as steam oxidized or ferrite transformed stainless steel cladding; however, the high percentage of magnetic pan fines is probably due to crud that was deposited on the core debris. The crud was probably only loosely adherent and was, therefore, partially removed during sieving.

3.2 Radionuclide Distribution

A comparison of the radionuclide results obtained is given in Table 15. The calculated core inventory of selected radionuclides based on the ORIGEN, LOR-2, CINDER-10 and RIBD computer codes corrected to November 11, 1983, is given in Table 16. The calculated range (in percent) of selected radionuclides retained is given in Table 17. The data compiled shows that large variations exist in the specific fission product activities for the size fractions, individual particles, and residue.

The fission product data for the individual particles show some interesting results when compared to the calculated specific activities given in Table 16. The range of percent retained fission products for the individual particles is given in Table 18. None of the code calculations used explain the high levels of some of the fission products obtained. However, LOR-2 calculates the most reasonable results based on the criteria that none of the numbers significantly exceed 100%. The LOR-2 results produce the minimum values of retained fission products for Ru-106, Cs-137, Sb-125, and Eu-154 and the maximum value for Ce-144. Therefore, for particle 4 this results in approximately 100% retained for Ru-106, about 30% retained for

Cs-137 and 80-90% retained for Ce-144, Sb-125, and Eu-154. Particle 6 showed similar results except that practically no Cs-137 was retained. Particles 2 and 3 results were similar (to each other), however, neither retained much Ru-106 and particle 3 retained little Sb-125. Based on Ce-144 and Eu-154 activities, particles 2, 3, 4, and 6 contain mostly fuel. The depletion of Ru-106 for particles 2 and 3 is not understood. Particle 1 probably contains less fuel and more Zr and/or stainless steel materials.

The undissolved residue has the highest specific Ru-106 activity by a factor of approximately 2.5. This indicates that the chemical dissolution process was either unable to dissolve particles containing the highest Ru-106 activity or approximately one-third of the Ru-106 inventory from the total sample remained undissolved and concentrated in the residue. The Ru-106 content in the residue is included in the weighted average value for the whole sample given in Table 5. A large amount of Ce-144 is also retained in the residue.

The core inventory results based on ORIGEN-2 were not listed. However, if results from this code were used, the Ru-106, Cs-137, and Ce-144 % retained would be reduced slightly in Tables 17 and 18. The Sb-125 and Eu-154 values would be reduced by more than a factor of two. It is recommended that future comparisons be referenced to a selected set of core inventory results. It should also be noted that all code calculations discussed are based on core average conditions. However, during power operation flux peaking of at least a factor of two occurs in local areas, and, therefore, this effect could show up in individual particle results.

3.3 Particle Size Distribution

A log-log plot of the particle size distribution is given in Figure 17 and compared to the EG&G data from Reference 4. The H8A results show smaller particle sizes than the EG&G results over the entire range, however, below

200 microns the difference is quite significant. It is suggested that the actual differences are due primarily to:

1. A difference in particle sizing technique. B&W used dry sieving in a stack which was shaken for one hour using a motor driven shaker. However, EG&G used liquid freon to wash the samples through the screens with manual shaking only.

2. The vigorous screening used by B&W caused loosely held surface deposits to come off larger particles, especially the orange-yellow material, believed to be iron oxides.

It is the opinion of the author that item 1 probably is responsible for most of the size differences noted. This is expected because significant energy is normally required to cause size separation of irregularly shaped fine particles during screening.

The sample loss that occurred during visual examination probably did not significantly affect the particle size distribution results. The reasons for this are summarized below.

1. The visual examination results of the material adhering to the tray indicated that all size fractions were stack rather than just fines.

2. The B&W sample contained a finer size distribution than the EG&G sample results over the entire range and the difference between the B&W and EG&G size distributions increased for the finer particles. These results would not be expected if finer particle sizes were preferentially removed. However, these results would be expected based on differences in screening techniques for the reasons given above.

3. The EG&G results indicate considerable variation in particle size distribution. The H8A sample has no greater deviation from the apparent median range than the E9A data.

4. Based on the types of sampling tools used to remove the debris samples and the nature of the debris bed, signi-

ficant variations in particle size distribution (and other results) would be expected.

The percentage of magnetic material in the pan fines is eight to ten times higher than the other size fractions as indicated in Table 2. This may indicate that a major part of the loosely held surface material on all particles is magnetic. This material may have been removed by screening or handling.

The fission product distribution as a function of size fraction (Table 4) shows large variations but significant trends of radionuclide concentration or depletion as a function of particle size are not seen. For water leachable fission products such as Cs-137, a slight depletion is seen between the +10 and (-10, +24) mesh fractions. Because the trend is not continuous over all the size fractions, the reduction for the (-10, +24) mesh fraction may not be significant. There is no indication, however, that Cs-137 was preferentially leached out of fines during residence in the TMI-2 core.

Based on the results presented in Table 1 and Figure 15, about 90 w/o of the sample contained particles greater than about 400 micron particle size and about 4 w/o of the sample was suspendible fines, i.e., less than 70-100 micron particle size. Based on 60 metric tons of rubble, this results in about 2,400 kgs of fines that might be collected in filter canisters during defueling. The EG&G results for the first set of samples indicate only about 150 kg fines calculated on the same basis. Because the differences are large, the particle size distribution results should be repeated based on a standard procedure accepted by GPUN.

Table 14. TMI-2 Active Core Region Materials Summary

	Weight (kg)
Zircaloy	23,050
304 stainless steel*	1,610
Inconel	1,210
Ag-In-Cd	2,750 ? correct
Al_2O_3-B_4C	630
Gd_2O_2-UO_2	130
ZrO_2	330
UO_2	93,130
Trace materials	110 ± 45
Total material	122,960 ± 5%
U/Zr ratio	3.6

*W/O assembly end fittings.

Table 15. Comparison of Radionuclide Results Obtained

Radionuclide	Weighted Average Whole Sample[1] (μCi/g)	Range for Non-magnetic Size Fractions[2] (μCi/g)	Range for Magnetic Size Fractions[2] (μCi/g)	Range for Individual Particles[4] (μCi/g)	Residue[1] (μCi/g)
Ru-106	422	109 - 287	225 - 1,680	73.3 - 1,650	4,090
Cs-134	56.2	41.8 - 74.2	74.1 - 101	8.54 - 127	13.3
Cs-137	1,060	826 - 1,370	1,330 - 1,680	166 - 2,530	232
Ce-144	3,650	3,070 - 3,820	1,400 - 3,420	911 - 4,160	2,500
Sb-125	122	66.2 - 479	157 - 1,070	17.1 - 148	88
Eu-154	41	ND[3] - 45	18 - 40	10.6 - 57.7	ND

[1] From Table 5.

[2] From Table 4.

[3] ND = not detected.

[4] Data from Table 12. Particle 5 not included. See Section 2.7.3. Pr-144 activity used rather than Ce-144 due to large self-attenuation for Ce-144.

Table 16. Calculated Core Inventory of Selected Radionuclides[1]

Radionuclide	T 1/2		ORIGEN[2] 3/28/79	ORIGEN[2] 11/11/83	LOR-2 3/28/79	LOR-2 11/11/83	CINDER-10 3/28/79	CINDER-10 11/11/83	RIBD 3/28/79	RIBD 11/11/83
Ru-106	369	d	3.08×10^6	1.37×10^5	3.20×10^6	1.43×10^5	2.89×10^6	1.29×10^5	2.20×10^6	9.80×10^4
Cs-134	2.062	Y	2.57×10^5	5.59×10^4	1.68×10^5	3.66×10^4	1.34×10^5	2.92×10^4	1.07×10^5	2.33×10^4
Cs-137	30.1	Y	8.14×10^5	7.33×10^5	8.45×10^5	7.61×10^5	8.40×10^5	7.57×10^5	8.45×10^5	7.61×10^5
Ce-144	284	d	2.35×10^7	4.13×10^5	2.34×10^7	4.11×10^5	2.39×10^7	4.20×10^5	2.81×10^7	4.44×10^5
Sb-125	2.7	Y	4.02×10^4	1.25×10^4	5.23×10^4	1.63×10^4	5.07×10^4	1.58×10^4	3.35×10^4	1.04×10^4
Eu-154	8.54	Y	4.09×10^3	2.82×10^3	8.30×10^3	5.73×10^3	6.80×10^3	4.70×10^3	1.67×10^3	1.15×10^3

[1] From GPUN Report TPO/TMI-043, Rev. 2, dated January 1984.

[2] Obtained from EPRI NP-2722, dated November 1982.

Table 17. Range of Specific Radionuclide Activity for Bulk Sample(1)

Radionuclide	Calculated Maximum Specific Activity(2) (microCuries/gram)		Calculated Minimum Specific Activity(2) (microCuries/gram)		Average Whole Sample Results From Table 5 (microCuries/gram)	Range of % Retained	
Ru-106	1,202	(1,536)	823.5	(1,053)	422	35-51	(27-40)
Cs-134	469.7	(600.4)	195.8	(250.3)	56.2	12-29	(9-22)
Cs-137	6,395	(8,174)	6,160	(7,874)	1,060	17	(13)
Ce-144	4,151	(5,306)	3,454	(4,415)	3,650	88-106	(69-83)
Sb-125	137	(175.1)	87.4	(111.7)	122	89-140	(70-109)
Eu-154	48	(61.4)	9.7	(12.4)	41	85-423	(67-331)

(1)Basis weight includes all UO_2, Zircaloy-4, stainless steel, and Inconel in active core (approximately 119×10^6 g). Numbers in parentheses are normalized per gram of UO_2. Basis weight is 93.1×10^6 g.

(2)Based on the data given in Table 14.

Table 18. Range of % Retained Fission Products for Individual Particles(1)

Radionuclide	Particle 1	2	3	4	6
Ru-106	13-18	5-7	5-7	104-151	107-157
Cs-134	10-25	9-21	16-37	21-51	1-3
Cs-137	12-13	11	18-19	31-32	2
Ce-144(2)	22-26	62-74	68-82	77-92	78-94
Sb-125	81-127	38-60	9-16	85-132	59-93
Eu-154	22-109	89-440	94-466	79-389	85-419

(1)All particles except 1 calculated per gram UO_2.

(2)Pr-144 peak used.

Figure 17. Plot of Particle Size (D) Versus Weight Percent Less Than D for the H8A Sample Subjected to Particle Sizing. Other distribution results given are from EG&G report (Reference 4).

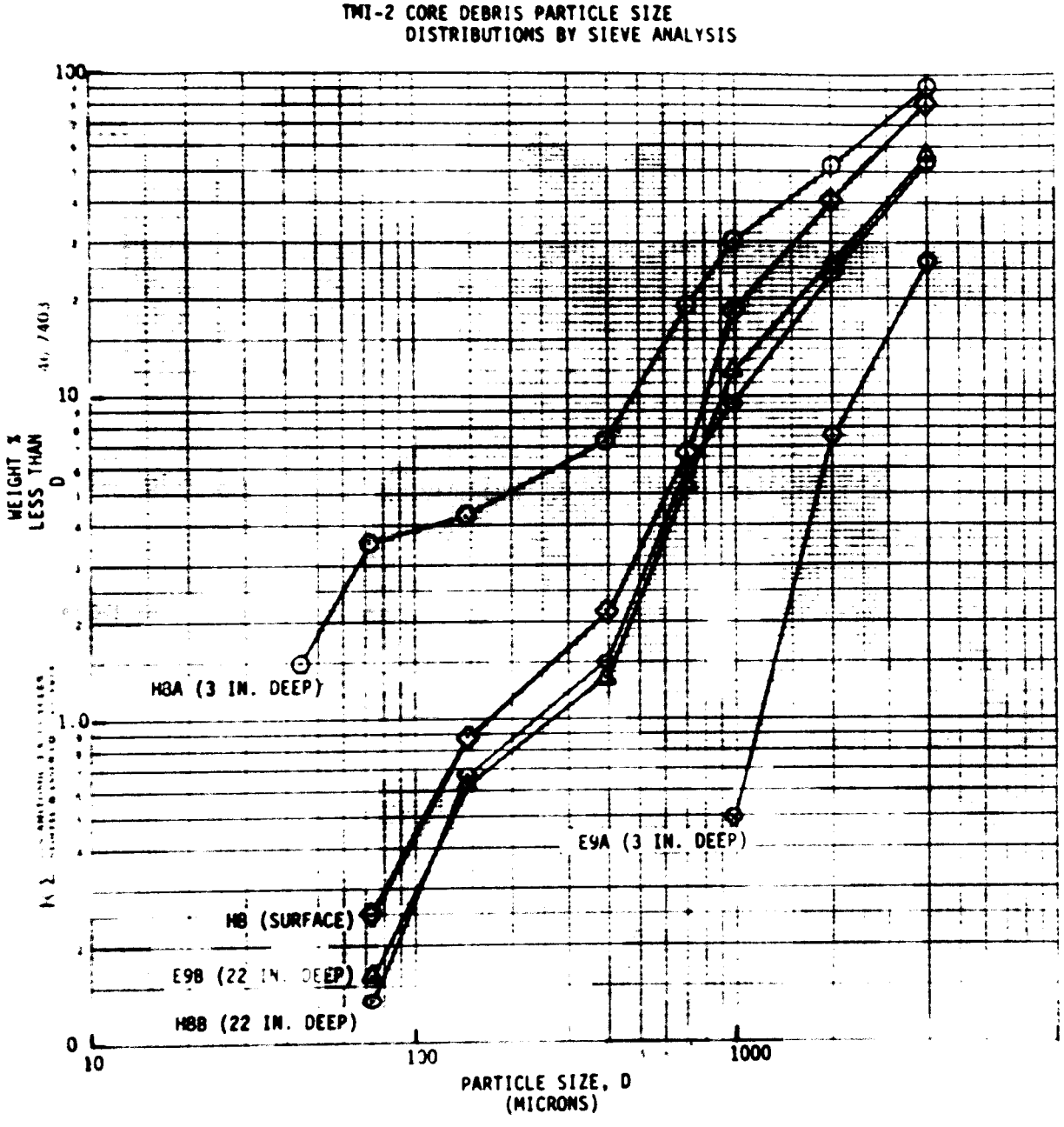

4. CONCLUSIONS

1. The H8A sample material was determined to be loose, free flowing and granular; to have a bulk density of approximately 4.2 g/cc; and consisted of at least four different categories of material.

2. Approximately 8.5 w/o of the sample was magnetic and contains higher amounts of Fe, Ni, Cr, and Ag.

3. Particle size distribution in the sample ranged from large particles approaching 1 cm to very fine material <325 mesh (44 microns). The weight median size was 2 mm; 90 w/o of the material was greater than 400 microns and 4 w/o of the material was less than 100 microns.

4. A large percentage of the sample material has the appearance of some type of solid solution and/or reaction product formed at high temperature by combination of two or more core components.

5. The sample material is very resistant to chemical dissolution in strong boiling mineral acids (HF, HCl and HNO_3).

6. The undissolved residue remaining following acid treatment contained significant amounts of U, Zr, Fe, and Cr and the bulk of the Ru-106 inventory.

7. The bulk sample radionuclide results indicate that 13% of the Cs-137, 27 to 40% of the Ru-106, and 70 to 100% of the Ce-144, Sb-125, and Eu-154 were retained.

8. Individual particles analyzed showed a wide range of % retention of radionuclides. These differences probably resulted from large compositional, density, and time/temperature TMI-2 exposure differences, superimposed on local differences in neutron fluence.

9. Most of the Curie content (about 70%) is from Ce/Pr-144 activity. Cs-137 accounts for most of the remaining Curie content (approximately 21%). Cs-137 accounts for most of the gamma activity. The total activity level for the sample was approximately 5,400 microCuries/gram on November 11, 1983 (excluding Sr-90).

10. The Cs-137 activity is depleted in all size fractions rather than preferentially depleted in fine size fractions.

11. The bulk sample was composed of 83 w/o U, 14 w/o Zr, 3 w/o Fe, and 1 w/o Ni with minor amounts of Cr, Sn, Al, In, and Ag. Elemental results varied considerably with regard to size fraction and magnetic/non-magnetic properties.

12. The metallographic/SEM/EDS examination performed on a reaction product particle (#3) indicated:

    a. Probable liquefaction and rapid cooling occurred from high temperature.

    b. Both fine and coarse internal porosity.

    c. The presence of at least three phases.

    d. U and Zr as the major elements detected in both major phases.

    e. U, Zr, Cr, Fe, and Al as the elements detected in a third minor phase present.

5. REFERENCES

1. Personal communication from D. Powers (Sandia National Laboratory) to C. S. Caldwell (B&W), August 20, 1984.

2. J. F. White, "Physico Chemical Studies of Clad UO_2 in Potential Meltdown Environments," AEC Fuels and Materials Development Progress Report 67, GEMP-1004, March 29, 1968, pp 18-22.

3. C. T. Fuji and R. A. Meussner, "High Temperature Oxidation of Iron-Chromium Binary Alloys in Water Vapor, Part 1," U.S. Naval Research Laboratory, NRL Report 5506 (1960).

4. D. W. Akers and B. A. Cook, Draft Preliminary Report, "TMI-2 Core Debris Grab Samples Analysis of First Group of Samples," EGG-TMI-6630.

APPENDIX A

Plots of Gamma-Ray Spectra Versus Length of Sample Contained in the Sampling Tool

The 49.0 inch dimension is furtherest away from the point of the sampler as seen in Figure 1.

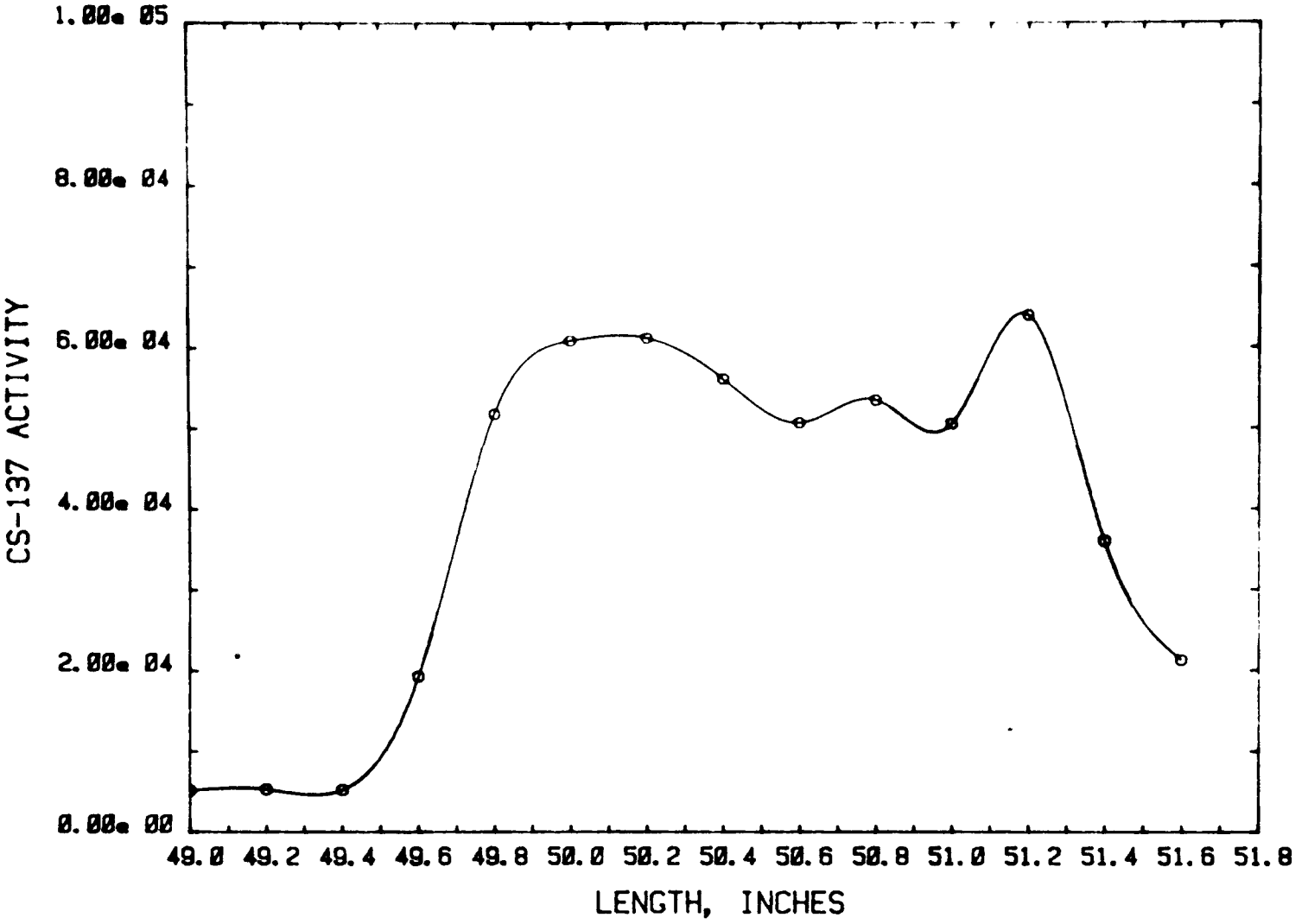

Cs-137 ACTIVITY vs. LENGTH at 0 deg.

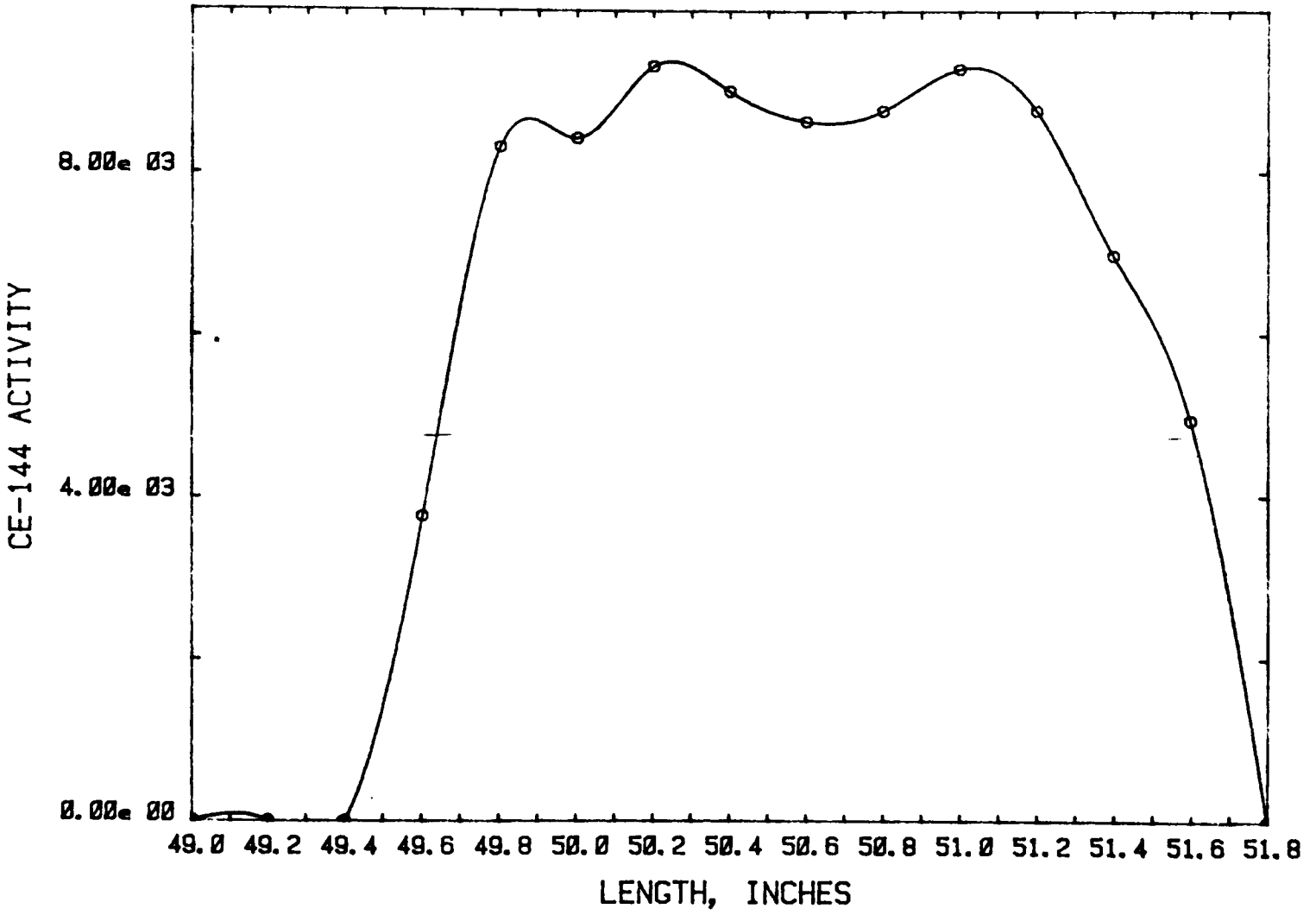

Ce-144 ACTIVITY vs. LENGTH at 0 deg.

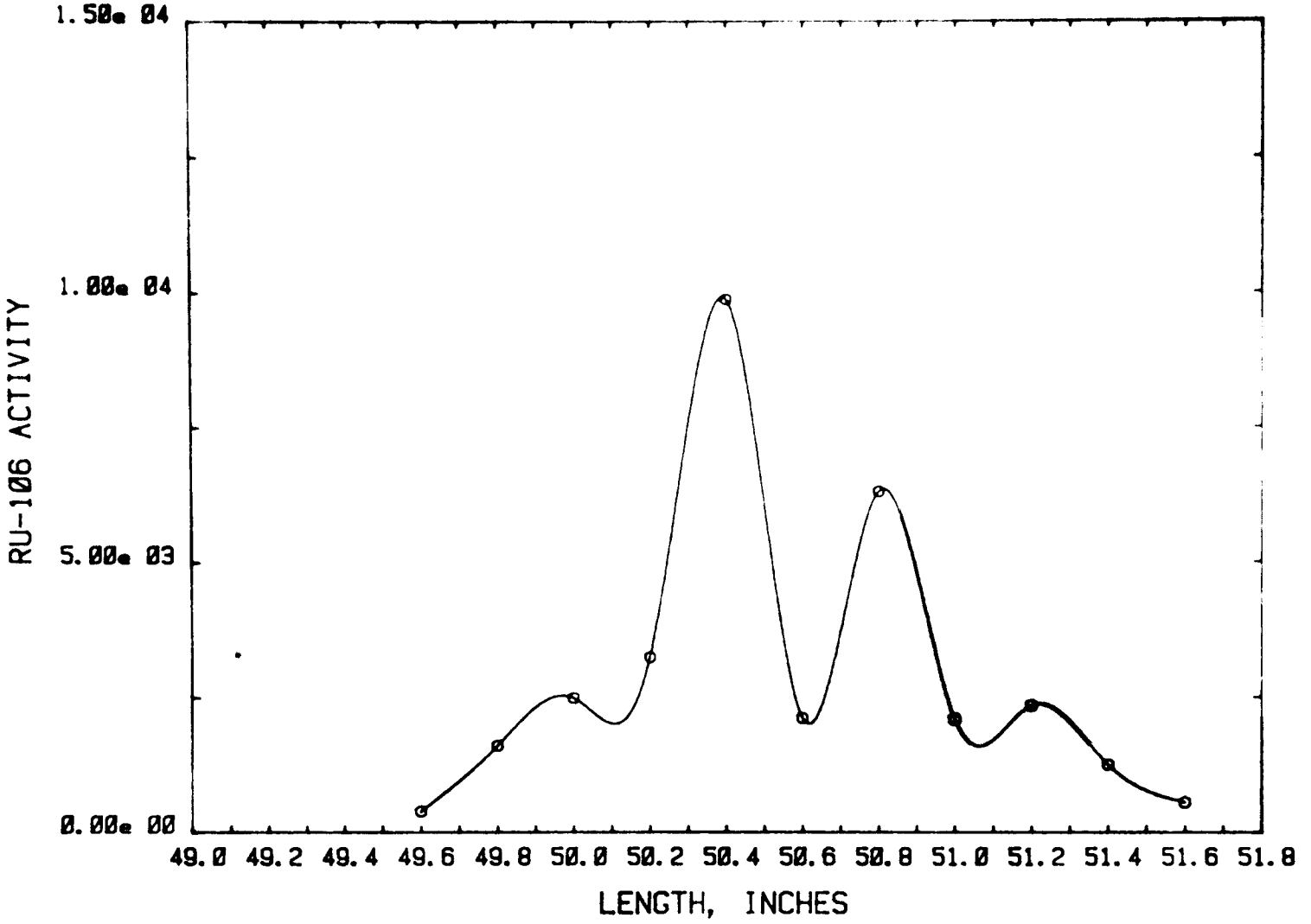

Ru-106 ACTIVITY vs. LENGTH at 0 deg.

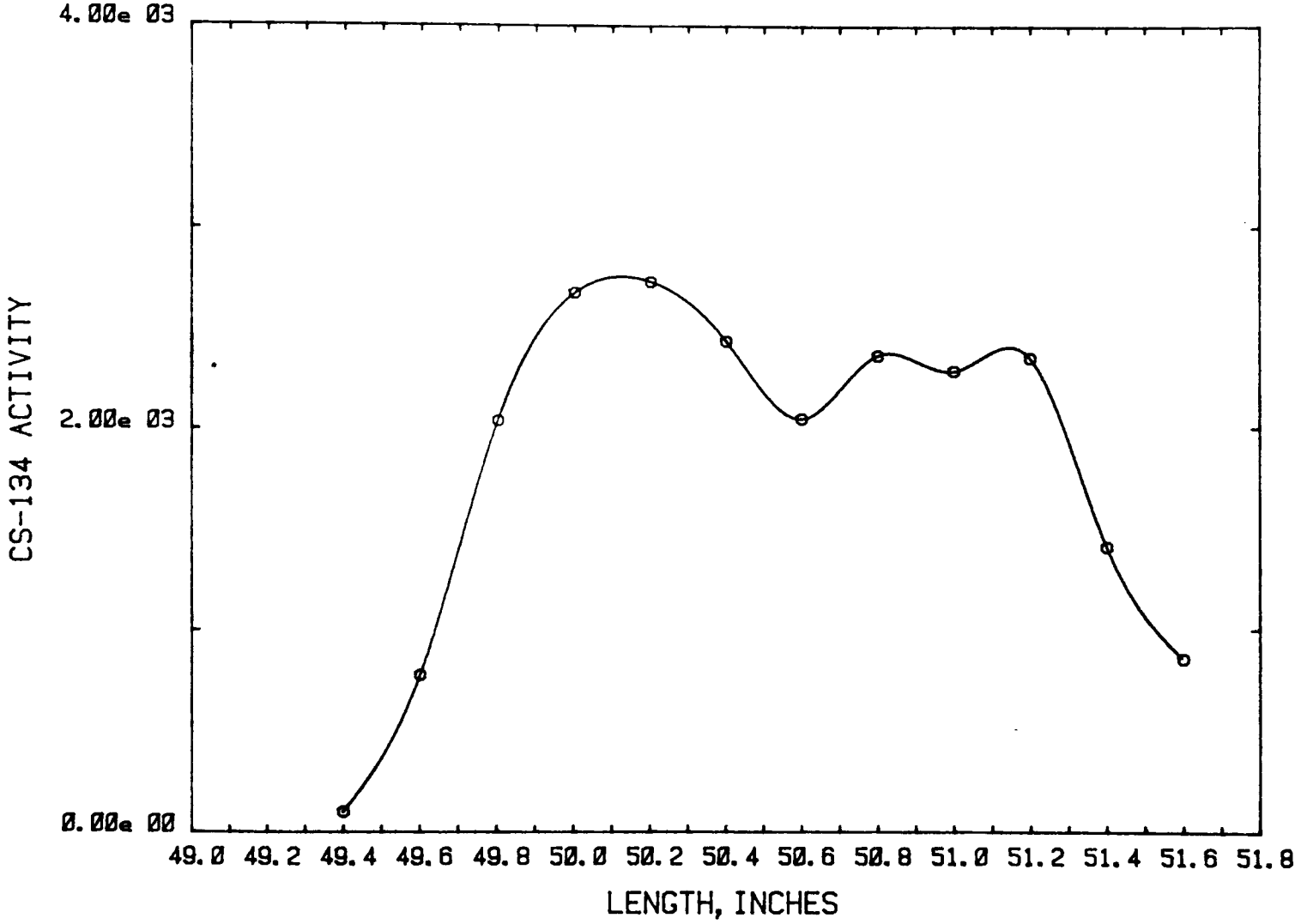

Cs-134 ACTIVITY vs. LENGTH at 0 deg.

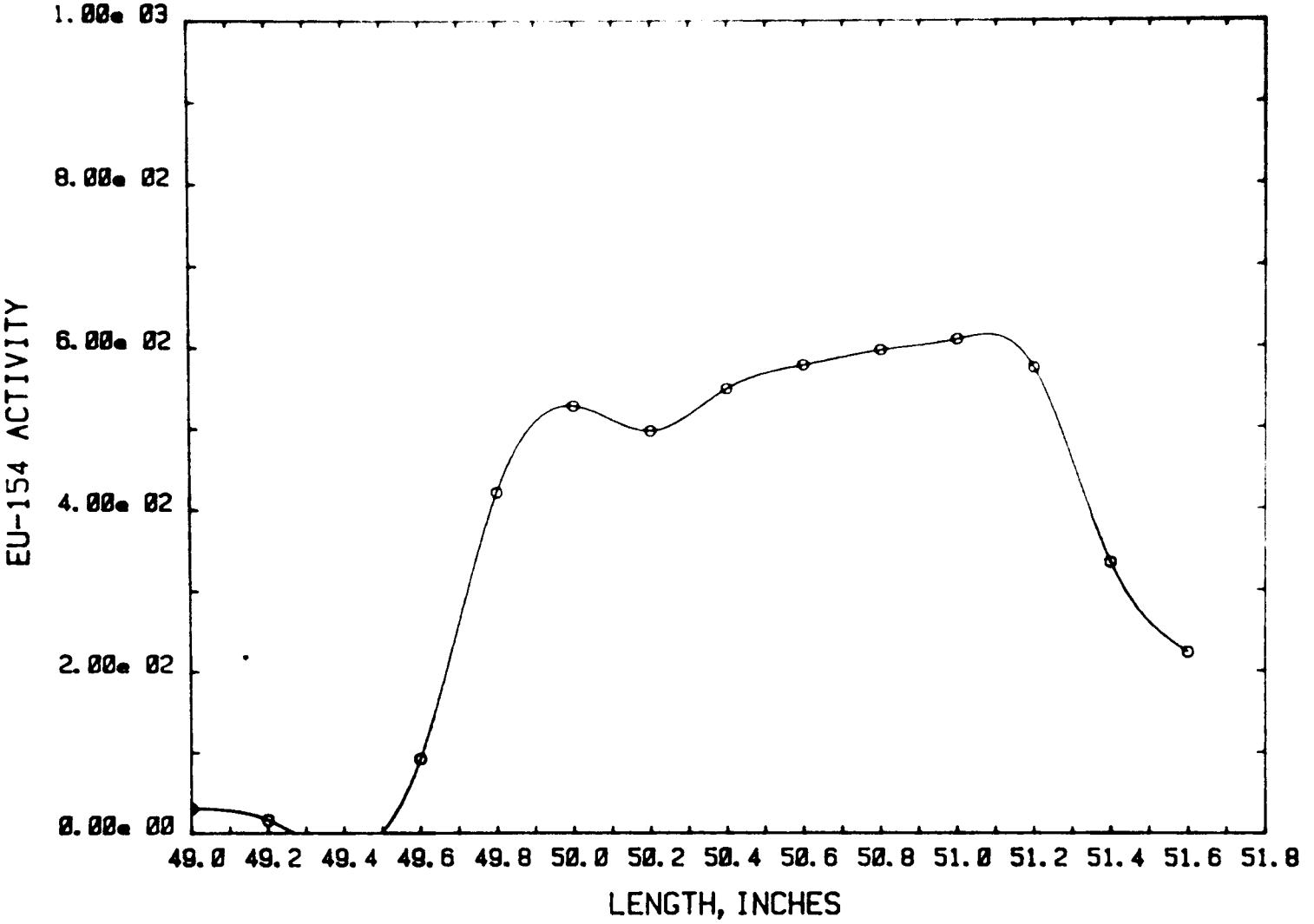

Eu-154 ACTIVITY vs. LENGTH at 0 deg.

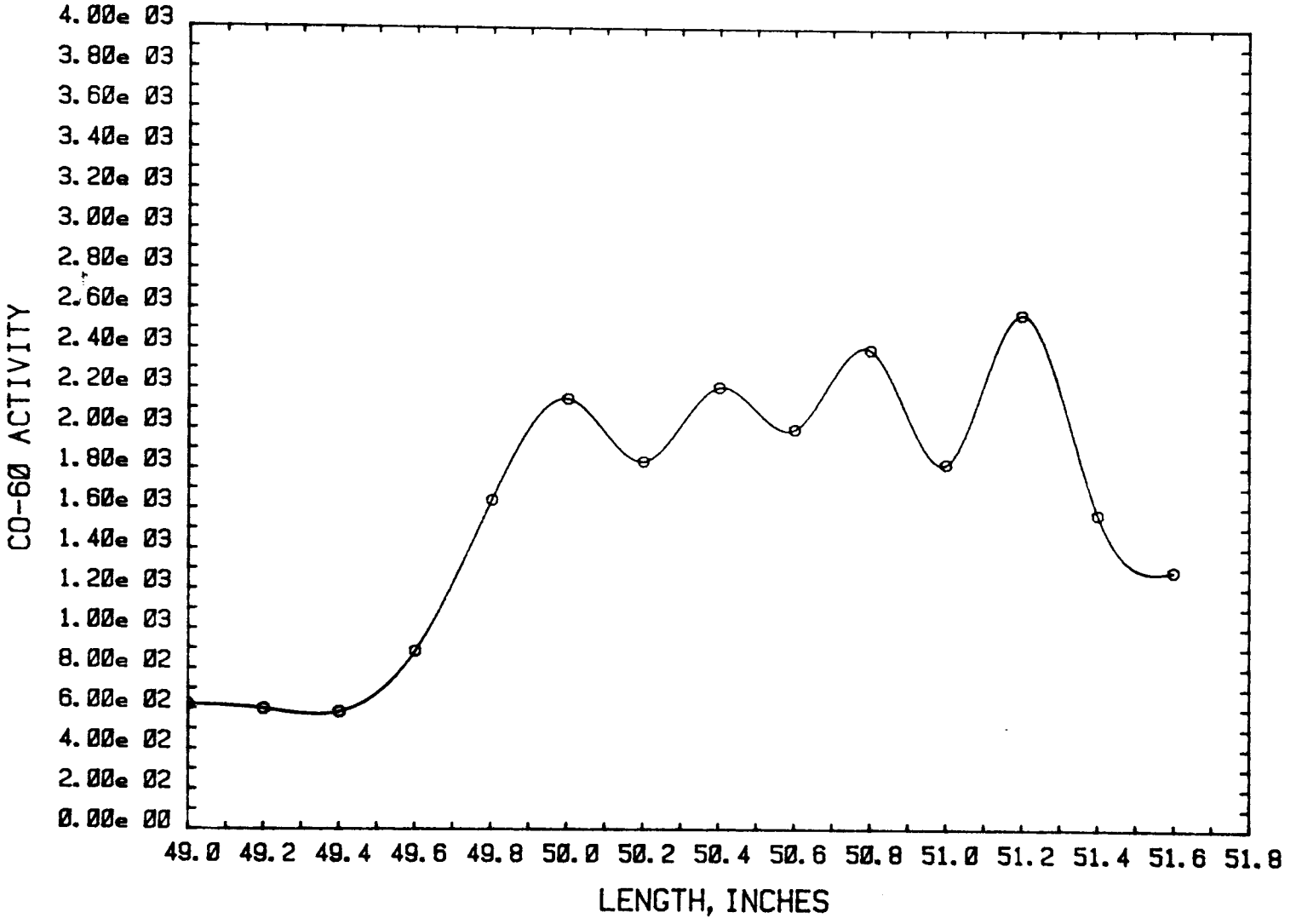

Co-60 ACTIVITY vs. LENGTH at 0 deg.

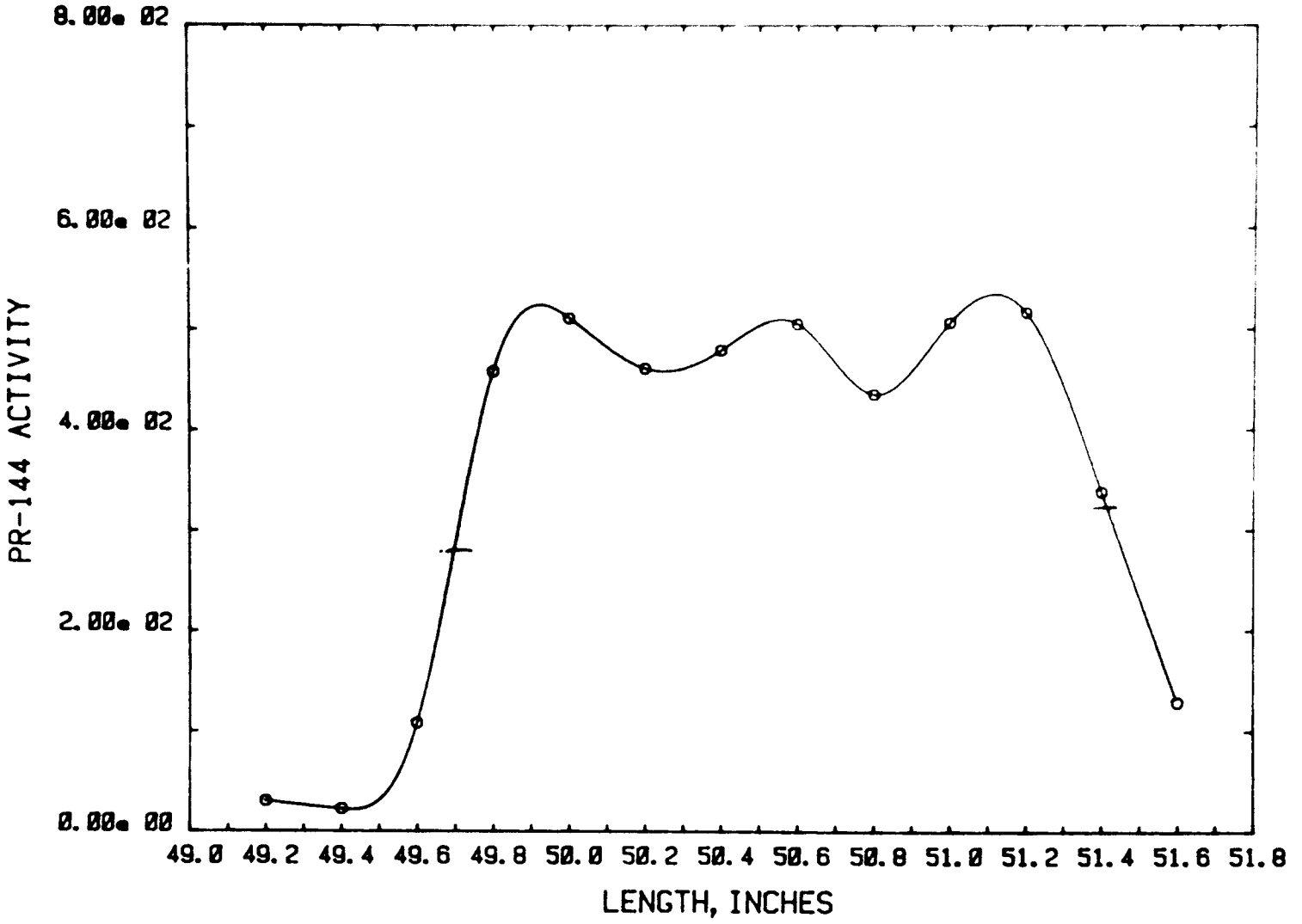

Pr-144 ACTIVITY vs. LENGTH at 0 deg.

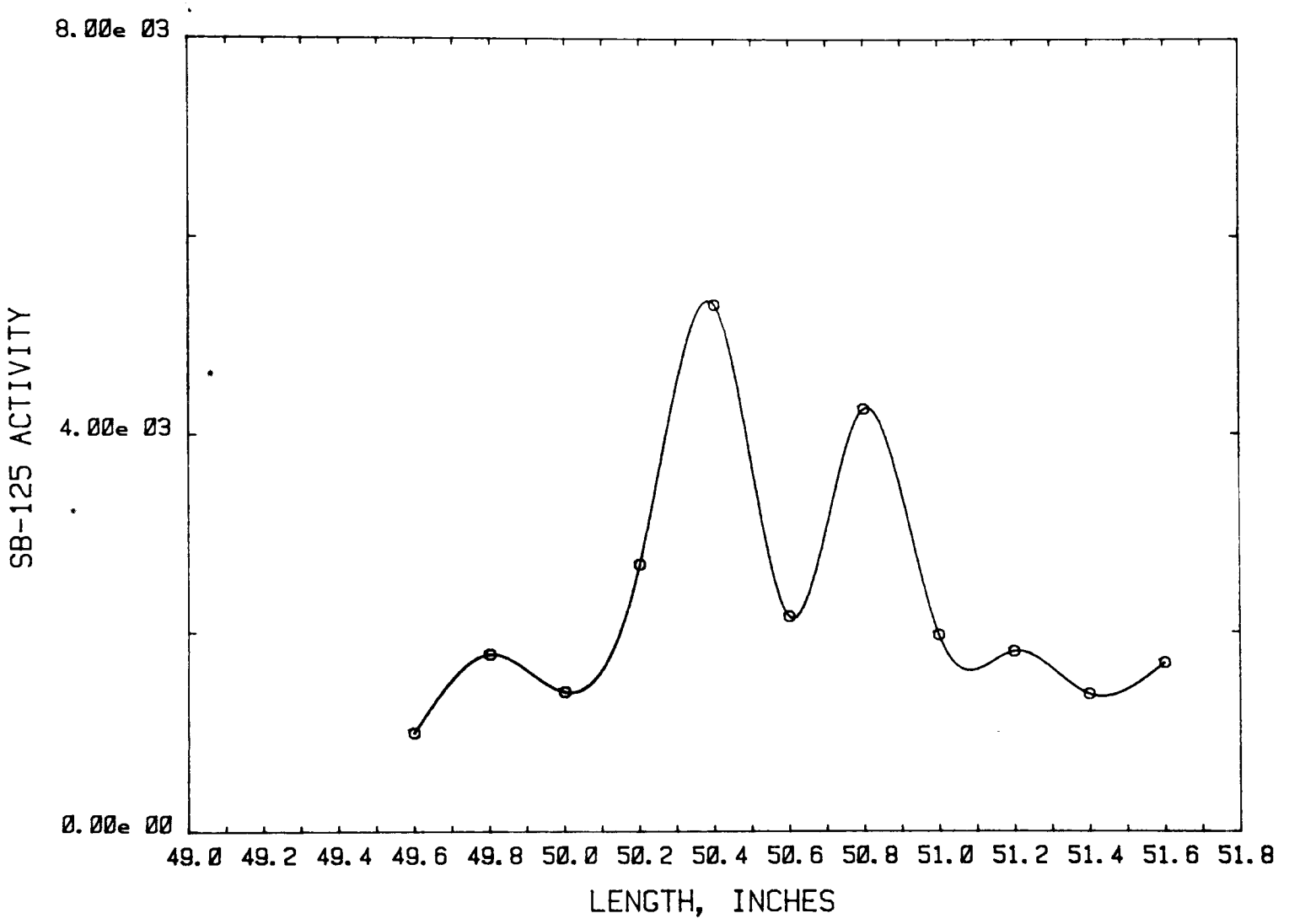

Sb-125 ACTIVITY vs. LENGTH at 0 deg.

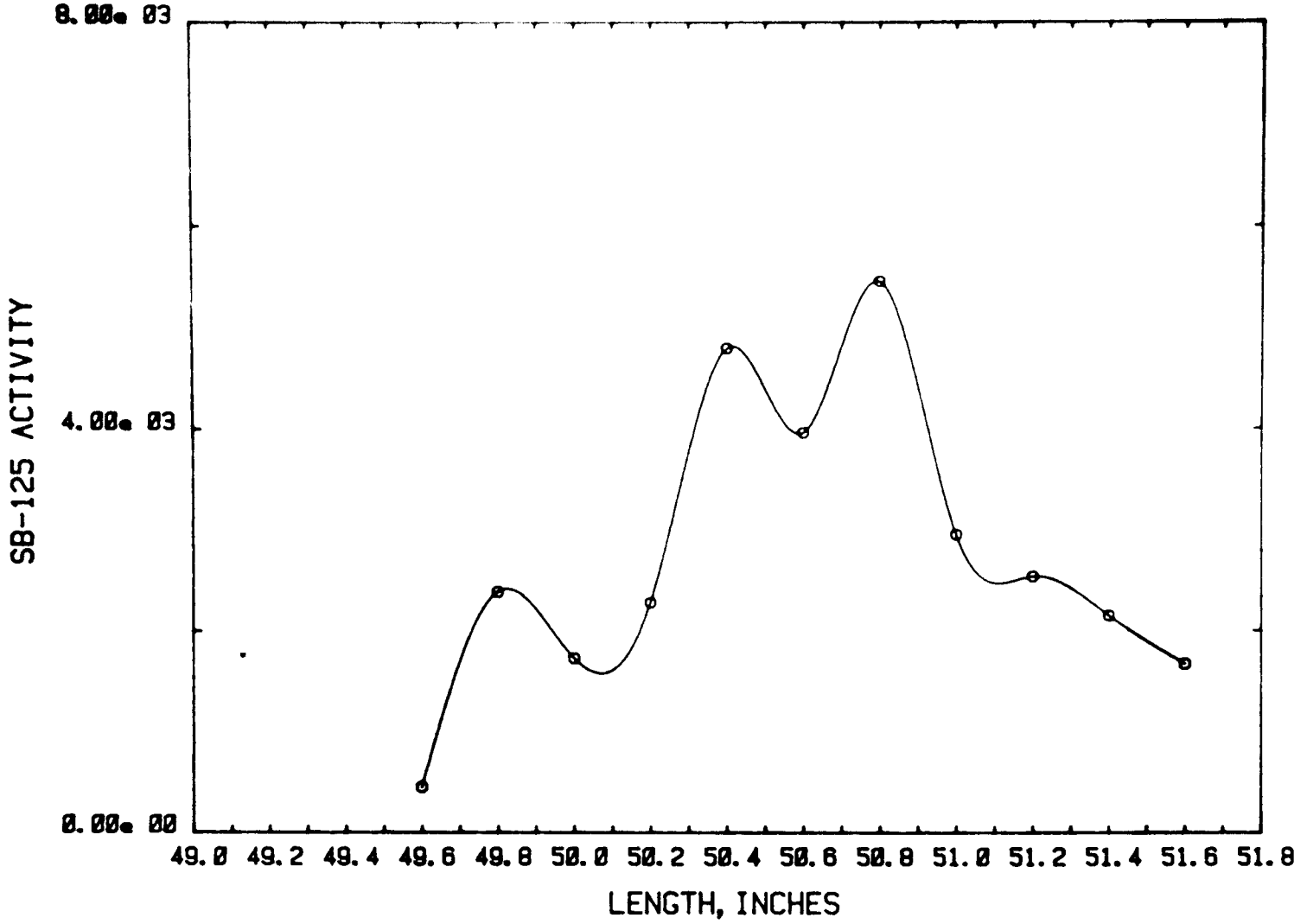

Sb-125 ACTIVITY vs. LENGTH at 180 deg.

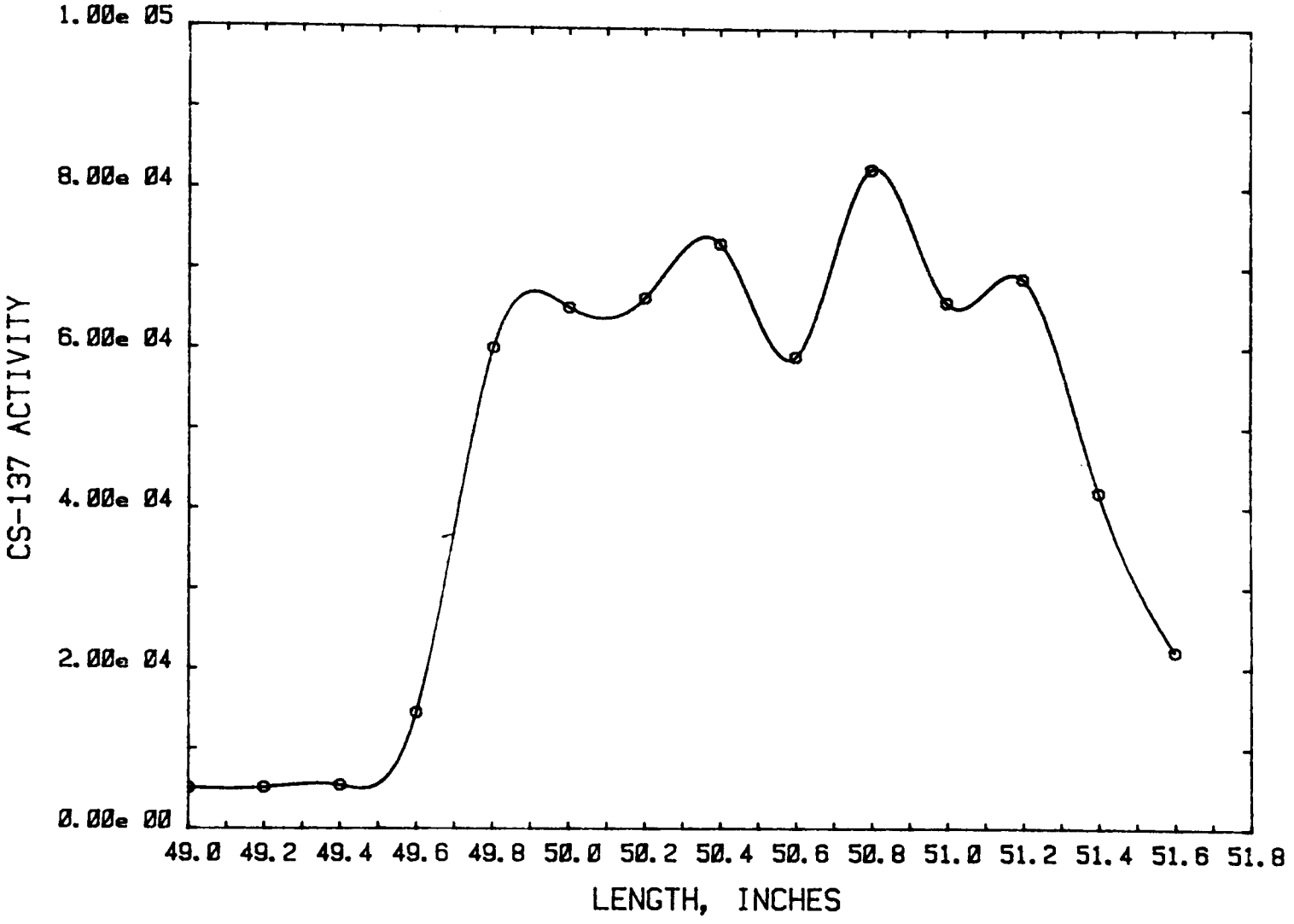

Cs-137 ACTIVITY vs. LENGTH at 180 deg.

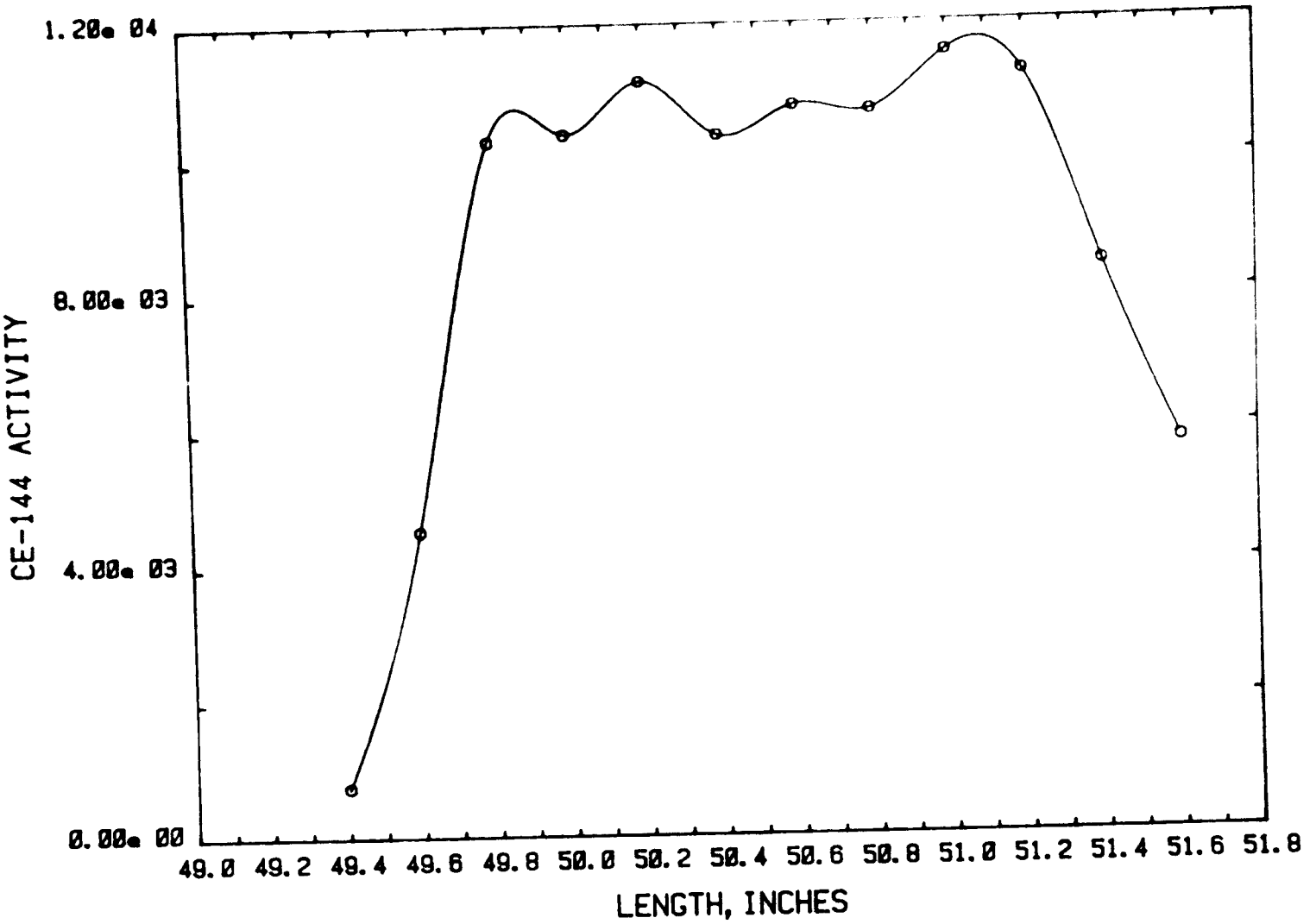

Ce-144 ACTIVITY vs. LENGTH at 180 deg.

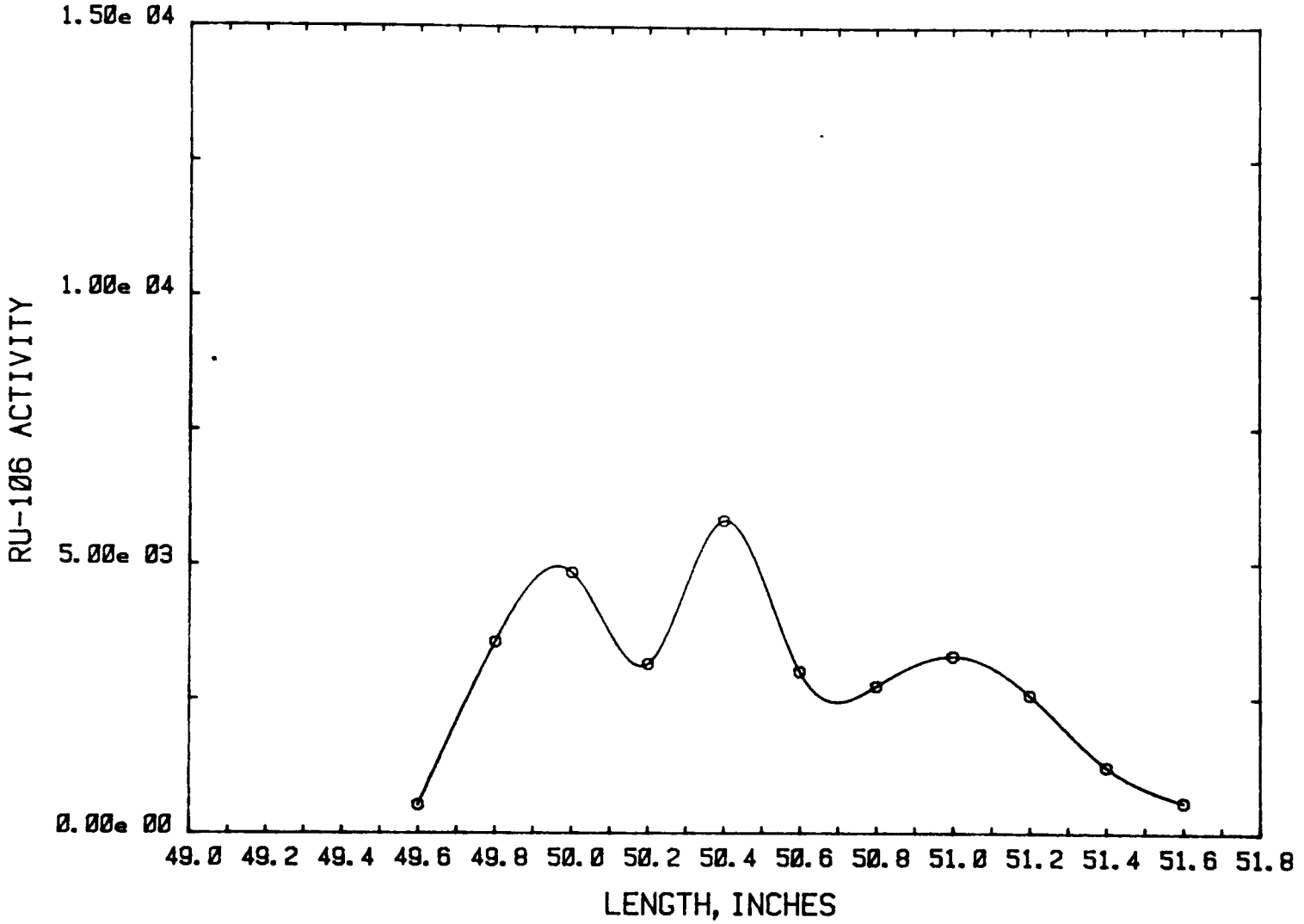

Ru-106 ACTIVITY vs. LENGTH at 180 deg.

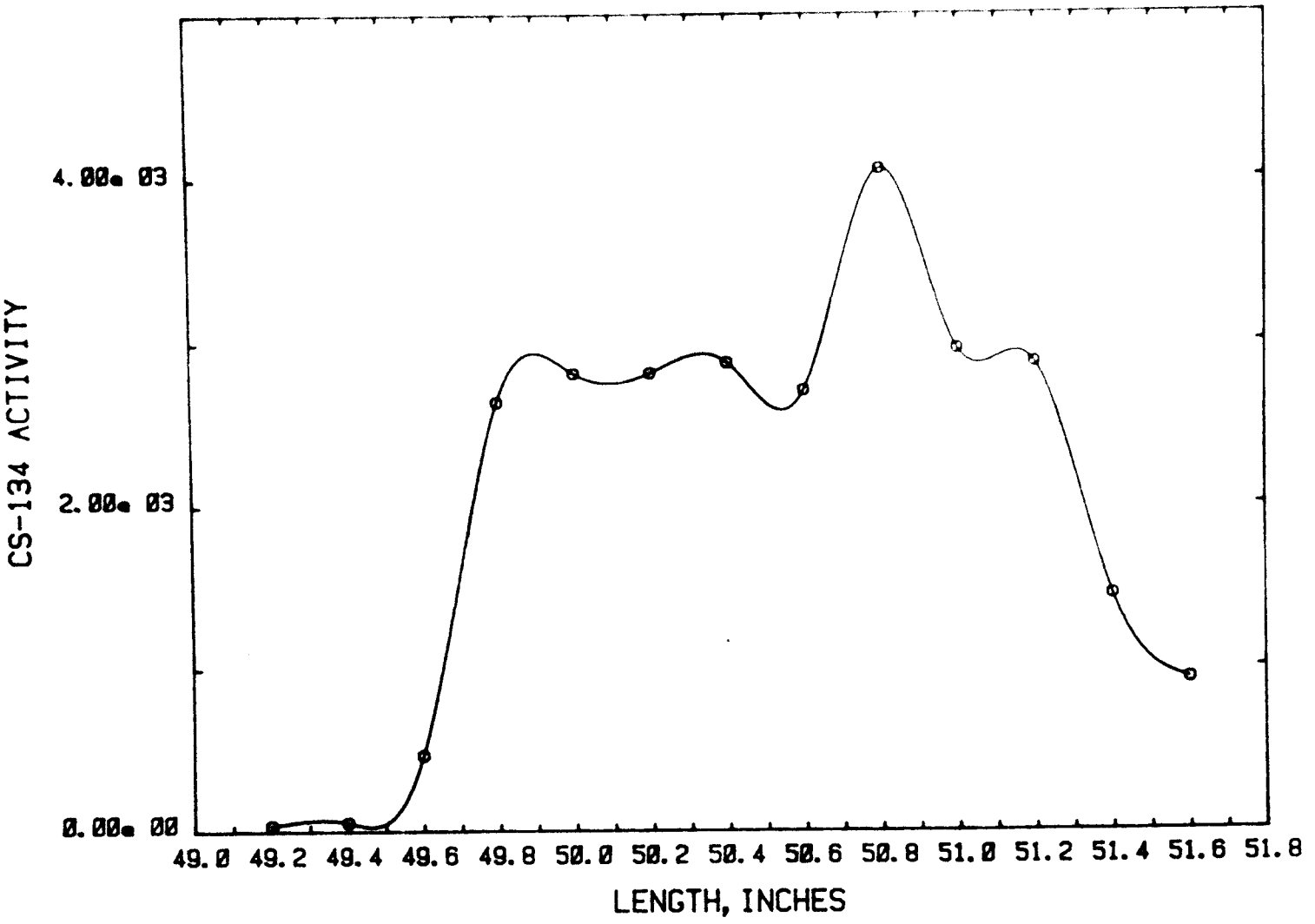

Cs-134 ACTIVITY vs. LENGTH at 180 deg.

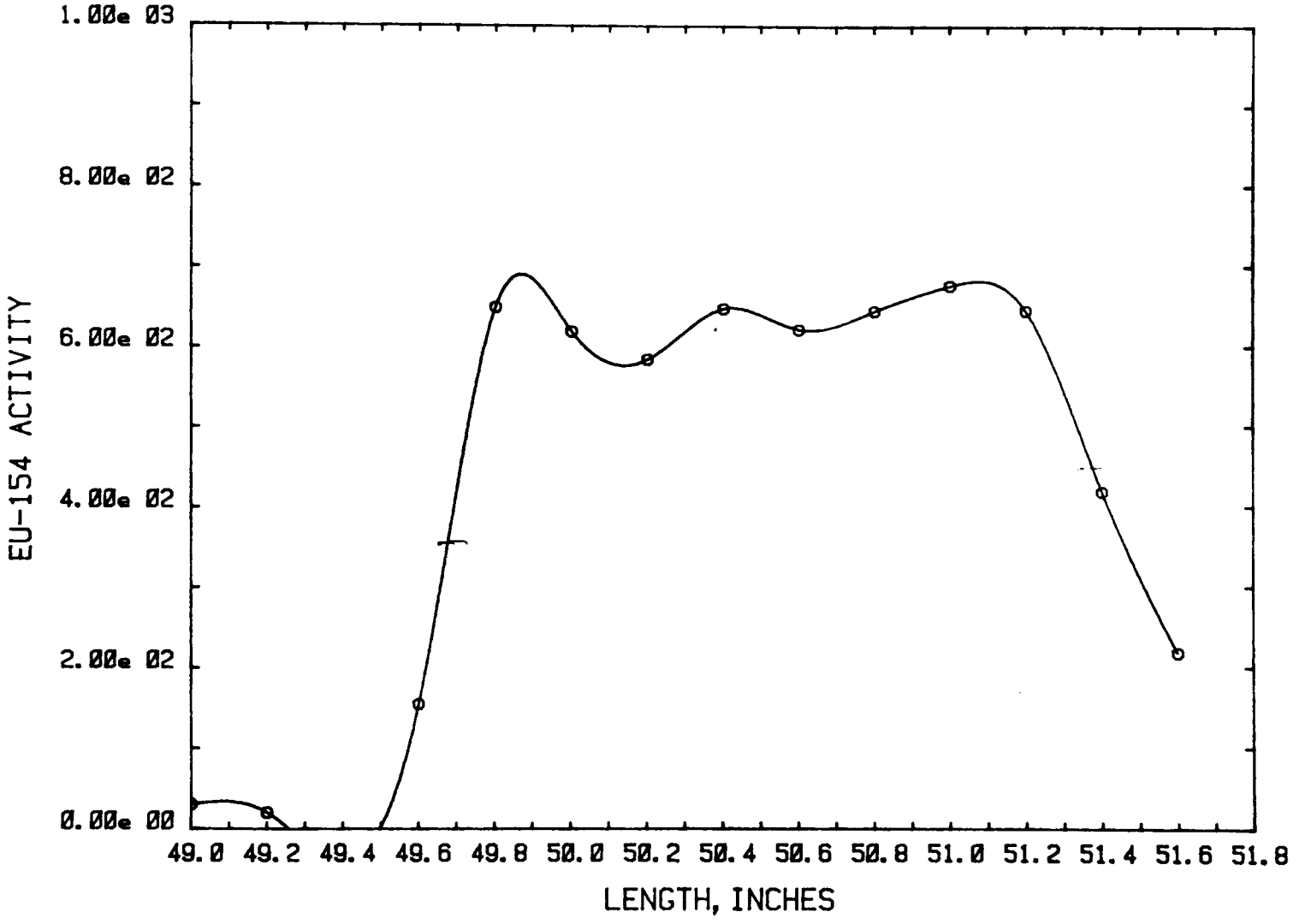

Eu-154 ACTIVITY vs. LENGTH at 180 deg.

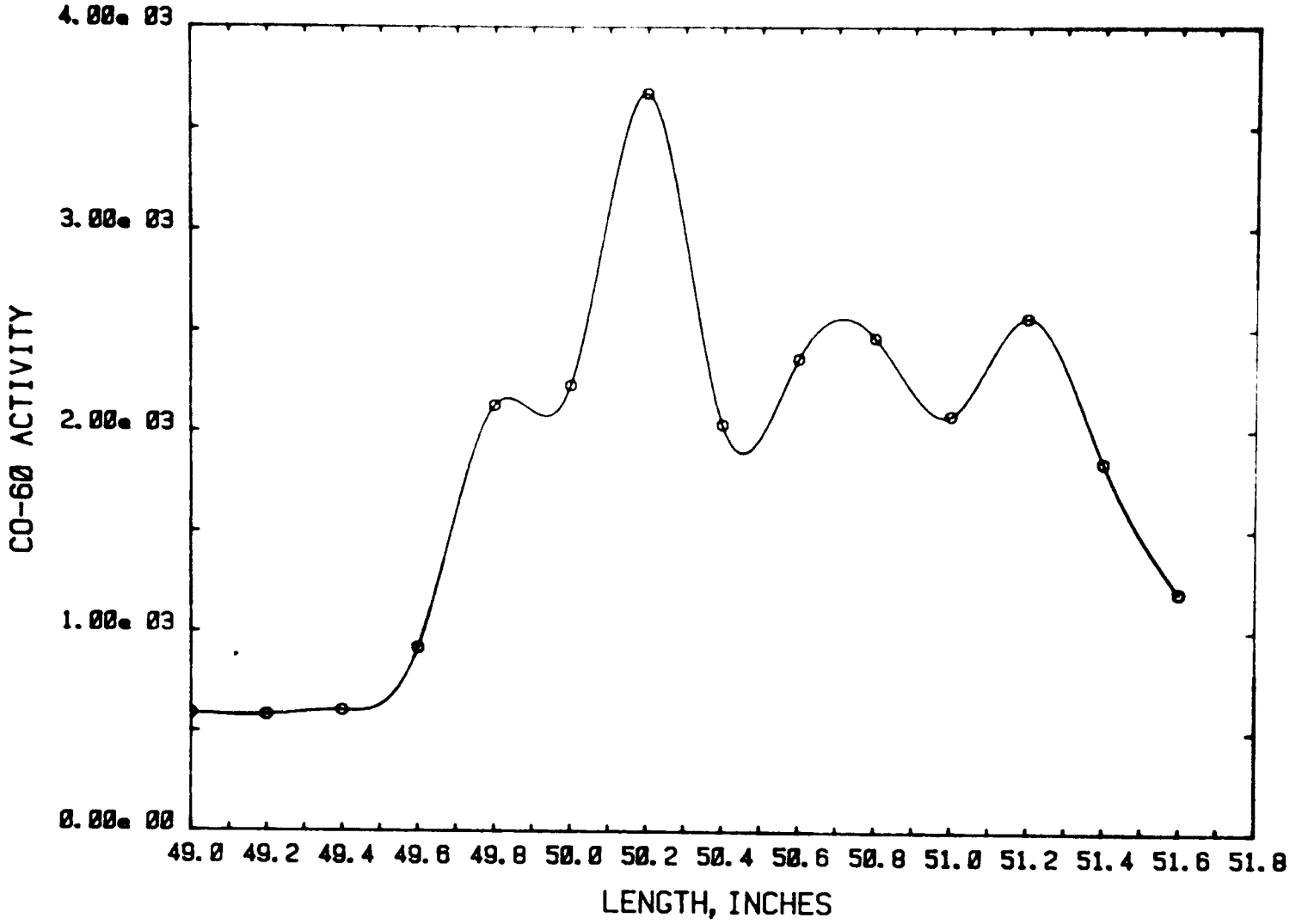

Co-60 ACTIVITY vs. LENGTH at 180 deg.

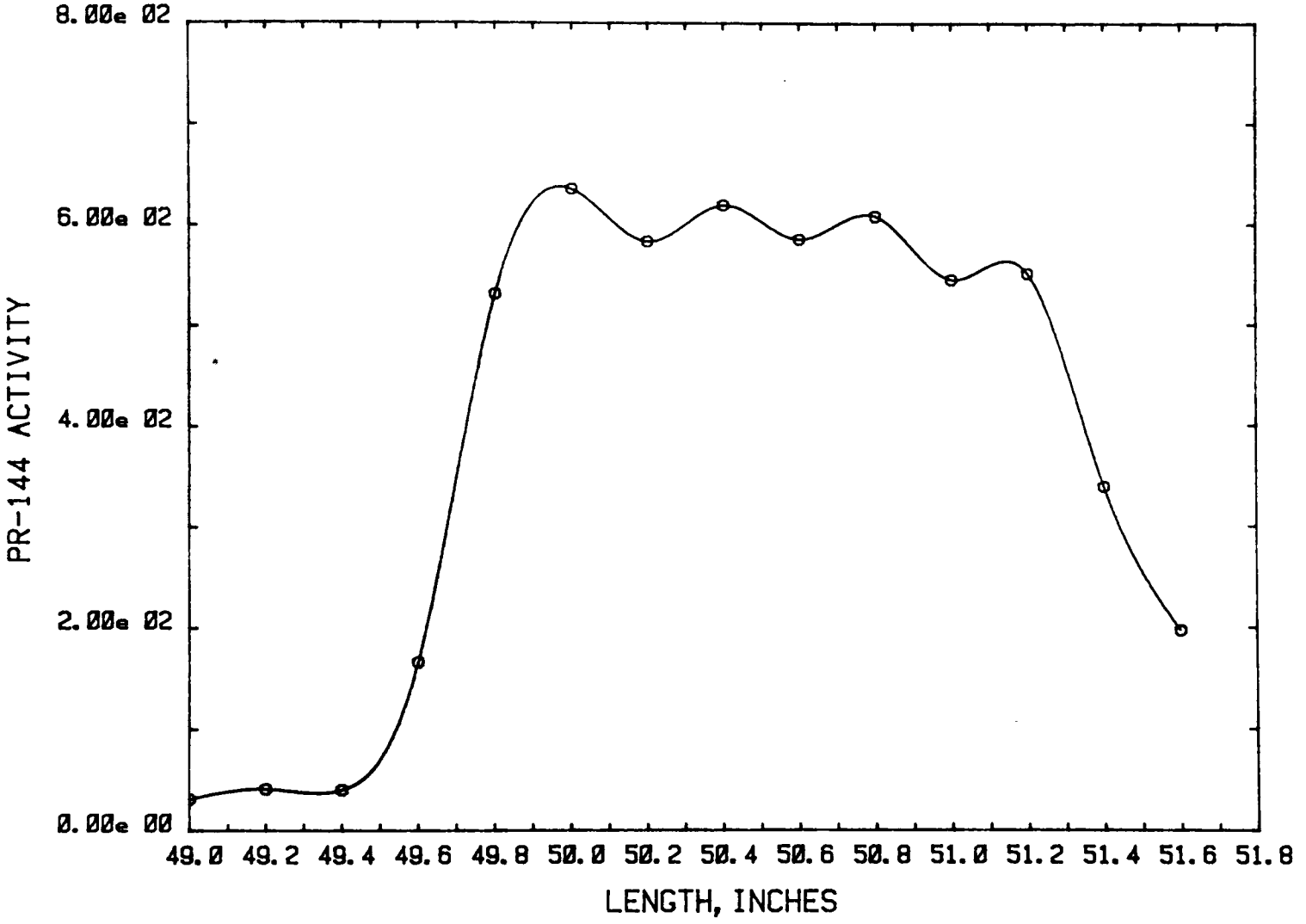

Pr-144 ACTIVITY vs. LENGTH at 180 deg.

APPENDIX B

Representative Photographs of Each Size Fraction

Squares on paper are 1/4-inch. The pan fines obtained (-325 mesh fraction) are abbreviated PF.

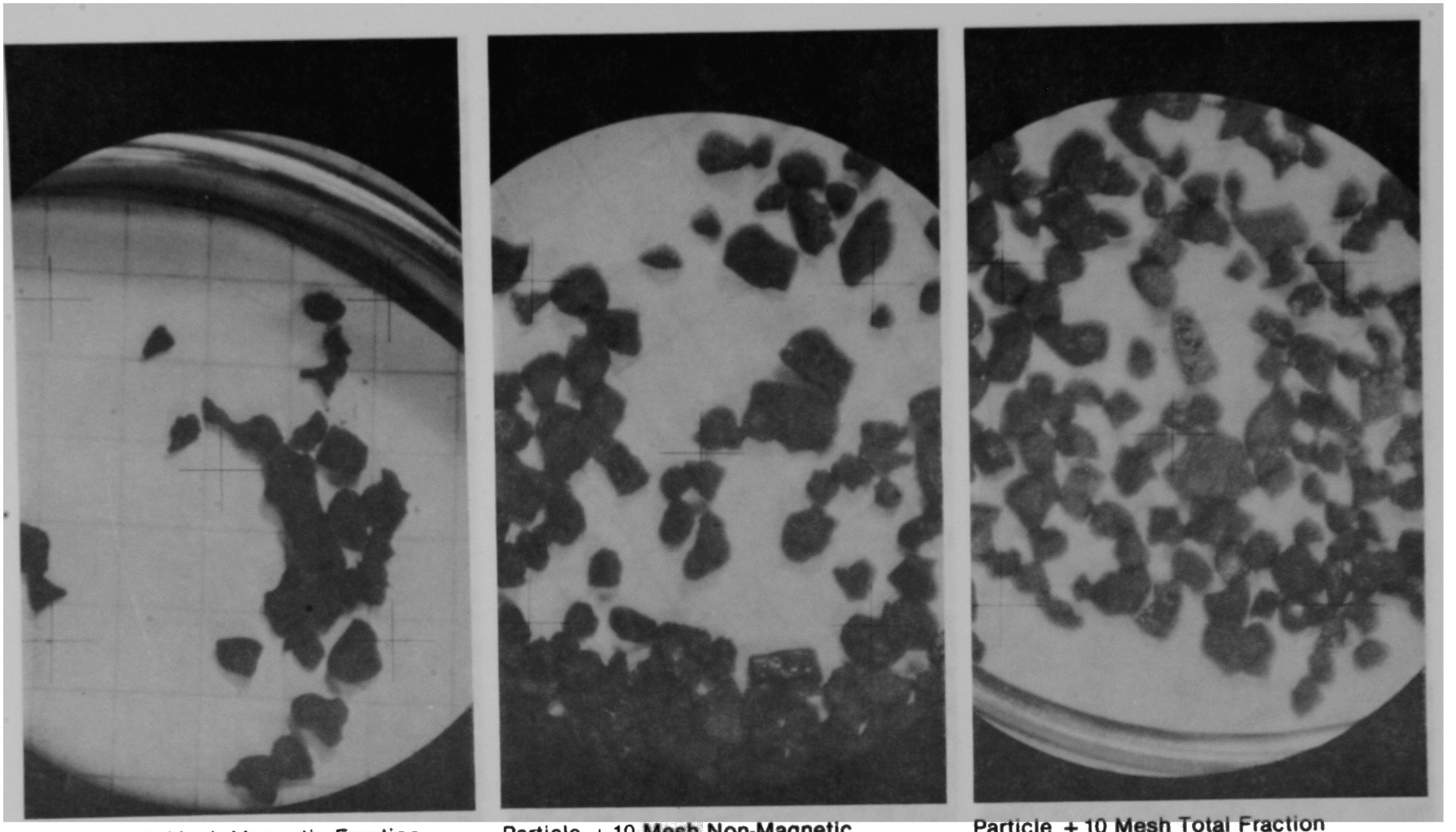

Particle + 10 Mesh Magnetic Fraction

Particle + 10 Mesh Non-Magnetic Fraction

Particle + 10 Mesh Total Fraction

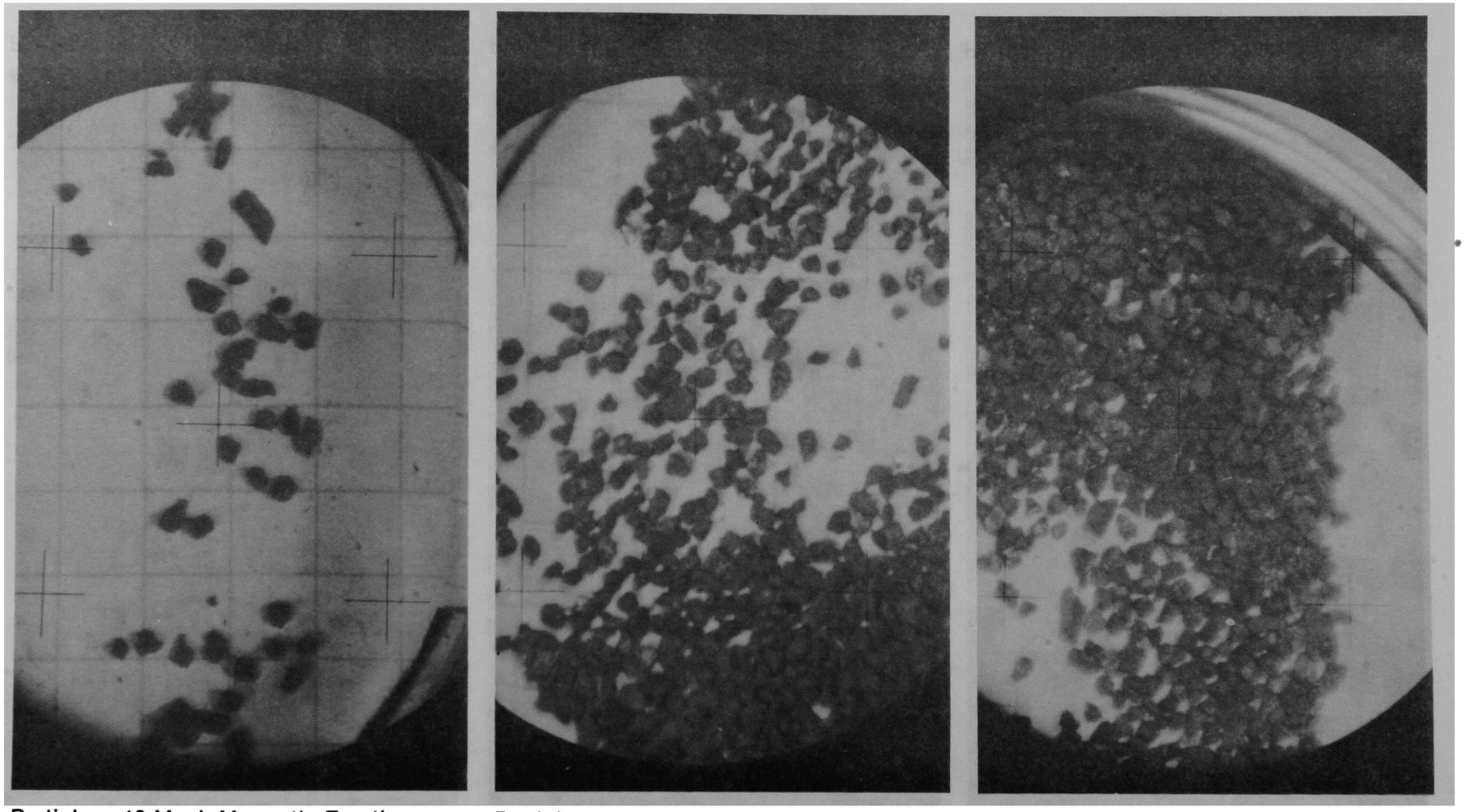

Particle + 16 Mesh Magnetic Fraction

Particle + 16 Mesh Non-Magnetic Fraction

Particle + 16 Mesh Total Fraction

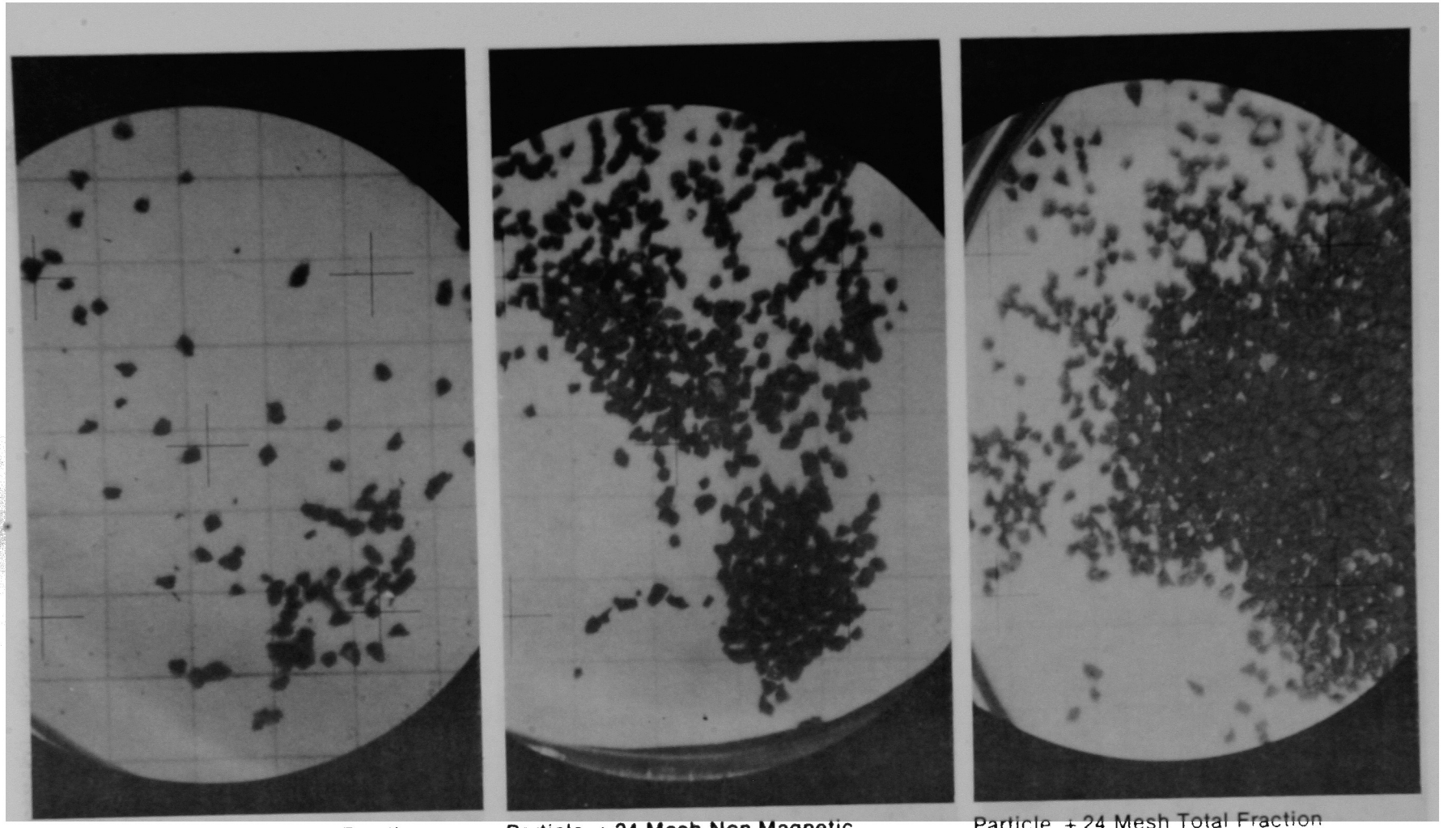

Particle +24 Mesh Magnetic Fraction

Particle +24 Mesh Non-Magnetic Fraction

Particle +24 Mesh Total Fraction

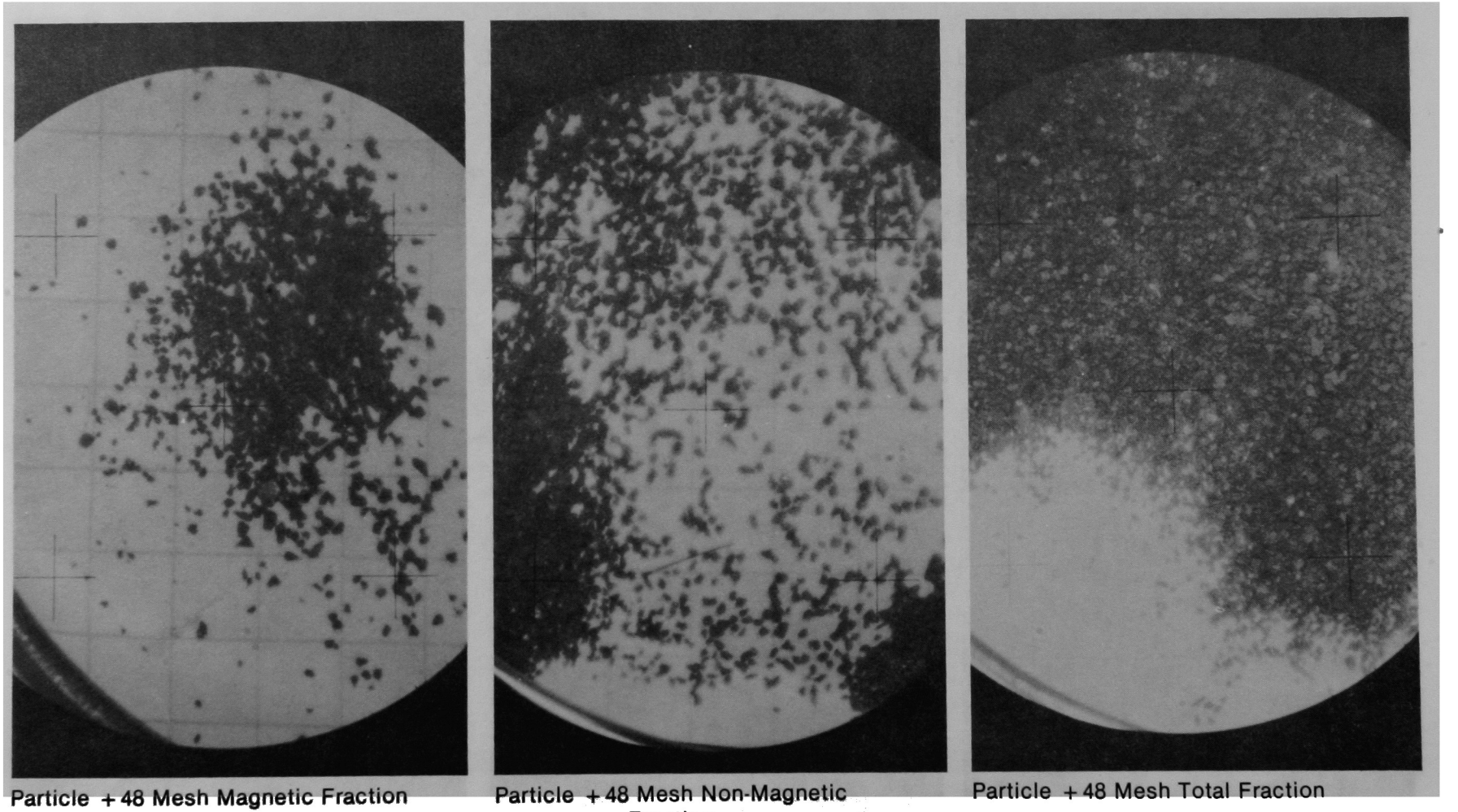

Particle + 48 Mesh Magnetic Fraction

Particle + 48 Mesh Non-Magnetic Fraction

Particle + 48 Mesh Total Fraction

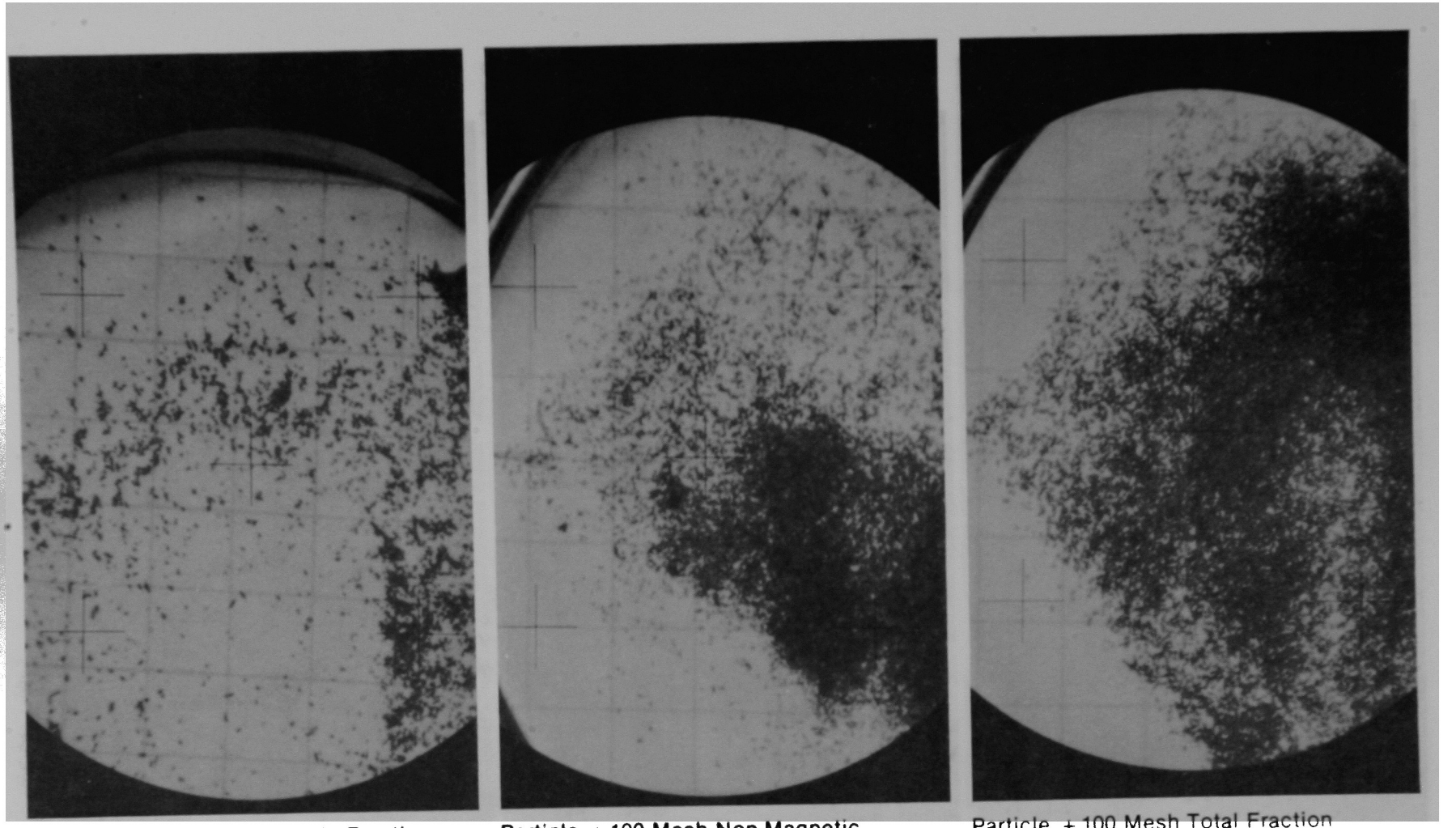

Particle + 100 Mesh Magnetic Fraction

Particle + 100 Mesh Non-Magnetic Fraction

Particle + 100 Mesh Total Fraction

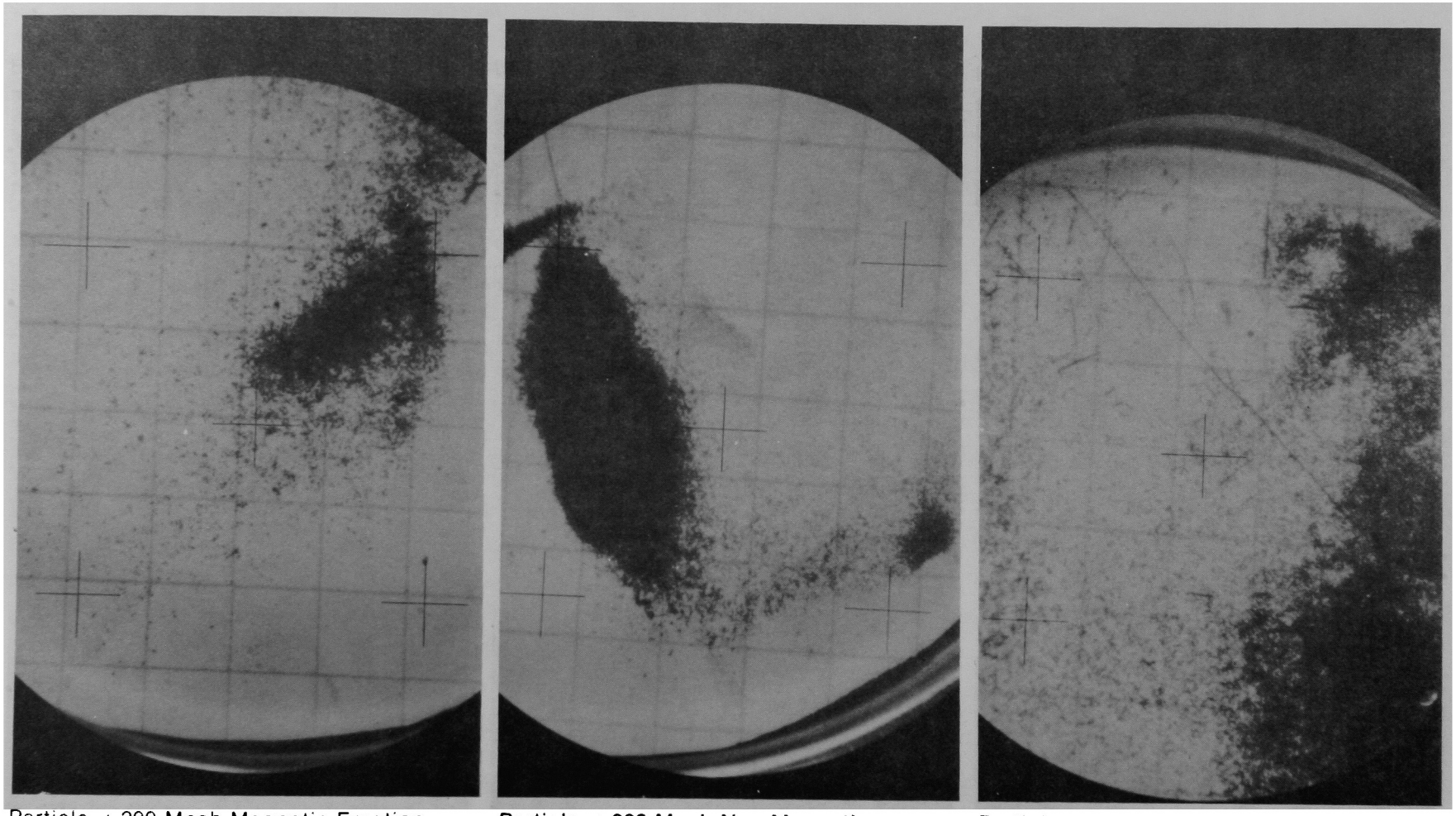

Particle +200 Mesh Magnetic Fraction

Particle +200 Mesh Non-Magnetic Fraction

Particle +200 Mesh Total Fraction

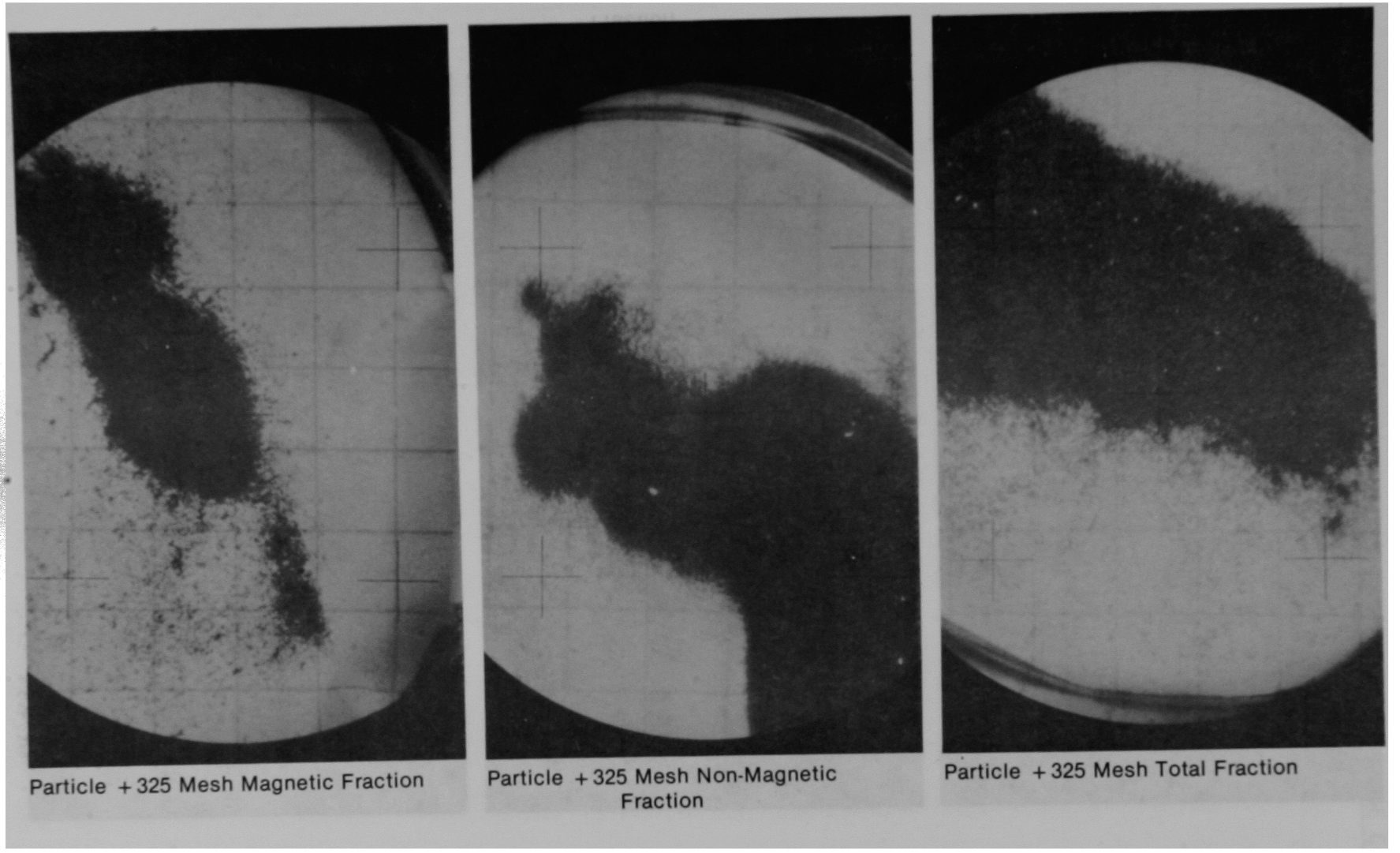

Particle +325 Mesh Magnetic Fraction

Particle +325 Mesh Non-Magnetic Fraction

Particle +325 Mesh Total Fraction

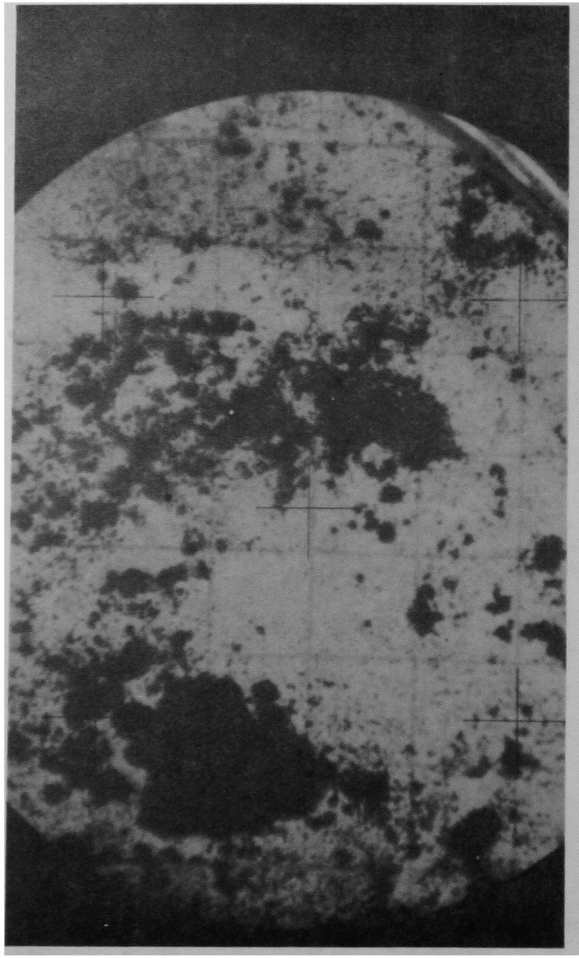

Particle PF Mesh Magnetic Fraction

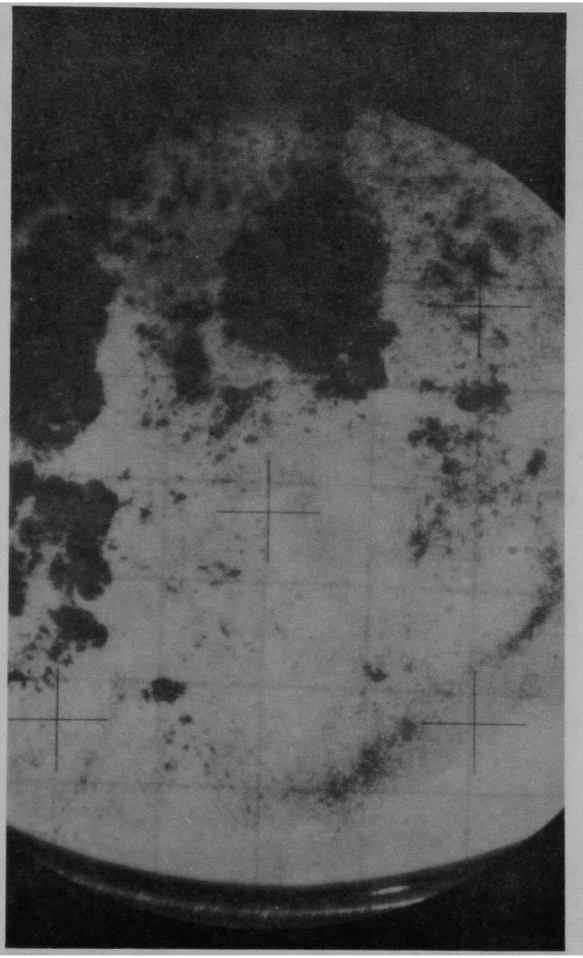

Particle PF Mesh Non-Magnetic Fraction

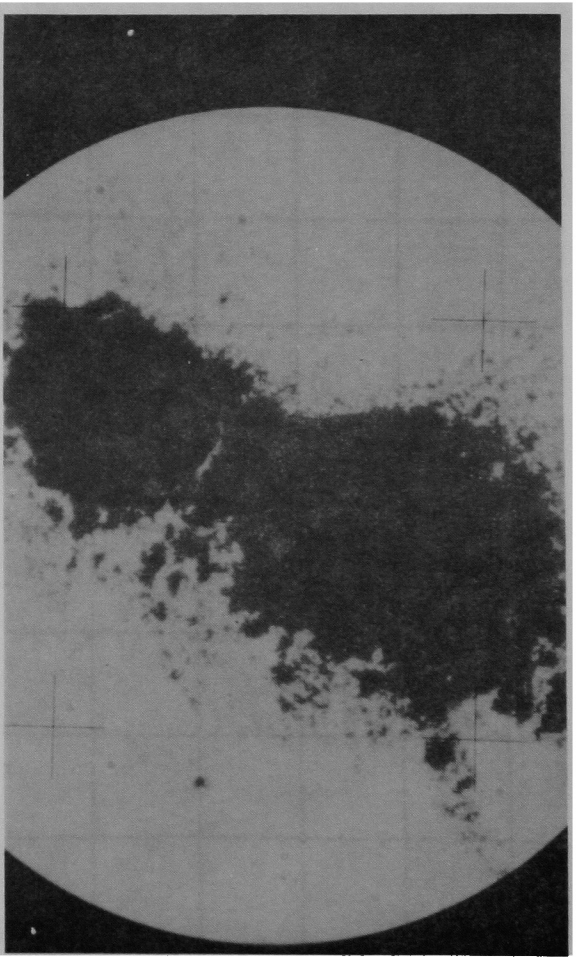

Particle PF Mesh Total Fraction

APPENDIX C

Gamma-Ray Spectra of the Six Coarse Particles Examined

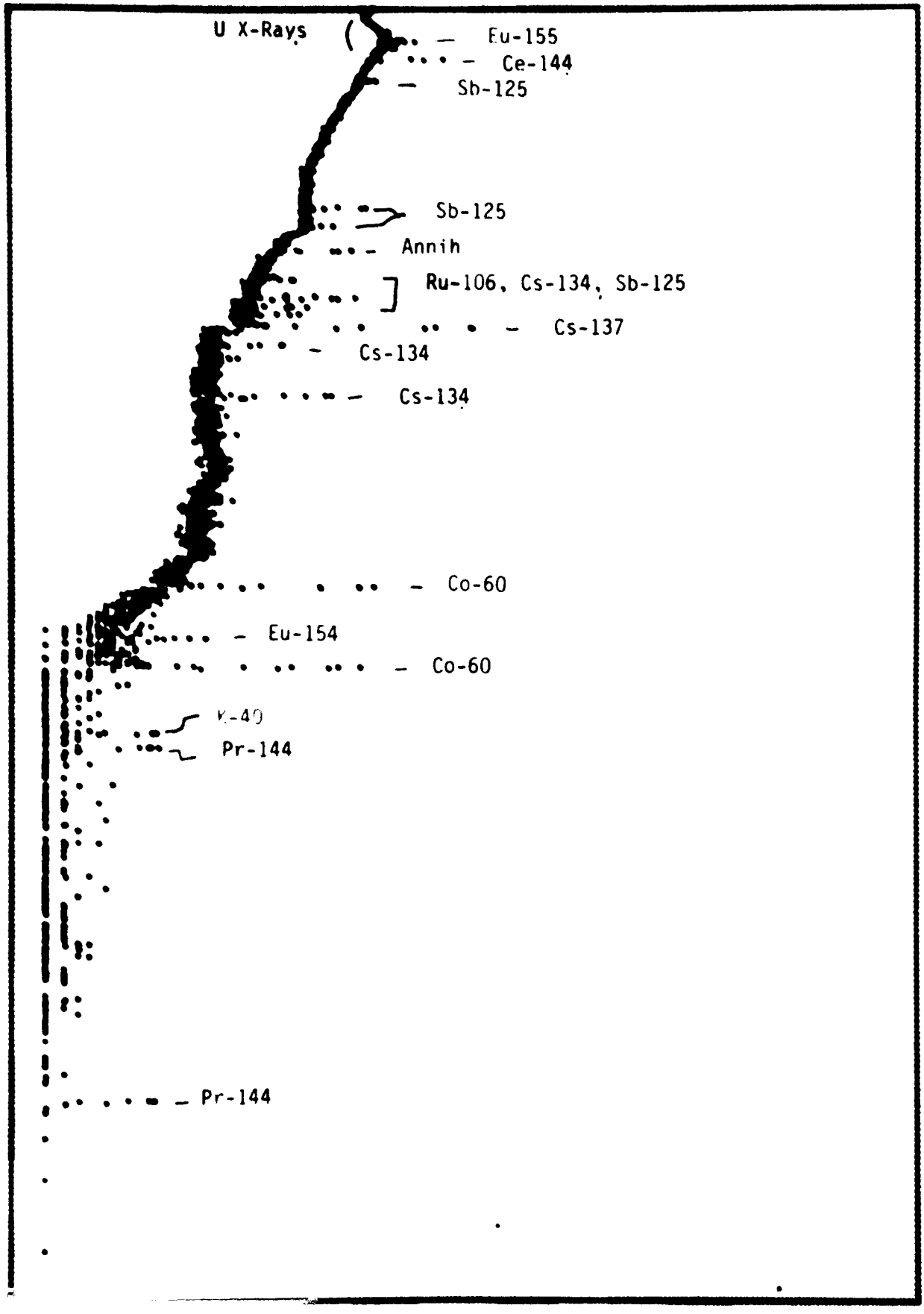
U X-Rays
Eu-155
Ce-144
Sb-125
Sb-125
Annih
Ru-106, Cs-134, Sb-125
Cs-137
Cs-134
Cs-134
Co-60
Eu-154
Co-60
K-40
Pr-144
Pr-144
Sample 1

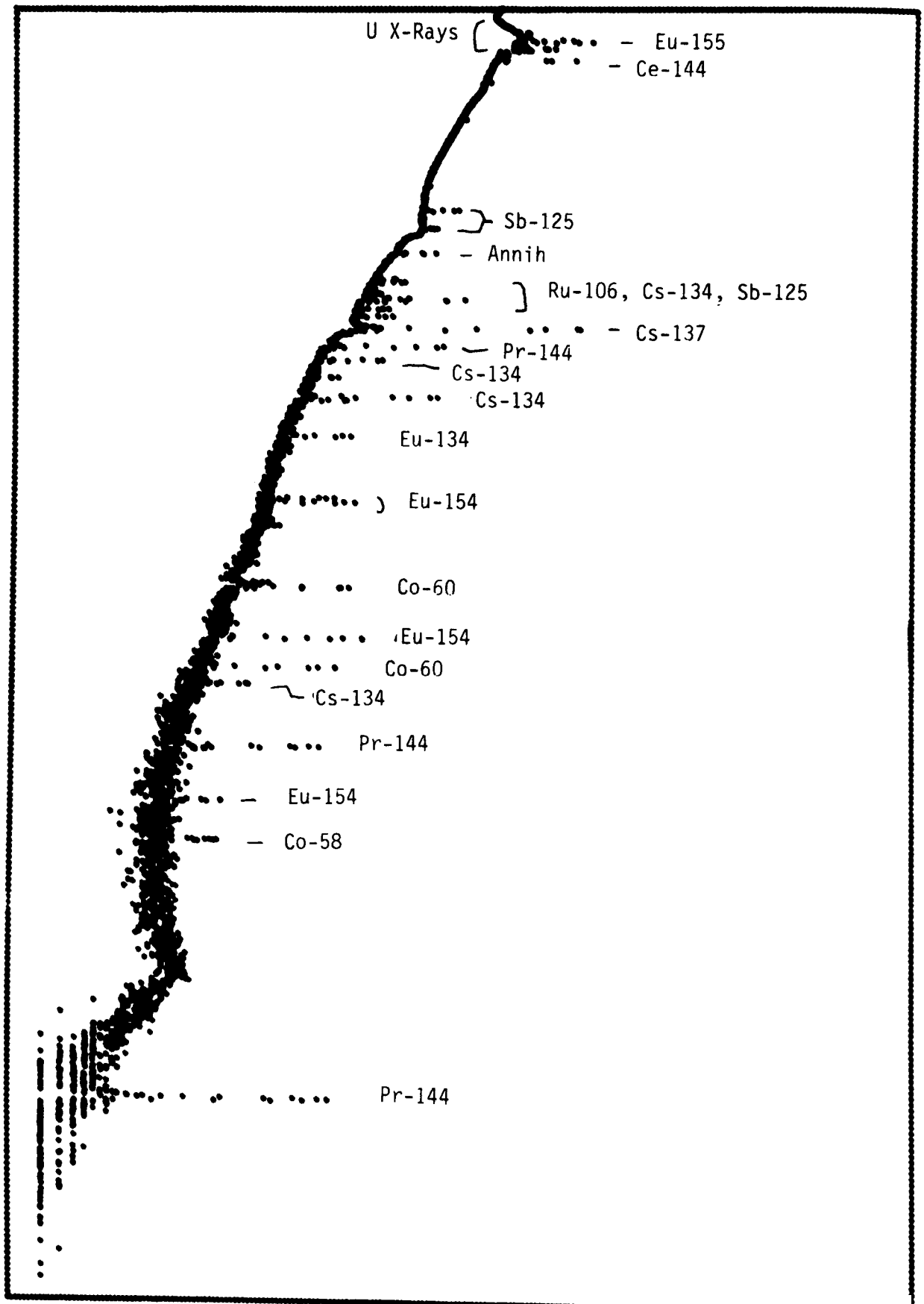
U X-Rays
Eu-155
Ce-144
Sb-125
Annih
Ru-106, Cs-134, Sb-125
Cs-137
Pr-144
Cs-134
Cs-134
Eu-134
Eu-154
Co-60
Eu-154
Co-60
Cs-134
Pr-144
Eu-154
Co-58
Pr-144

Sample 2

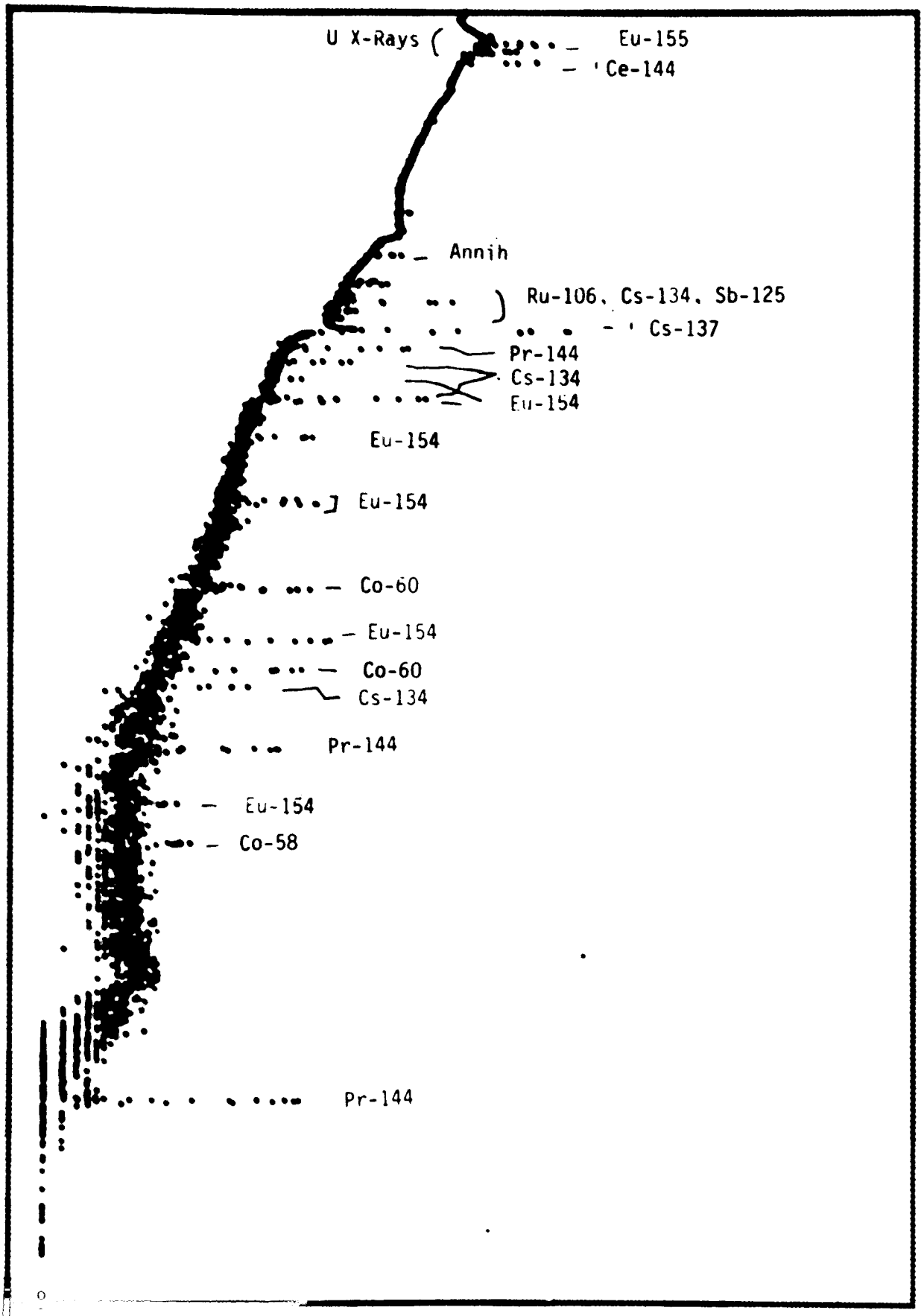
U X-Rays
Eu-155
Ce-144
Annih
Ru-106, Cs-134, Sb-125
Cs-137
Pr-144
Cs-134
Eu-154
Eu-154
Eu-154
Co-60
Eu-154
Co-60
Cs-134
Pr-144
Eu-154
Co-58
Pr-144

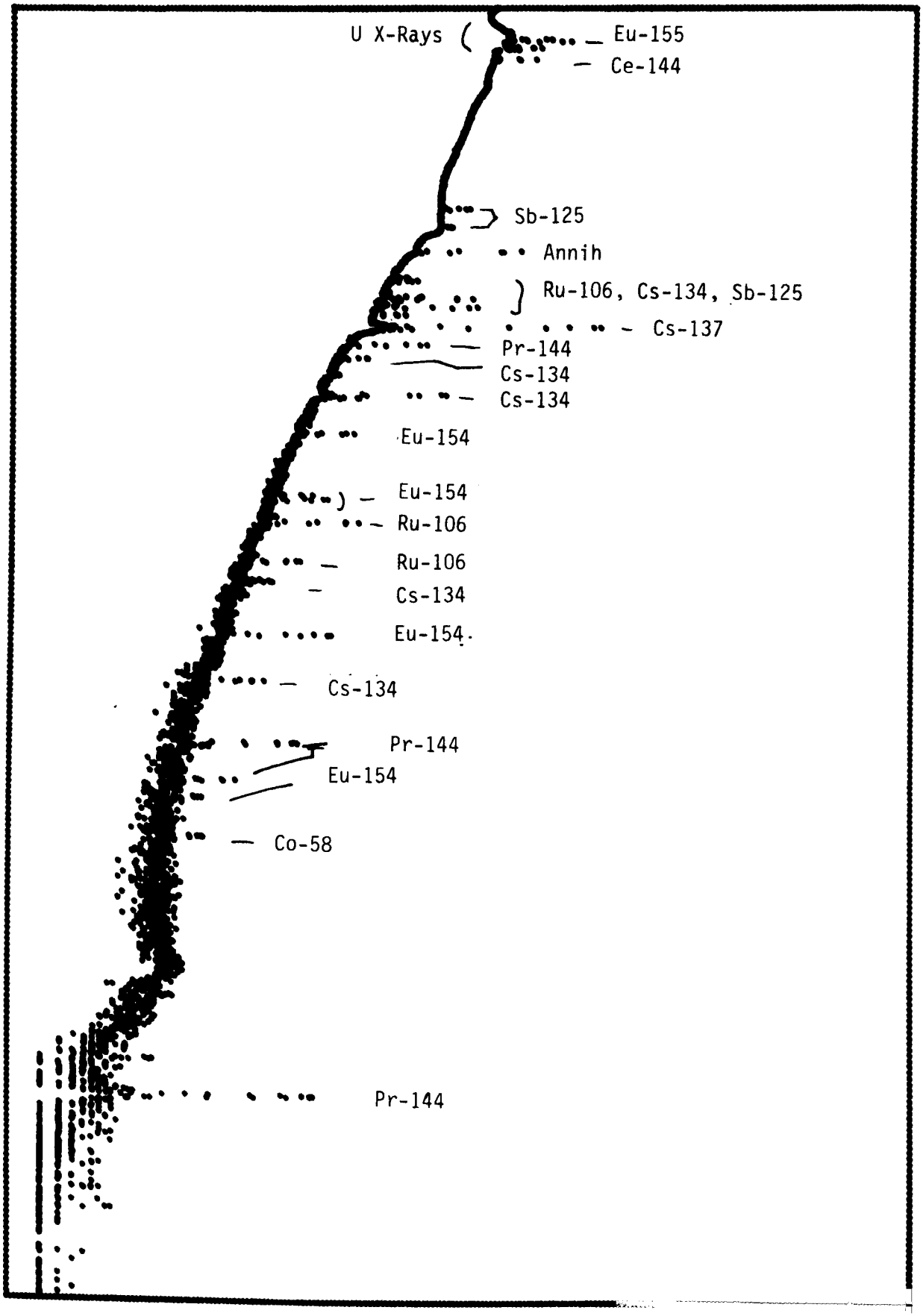
U X-Rays
Eu-155
Ce-144
Sb-125
Annih
Ru-106, Cs-134, Sb-125
Cs-137
Pr-144
Cs-134
Cs-134
Eu-154
Eu-154
Ru-106
Ru-106
Cs-134
Eu-154
Cs-134
Pr-144
Eu-154
Co-58
Pr-144

Sample 4

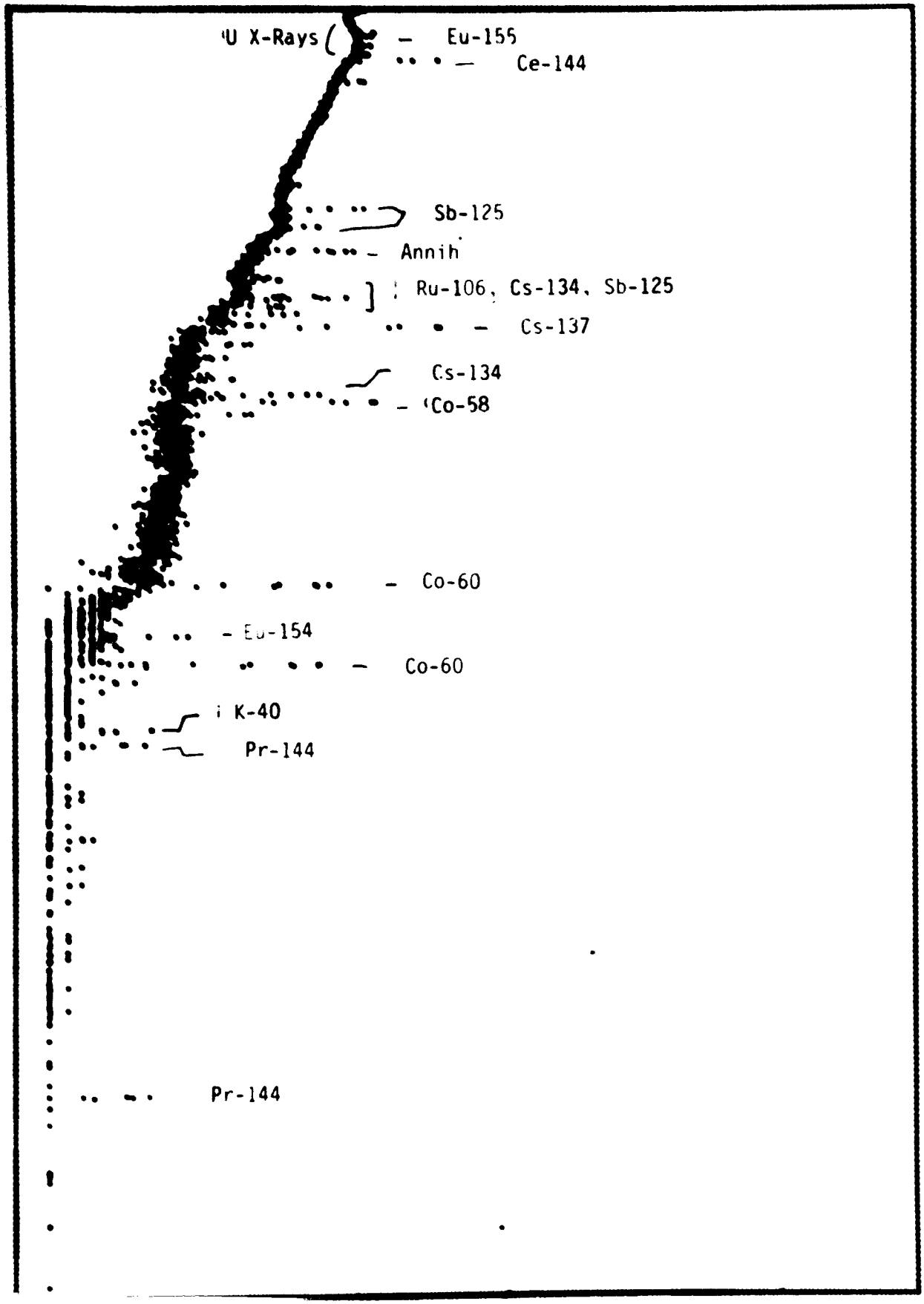
U X-Rays
Eu-155
Ce-144
Sb-125
Annih
Ru-106, Cs-134, Sb-125
Cs-137
Cs-134
Co-58
Co-60
Eu-154
Co-60
K-40
Pr-144
Pr-144

Sample 5

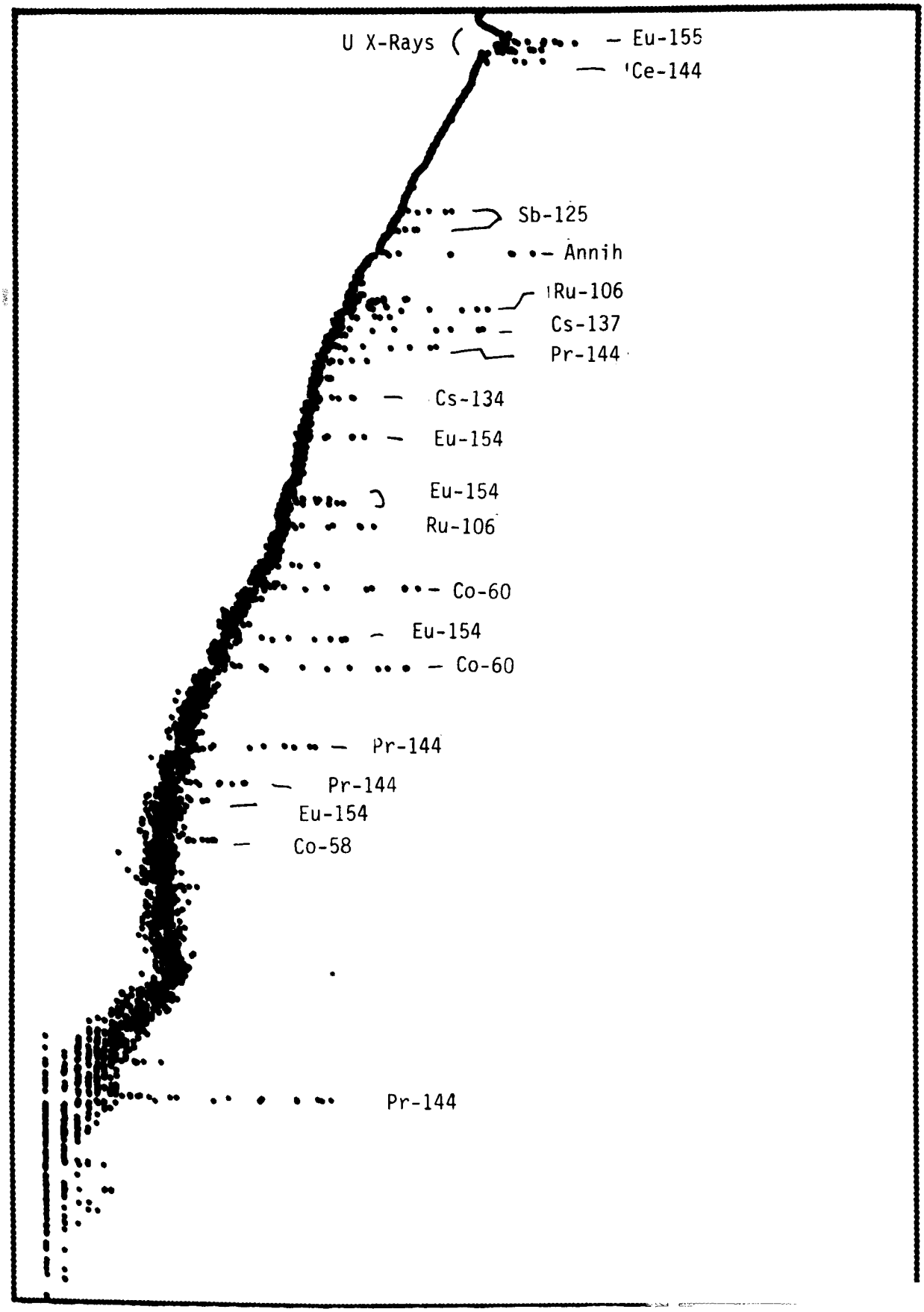
U X-Rays
Eu-155
Ce-144
Sb-125
Annih
Ru-106
Cs-137
Pr-144
Cs-134
Eu-154
Eu-154
Ru-106
Co-60
Eu-154
Co-60
Pr-144
Pr-144
Eu-154
Co-58
Pr-144

Sample 6

APPENDIX D

Photographs Taken of the Six Coarse Particles During Visual Examination

In some photographs a 1/4-inch square background grid can be seen.

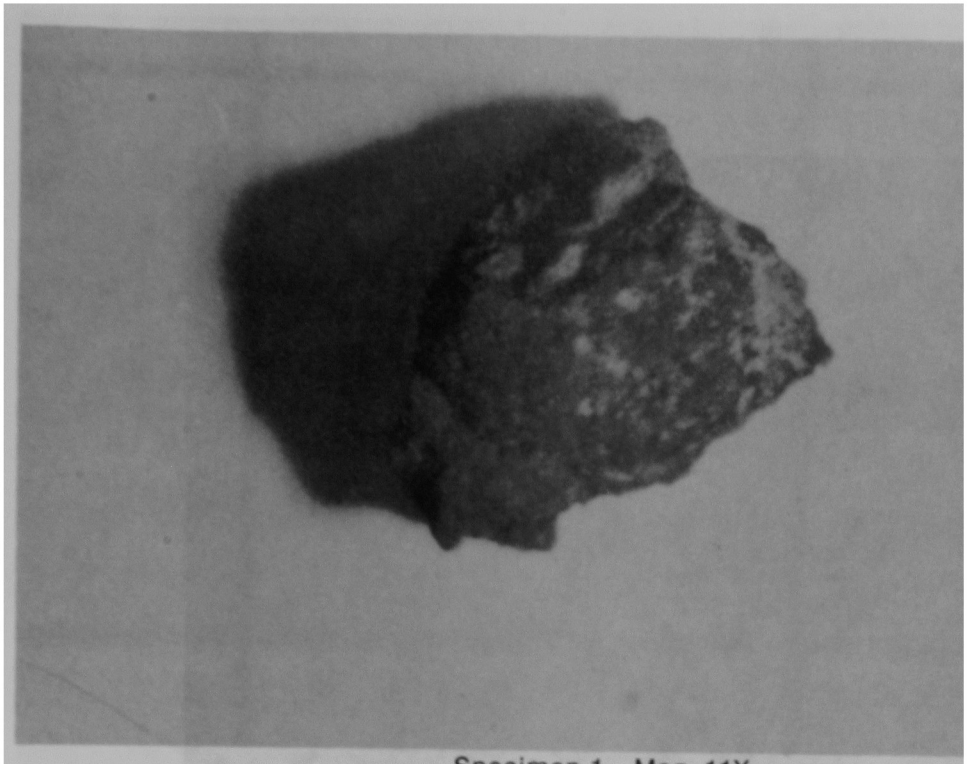

Specimen 1—Mag. 11X

Specimen 1—Mag. 25X

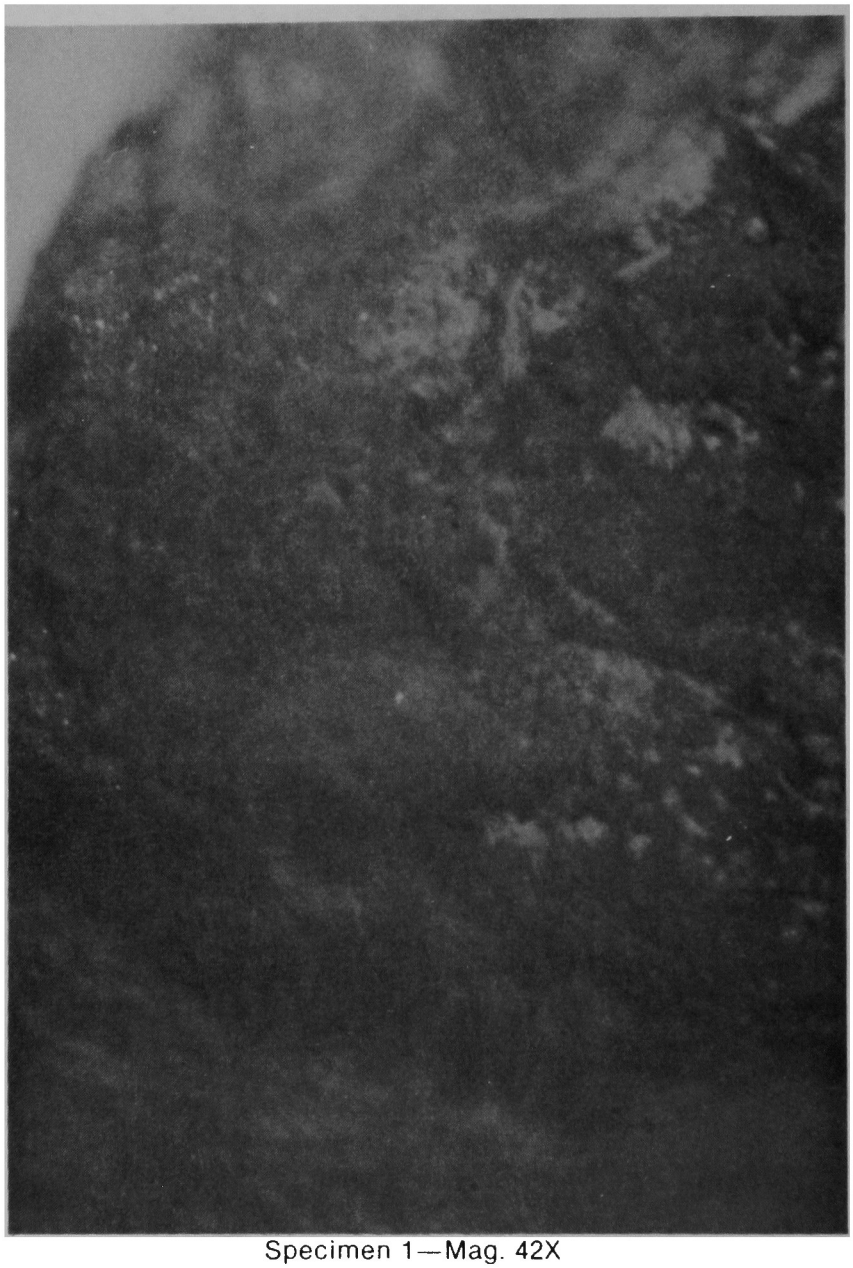

Specimen 1—Mag. 42X

Specimen 2—Mag. 11X

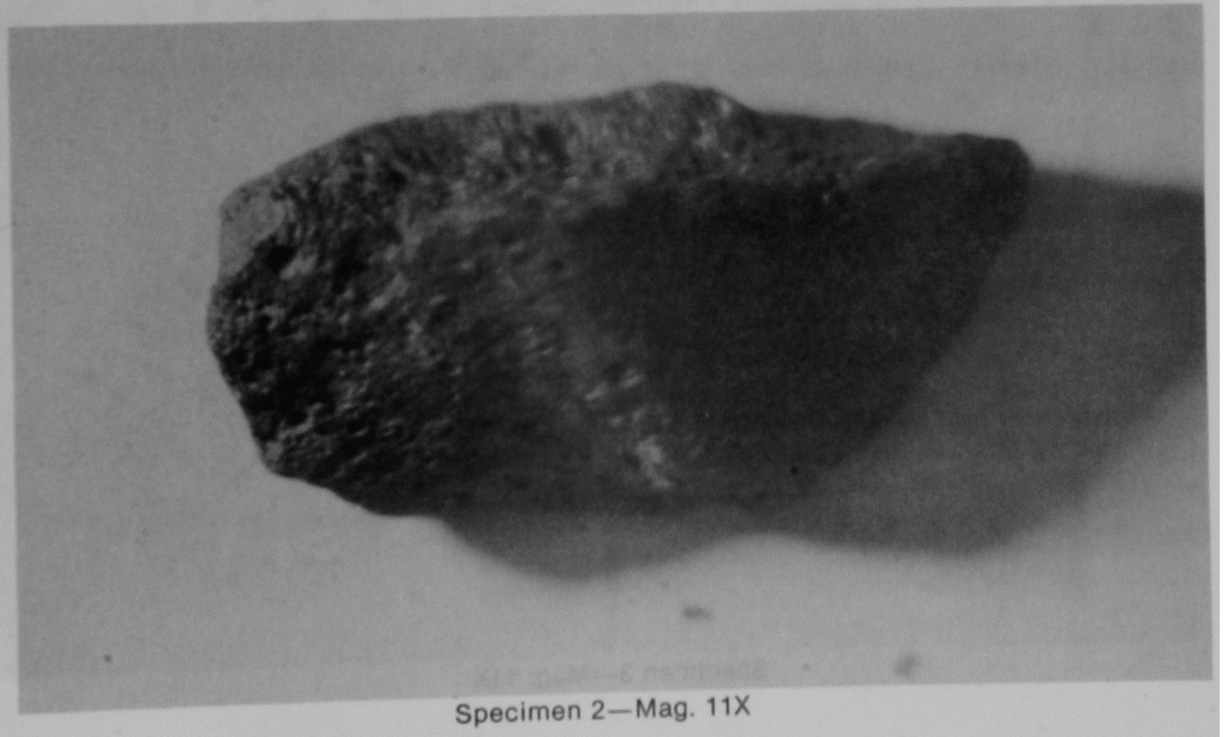

Specimen 2—Mag. 11X

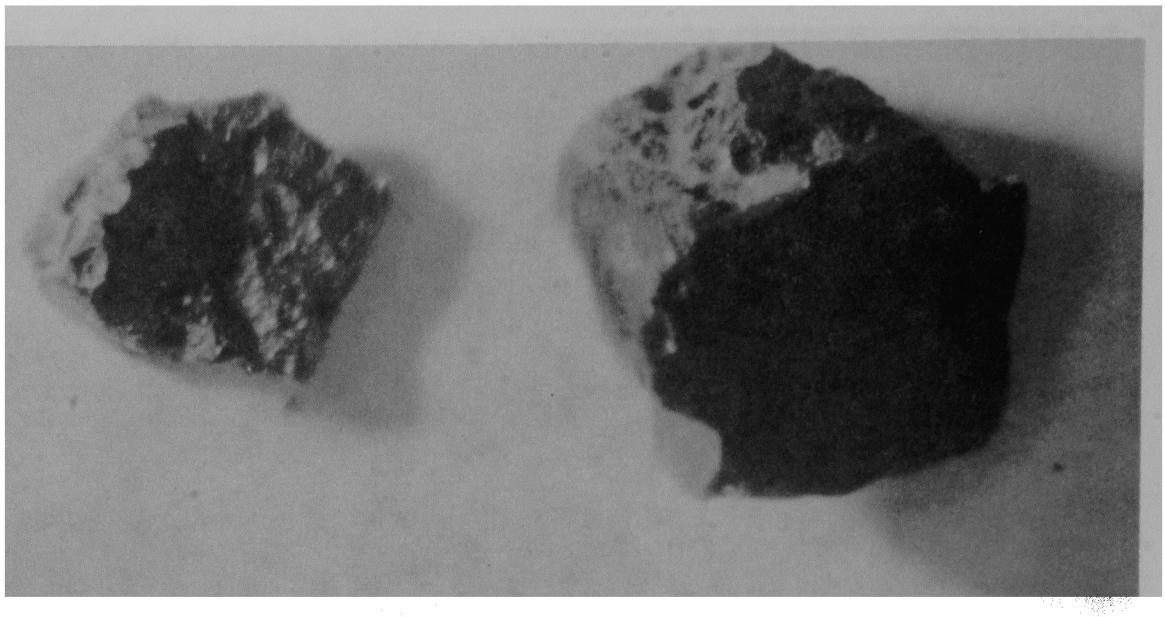

Specimen 3—Mag. 11X

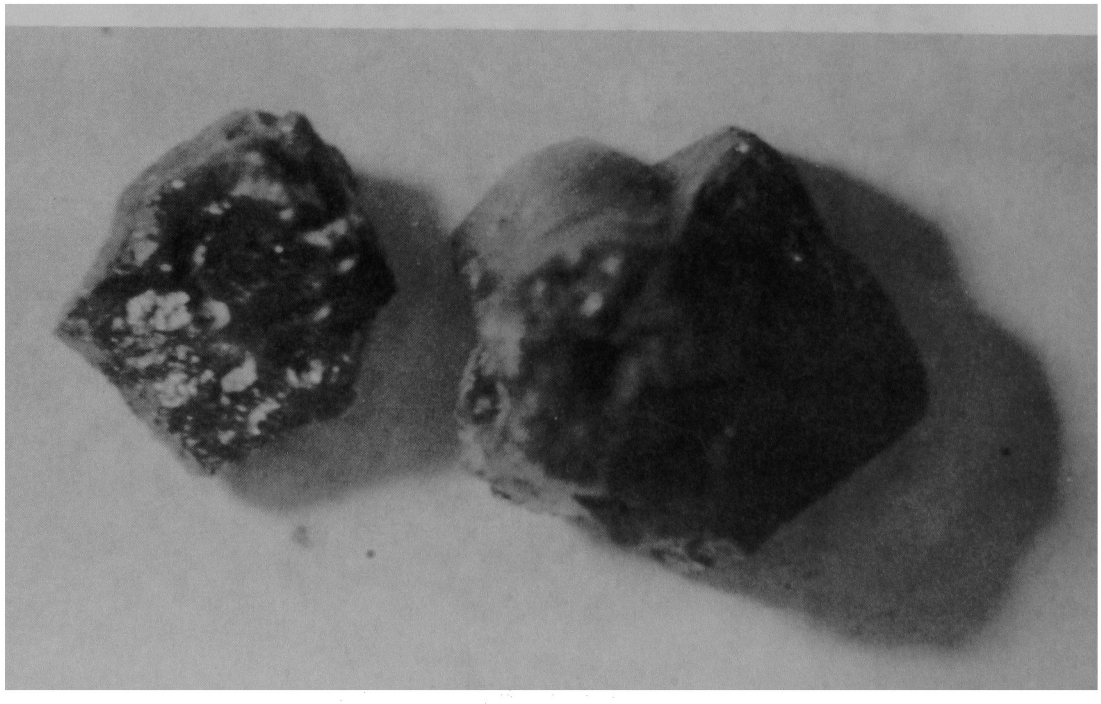

Specimen 3—Mag. 11X

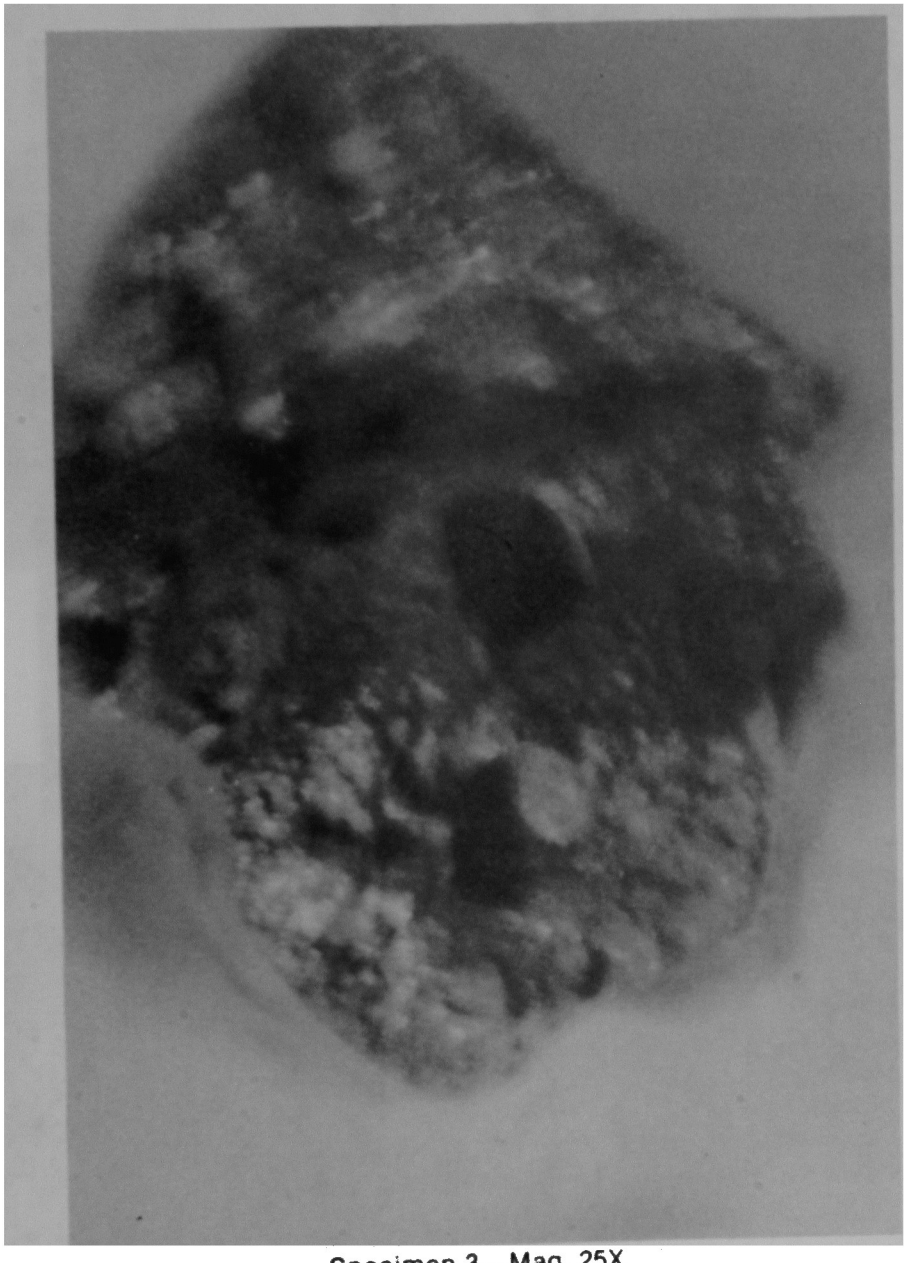

Specimen 3—Mag. 25X

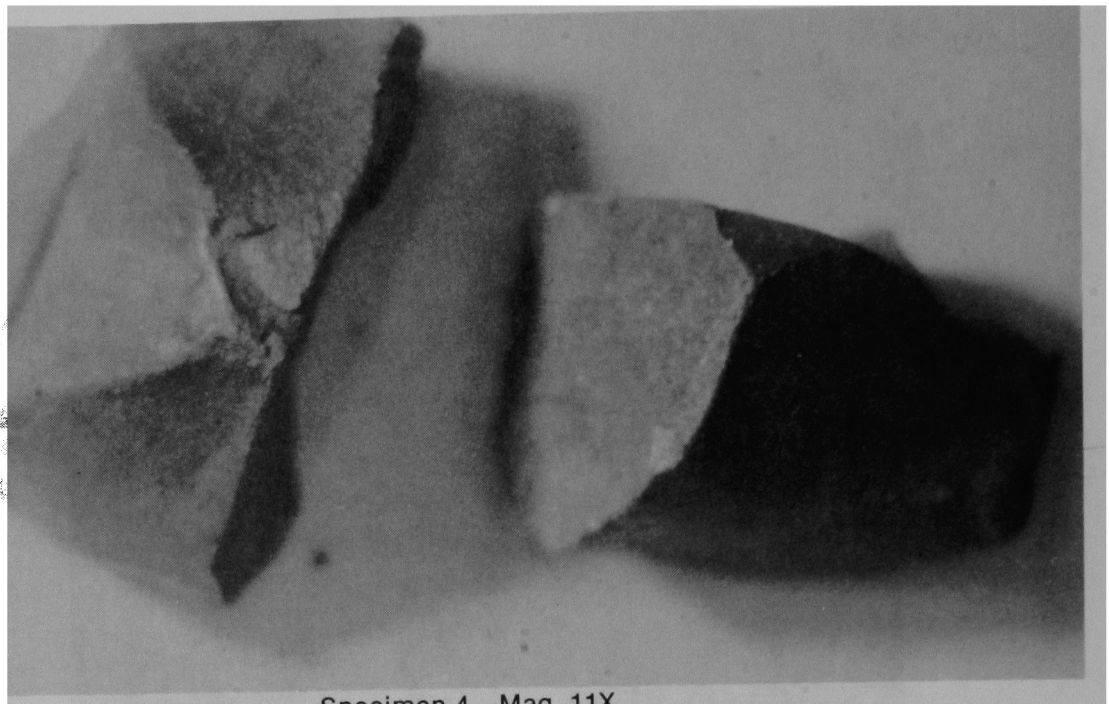

Specimen 4—Mag. 11X

Specimen 4—Mag. 11X

Specimen 4—Mag. 25X

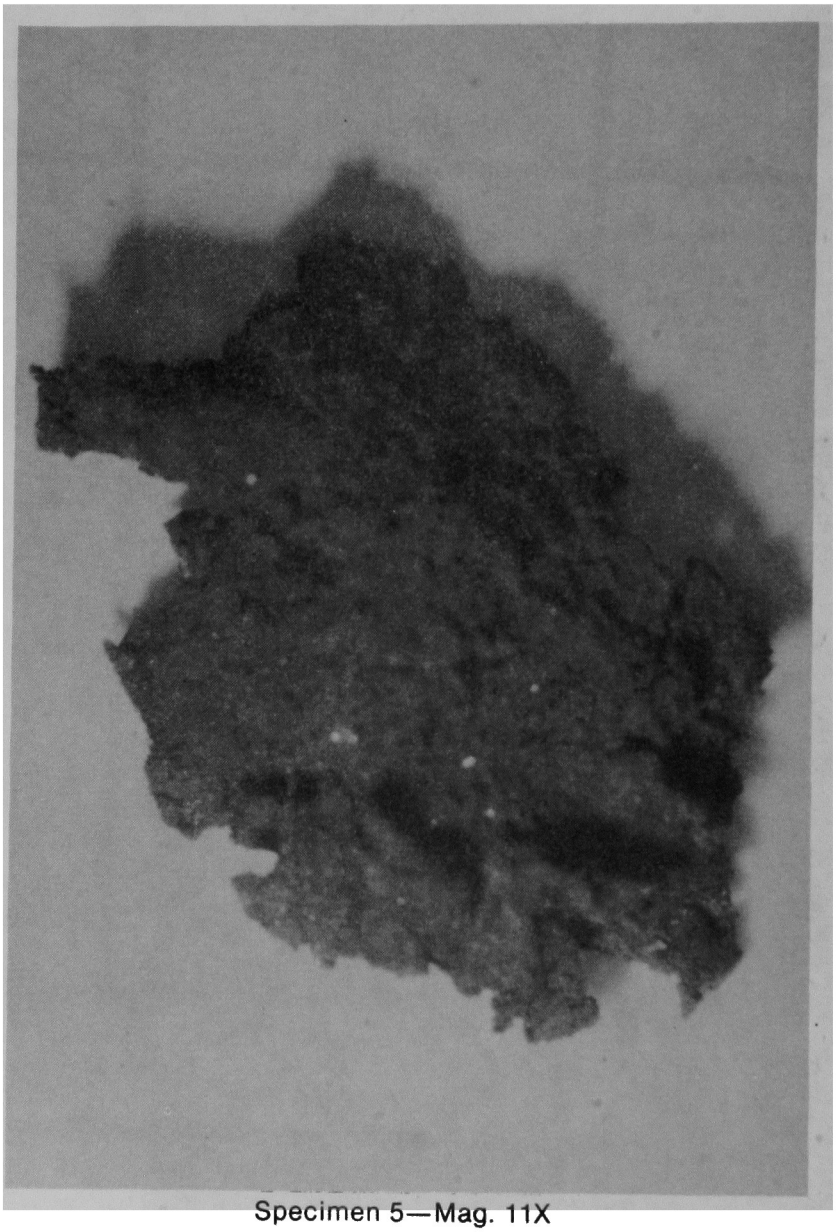

Specimen 5—Mag. 11X

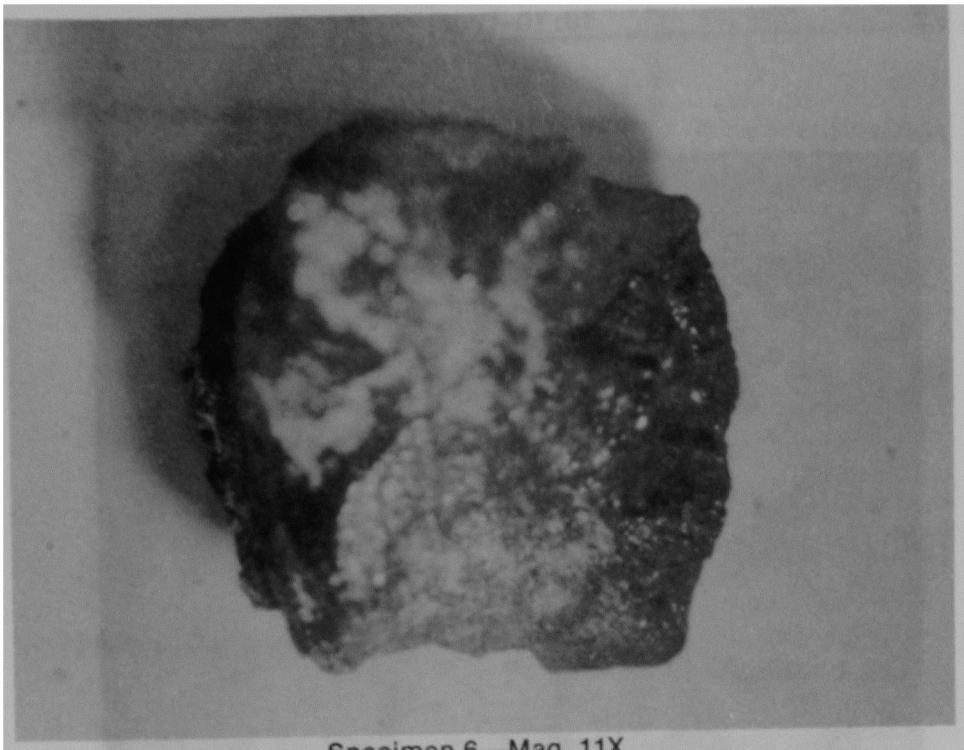

Specimen 6—Mag. 11X

Specimen 6—Mag. 11X

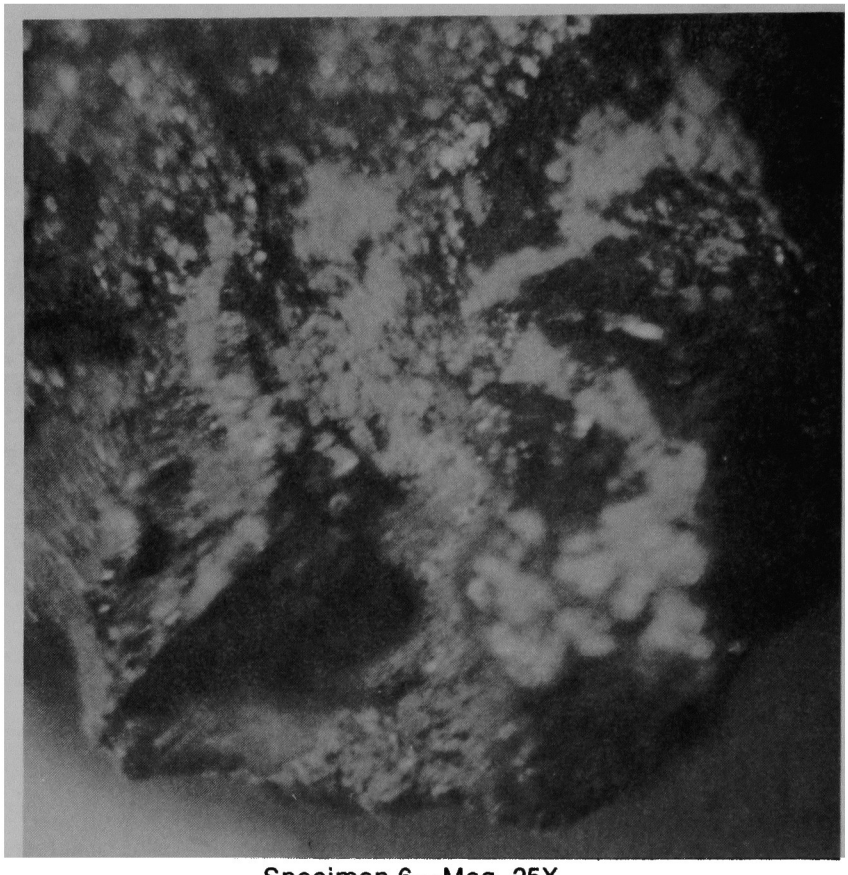

Specimen 6—Mag. 25X

APPENDIX E

X-Ray Diffraction Results

Table E-1. X-Ray Diffraction Results

Interplanar (d) Spacing (Angstroms)	Intensity*
10.5	MS
5.3 (broad)	MS
4.8	W
4.45	MW
3.85	W
3.65	VW
3.30	W
3.17	S
2.83	M
2.74	W
2.65	W
2.60	W
2.48 (broad)	S
2.27	VW
2.20	VW
2.05	VW
1.95	W
1.85	W
1.80	MW
1.73	VW
1.67 (broad)	VW
1.60	W
1.58	W
1.47	W

*S = strong
MS = medium strong
W = weak
MW = medium weak
VW = very weak
M = medium